UNIVERSITÀ
DEGLI STUDI
DI PADOVA

Università degli Studi di Padova

Dipartimento Territorio e Sistemi Agro Forestali

SCUOLA DI DOTTORATO DI RICERCA IN

TERRITORIO AMBIENTE RISORSE E SALUTE

CICLO XXVI

DNA Repair is Modulated by Cellular and Circadian Cycles

Direttore della scuola: Ch.mo Prof. Mario Aristide Lenzi

Supervisore: Ch.mo Prof. Lucia Celotti

Co-supervisore: Ch.mo Prof. Urs Albrecht

Dottorando: Leonardo Bee

Summary

Background

DNA repair is an essential cellular function aiming to maintain genomic stability during dangerous environmental conditions, such as exposure to UV light and ionizing radiation. At the molecular level, cell life is marked by rhythmic events resulting from the two major oscillatory systems: the circadian clock and the cell cycle, which share some striking similarities. Both consist of interlocked auto-regulatory feedback loops and both rely on chromatin remodeling events that produce sequential transcription, translation, post-translational modification, and degradation phases. In mammals, DNA double-strand breaks (DSBs) are rejoined by two highly regulated pathways: non-homologous end joining (NHEJ), which is always operative, and homologous recombination (HR), which is active only in late S- and G2-phases when both sister chromatids are present. DNA adducts induced by exposure to UV light, such as cyclobutane pyrimidine dimers (CPDs) and pyrimidine pirimidone photoproducts ([6-4]PPs), can be repaired only by the nucleotide excision repair (NER) system. DNA damage response (DDR), which includes DNA repair, checkpoint activation, chromatin remodeling, and apoptosis, seems to be strictly modulated by the rhythmicity induced by the cell cycle and the circadian clock, and this could affect its efficiency, making the cells more sensitive or resistant to genotoxic stress at different times of the day.

Methodology and Principal Findings

DNA double-strand break repair is modulated by cell cycle progression

Human lung fibroblasts were tested for DNA repair efficiency during some phases of the cell cycle by monitoring formation and disappearance of γ-H2AX foci at the sites of DSBs induced by γ-ray irradiation. The decrease in γ-H2AX signals at DSB sites was more pronounced in G2- with respect to G1-phase cells. Moreover, G2 cells treated with the HR inhibitor (RI-1) exhibited a higher level of unrepaired DSBs starting six hours after irradiation, showing that HR is active early after DNA damage. Our data demonstrated that in G2-phase cells, NHEJ and

HR repair systems cooperate in DSB rejoining not only long times after irradiation but also during the first hours of post-irradiation incubation. The relevance of HR during DSB repair and, in particular, the possibility that this pathway could compensate for NHEJ deficiency, was assayed in DNA-PKcs deficient cells as well as in those treated with DNA-PKcs inhibitor. In both conditions, the kinetics of γ-H2AX demonstrated that DSB repair was strongly affected during all phases of the cell cycle, even in the G2-one when HR should have been active, confirming previous observations according to which DSB rejoining is strictly dependent on the integrity of the NHEJ repair system (Bee e al. 2013).

DNA repair efficiency is modulated during the circadian cycle

We evaluated whether the circadian clock affects the efficiency of DNA repair in non-proliferating human primary skin fibroblasts irradiated with UV light. Quiescent fibroblasts (in the G0 phase) were synchronized by dexamethasone incubation to induce rhythmic expression of the circadian clock genes. We found, by using qRT-PCR, a strong circadian rhythmicity in PER2 mRNA levels, which showed two negative peaks at 16 h and 40 h after dexamethasone incubation and a positive one at 28 h, with an overall period of about 24 h. BMAL1 mRNA expression also showed robust oscillations in the anti-phase of PER2 transcript (as expected). The rhythmicity of the transcripts was confirmed by Western blot analyses showing clear oscillations of BMAL1 and PER2 protein levels. We identified, thus, two time-points separated by a 12 h interval during which administration of UV light occurred at the two opposite levels of clock gene expression.

Following the PER2 protein expression level, the cells were irradiated at 16 h after dexamethasone, which corresponded to the PER2 nadir, and at 28 h after dexamethasone, corresponding to the PER2 zenith. By measuring H2AX phosphorylation, a marker of damaged DNA, we found that zenith-irradiated cells exhibited a significantly higher extension of γ-H2AX, especially 2 and 4 h after irradiation. Analyzing the renjoining of the gaps in DNA molecules produced during the NER process, using fluorometric analysis of DNA unwinding (FADU),

we uncovered, moreover, that the cells irradiated at the PER2 zenith contained less dsDNA than those irradiated at the nadir, suggesting that a greater residual damage results from slower repair kinetics. By measuring the removal of [6-4]PPs, we were able to determine that both treatment groups efficiently removed photoproducts within the first 3 h after irradiation, but the fibroblasts irradiated at the zenith exhibited a significantly slower kinetic of [6-4]PPs removal with respect to those irradiated at the nadir. By assessing XPA protein expression, we did not, as opposed to other authors, find any evidence of an oscillating pattern. Analysis of the XPA promoter using luciferase assay or by blocking the core clock machinery by RNA interference of BMAL1 expression and in BMAL1 mutant cells revealed no connection between this protein and circadian clock transcription factors. Interestingly, our results showed that in addition to the faster kinetics of [6-4]PPs removal, fibroblasts irradiated at the nadir of PER2 induced a significantly higher formation of both [6-4]PPs and CPDs with respect to zenith-irradiated cells. These data were confirmed by Unscheduled DNA Synthesis assay (UDS), which showed an higher incorporation of [3H]-TdR at the nadir- with respect to the zenith-irradiated cells. Transfection of fibroblasts with siRNAs targeting BMAL1 gene expression abrogated the difference observed in the amount of [6-4]PPs formed and reduced the photoproduct removal efficiency of nadir-irradiated cells. In this condition we observed no differences between nadir and zenith-irradiated cells, confirming BMAL1's role in UV light sensitivity and DNA damage repair.

Conclusions

Taken as a whole, even if preliminary, our results indicate that DNA damage response is an event that is strictly modulated by the rhythmicity of the cell cycle and the circadian clock and that its efficiency varies over a 24 h interval. This indicates that the time of exposure to genotoxic stress, such as ionizing radiation and/or UV light, could increase the risk of genomic instability. We observed that both the sensitivity of DNA to UV and repair were higher when PER2 reached its nadir (and therefore BMAL1 its zenith), perhaps as a

consequence of a particular chromatin structure which leads to higher DNA accessibility. We observed, nevertheless, that DSB rejoining was more efficient in the S-G2 phases, when both HR and NHEJ cooperate in DNA repair. In mice PER2 nadir was found to occur during the day while the PER2 zenith and S-G2 phases occurred during the night far from the UV component of sunlight. We speculate that the temporal separation of these events is a form of adaptation to environmental conditions (such as sunlight) and that the disruption of this oscillatory equilibrium affects DNA repair process.

Riassunto

Contesto

La riparazione dei danni al DNA è una funzione essenziale per il mantenimento della stabilità genomica in seguito all'esposizione a particolari condizioni ambientali, tra le quali le radiazioni UV e le radiazioni ionizzanti. A livello molecolare la vita della cellula è scandita da eventi ritmici risultanti dai due principali sistemi oscillatori: l'orologio circadiano e il ciclo cellulare, i quali condividono notevoli somiglianze. Entrambi, infatti, consistono in cicli di auto-regolazione ed entrambi si basano su eventi di rimodellamento della cromatina per produrre fasi sequenziali di trascrizione, traduzione, modificazione post-traduzionale, e fasi di degradazione. Nei mammiferi, le rotture del doppio filamento del DNA sono riparate mediante due vie altamente regolate: la saldatura delle estremità non omologhe (NHEJ), attiva in tutte le fasi del ciclo cellulare, e la ricombinazione omologa (HR), attiva solamente nelle fasi S e G2, quando sono presenti entrambi i cromatidi fratelli. Gli addotti di DNA indotti dall'esposizione ai raggi UV, come i dimeri ciclo butano-pirimidina (CPD) ed i fotoprodotti pirimidina-pirimidone ([6-4]PP), sono, invece, riparati unicamente dal sistema di rimozione dei nucleotidi (NER). La risposta ai danni al DNA (DDR) che include la riparazione del DNA, l'attivazione dei checkpoint del ciclo cellulare, il rimodellamento della cromatina e l'apoptosi, sembrano essere strettamente modulati dalla ritmicità indotta sia dal ciclo cellulare sia da quello circadiano. Questa interazione può quindi influenzare la risposta ai danni al DNA, rendendo la cellula più sensibile o più resistente agli stress genotossici nei diversi momenti del giorno.

Scopo dello studio

1. Analizzare in fibroblasti umani irradiati con raggi γ (a) il coinvolgimento e l'efficienza dei due sistemi di riparazione principali durante le fasi del ciclo cellulare e (b) la tempistica del reclutamento di HR nella riparazione delle doppie rotture al DNA.

2. Investigare se difetti nella NHEJ coinvolgono anche l'efficienza di HR nella riparazione delle doppie rotture in fase G2.
3. Sviluppare un sistema per il mantenimento delle colture cellulari in quiescenza a lungo termine e validare un insieme di tecniche che consentano di saggiare con precisione la riparazione dei danni al DNA indotti dalla luce UV.
4. Sincronizzare colture cellulari umani e indurre l'espressione circadiana dei vari geni orologio che oscillano in animali vivi.
5. Investigare se l'efficienza della risposta ai danni al DNA è influenzata dalla fase circadiana nella quale le cellule vengono trattate con agenti genotossici.

Metodologie e Risultati Principali

La riparazione delle doppie rotture al DNA è regolata dalla progressione del ciclo cellulare

In questo lavoro, è stata valutata l'efficienza della riparazione del DNA nelle varie fasi del ciclo cellulare in colture di fibroblasti umani di polmone seguendo la formazione e la scomparsa dei foci di γ-H2AX nei siti delle doppie rotture al DNA indotte da raggi γ. I risultati ottenuti hanno evidenziato una diminuzione del segnale di γ-H2AX più elevata nelle cellule in fase G2 rispetto a quelle in G1. Dopo sei ore dall'irradiazione, inoltre, le cellule in fase G2 trattate con l'inibitore di HR (RI-1), esibiscono un livello più elevato di DSBs non riparate, indicando che HR opera attivamente dopo tempi brevi dall'irradiazione. I dati dimostrano, quindi, che nelle cellule in fase G2, NHEJ e HR cooperano nella risoluzione delle DSB non solo a tempi lunghi dall'irradiazione, ma anche durante le prime ore di incubazione post-irradiazione. Data la rilevanza di HR nelle riparazione delle DSB, è stata valutata la capacità di HR di sopperire alla mancanza di NHEJ, utilizzando cellule difettive per DNA-PKcs o trattate con il suo specifico inibitore. In entrambe le condizioni, la cinetica dei foci di γ-H2AX ha dimostrato che la riparazione delle doppie rotture del DNA è fortemente

compromessa in tutte le fasi del ciclo cellulare, perfino in G2 dove HR dovrebbe essere attiva, confermando che la riparazione delle DSB è strettamente dipendente dall'integrità del sistema NHEJ.

L'efficienza della riparazione del DNA è controllata dall'orologio circadiano

In questo lavoro è stata valutata la possibilità che l'orologio circadiano possa influenzare l'efficienza della riparazione del DNA in fibroblasti primari di pelle umana quiescenti irradiati con luce UV. Attraverso un trattamento con dexametasone, i fibroblasti quiescenti (fase G0) sincronizzati al fine di indurre l'espressione ritmica dei geni orologio. Mediante qRT-PCT, è stato possibile apprezzare una forte induzione nella ritmicità del mRNA di PER2, che mostra due picchi negativi a 16 h e 40 h dopo l'incubazione con dexametasone, e un picco positivo a 28 h, con un periodo complessivo di circa 24 h. L'espressione di BMAL1 mostra anch'essa robuste oscillazioni e, come atteso, in anti-fase con il trascritto di PER2. La ritmicità dei trascritti è stata confermata mediante Western blot, la quale ha evidenziato chiare oscillazioni dei livelli delle proteine PER2 e BMAL1. È stato possibile identificare, quindi, due momenti temporali, separati da 12 h , nei quali la somministrazione di luce UV avviene in due livelli opposti di espressione dei geni orologio. Seguendo l'espressione della proteina PER2, le cellule sono state irradiate a 16 e 28 h in seguito al trattamento con dexametasone, corrispondenti rispettivamente al nadir e allo zenit di PER2. Quantificando la fosforilazione dell'istone H2AX, come marcatore dei danni al DNA, abbiamo trovato che le cellule irradiate allo zenit esibiscono un'estensione significativamente più elevata di γ-H2AX, in modo particolare a 2 e 4 h post-irradiazione. È stata quindi esaminata la risaldatura delle regioni di DNA a singolo filamento, prodotte durante il processo NER, mediante l'analisi fluorimetrica dello svolgimento del DNA (FADU). I risultati hanno evidenziato che le cellule irradiate allo zenit di PER2 contengono meno DNA a doppia elica rispetto a quelle irradiate al Nadir, suggerendo un maggiore danno residuo, come riflesso di una cinetica di riparazione più lenta. In accordo con ciò, quantificando la rimozione dei [6-4]PP è stato osservato che entrambi i gruppi rimuovono i foto

prodotti in modo efficiente entro le prime 3 h dall'irradiazione, ma i fibroblasti irradiati allo zenit di PER2 mostrano una cinetica di rimozione significativamente più lenta rispetto a quella osservata per il gruppo irradiato al nadir di PER2. Osservando l'espressione della proteina XPA, contrariamente dai risultati riportati da altri autori, non abbiamo trovato nessuna evidenza che segua un andamento oscillatorio. Una serie di analisi sul promotore di XPA mediante saggio della luciferasi, mediante il silenziamento di BMAL1 e in cellule mutanti in BMAL1 hanno dimostrato che non c'è una diretta connessione tra questa proteina e i fattori di trascrizione dell'orologio circadiano. Interessante, analizzando la formazione dei CPD e dei [6-4]PP immediatamente dopo l'irradiazione mediante saggio ELISA, abbiamo trovato che i fibroblasti irradiati al nadir di PER2 sono soggetti a una formazione significativamente più elevata di entrambi i CPD e [6-4]PP rispetto alle cellule irradiate allo zenit di PER2. Questi dati sono stati confermati dal saggio della Sintesi del DNA Non Programmata (UDS), che rivela una un'incorporazione più elevata di [3H]-TdR nelle cellule irradiate al nadir di PER2 rispetto a quelle irradiate al suo zenit. La trasfezione dei fibroblasti con siRNA aventi come target l'espressione del gene BMAL1, elimina la differenza osservata nell'ammontare dei [6-4]PP formati e riduce l'efficienza di rimozione dei dimeri delle cellule irradiate al nadir di PER2. In queste condizioni non è stato più possibile apprezzare differenze tra le cellule irradiate al nadir o allo zenit di PER2, suggerendo che BMAL1 giochi un ruolo importante nella sensibilità e nella riparazione dei danni al DNA indotti dalla luce UV.

Conclusioni

Nel loro insieme i dati, anche se preliminari, indicano che la risposta ai danni al DNA è un evento che è strettamente modulato dalla ritmicità del ciclo cellulare e dall'orologio circadiano, e la sua efficienza varia nel corso delle 24 ore. Questo significa che il tempo in cui avviene l'esposizione a stress genotossici, quali le radiazioni ionizzanti e UV, rappresenta un ulteriore fattore di pericolo per la stabilità genomica. È stato osservato, infatti, che sia la sensibilità che la

riparazione del DNA alla luce UV è elevata quando PER2 raggiunge il suo nadir (e quindi BMAL1 il suo zenit), forse come conseguenza di particolari conformazioni della cromatina che incrementano l'accessibilità del DNA. D'altra parte, è stato osservato che la riparazione delle doppie rotture al DNA è più efficiente nelle fasi S-G2 del ciclo cellulare, quando HR e NHEJ possono cooperare. Nel topo è stato osservato che il nadir di PER2 avviene durante il giorno, mentre lo zenit di PER2 e le fasi S-G2 avvengono durante la notte, lontano dal componente UV della luce del sole. Possiamo quindi ipotizzare che la separazione temporale di questi eventi sia una forma di adattamento alle condizioni ambientali (come la luce del sole) e che la rottura di questo equilibrio oscillatorio possa influenzare i processi di riparazione del DNA.

Introduction

DNA repair is an essential cellular function aiming to maintain genomic stability during dangerous environmental conditions, such as exposure to UV light and ionizing radiation. At the molecular level, cell life is marked by rhythmic events resulting from the two major oscillatory systems: the circadian clock and the cell cycle, which share some striking similarities. Both consist of interlocked auto-regulatory feedback loops and both rely on chromatin remodeling events that produce sequential transcription, translation, post-translational modification, and degradation phases. After damage has been induced, the cells activate a complex DNA damage response (DDR) process, which includes checkpoint activation, chromatin remodeling, DNA repair, and/or apoptosis, all seemingly strictly modulated by the rhythmicity linked to the cell cycle and the circadian clock. Both systems are able to control the DDR by affecting its efficiency and consequently making the cells more sensitive and/or resistant to genotoxic stress at different times in their cycle.

The environment surrounding us is saturated with high levels of radiation that can generate severe damage to DNA molecules such as single and double strand breaks, cross-links between DNA and proteins, and modifications in the double helix structure due to incorrect bond formation between adjacent nucleobases.

All organisms are, nevertheless, equipped with sophisticated, efficient systems to detect and repair radiation-damaged DNA. In many organisms, including humans, Nucleotide Excision Repair (NER) corrects any type of DNA lesions, such as cyclobutane pyrimidine dimers (CPDs) and pyrimidine pirimidone photoproducts ([6-4]PPs) induced by exposure to UV light. In mammals, DNA double strand breaks are rejoined by two highly regulated pathways: Non-Homologous End Joining (NHEJ), which is always operative, and Homologous Recombination (HR), which is active only in late S- and G2-phases when both sister chromatids are present.

This work focuses on research aiming to elucidate two important questions linked to this subject:

1. The involvement and the efficiency of the two main repair systems during cell cycle phases.
2. How the effectiveness of DDR is affected by the specific circadian time when the cells are stressed.

Radiation qualities

Radiation may be defined as energy in transit in the form of electromagnetic waves or particles. The environment that surrounds us is saturated with radiation, some forms perceptible to the senses (light, heat) and others requiring special instruments to be detected (radio waves, cosmic radiation, decay of radioactive isotopes). Depending on the amount of energy it possesses, radiation can be divided into two large groups: ionizing (e.g. γ-rays) and non-ionizing (e.g. ultraviolet light). The difference between the two groups lies in the higher energy possessed by the former, allowing it to induce the ionization of atoms and molecules with respect to the latter that does not possess enough energy to trigger the loss of electrons. Radiation's ability to cause biological effects does not, however, depend solely on the amount of energy it possesses but also on its capacity to penetrate substrates, which corresponds to the linear energy transfer (LET), representing the quantity of energy released per unit of distance traveled. In view of the complex nature of high LET radiation-induced damage, it is generally acknowledged that high-LET radiation forms (protons, alpha and beta particles) are biologically more effective than low-LET ones (γ- and X-rays) (Xue et al., 2009).

As far as non-ionizing radiations are concerned, due to solar irradiance, ultraviolet light (UV) is considered the kind of radiation to which organisms are most frequently exposed. UV light is an electromagnetic radiation with a wavelength between 100 and 400 nm that can be broken down into three bands: UV-A (400-320 nm), UV-B (320-280 nm), and UV-C (280-100 nm). Since frequency is inversely proportional to wavelength, despite its lower energy, UV-A penetrates the skin reaching the dermal layer damaging fibroblasts, the cells responsible for collagen secretion. UV-A is, as a result, the major contributor to

skin aging. While UV-C possesses low penetration proprieties, due to its higher energy (4.43-12.4 eV of UV-C vs. 3.10-3.94 eV of UV-A), direct exposure can cause more severe damage over time with respect to UV-A and UV-B. Despite the solar emission that covers all three bands, following absorption by the atmosphere, 95% of the rays that reach the earth's surface are represented by UV-A and the remaining 5% by UV-B. The ozone layer, in fact, absorbs 100% of UV-C and most of the UV-B rays.

The Biological Effect of Radiations

DNA damage represent the more serious kind of biological effect induced to organisms by radiations because they can potentially alter several fundamental cell life processes, such as cell cycle control and apoptosis, leading to cancer development. Consisting in chemical and structural modifications, DNA damage can be produced directly by energy absorption or indirectly through the production of reactive oxidative species (ROS), such as hydrogen peroxide (H_2O_2), superoxide anion (O2°-) and/or the hydroxyl radical (OH°). Following exposure to radiation, single (SSBs) and double-stranded DNA (DSBs) breaks, cross-links between DNA and proteins, and/or modifications in the double helix structure consequent to incorrect bond formation between adjacent nucleobases can be generated.

UV light can be directly absorbed by DNA, which contains many ring structures with conjugated double bonds, leading to damage caused by photochemical reactions. Adjacent pyrimidine bases react to form cyclobutane pyrimidine dimers (CPDs), accounting for the most common damage induced by UV (75%), with pyrimidine-pirimidone photoproduct [6-4]PPs, representing the remaining 25% (Figure 1). Dimers, in turn, cause a distortion in the DNA helix, which appears to be more pronounced in the case of photoproducts, which interfere with the integrity and stability of the genome as well as with fundamental processes such as DNA replication and gene transcription.

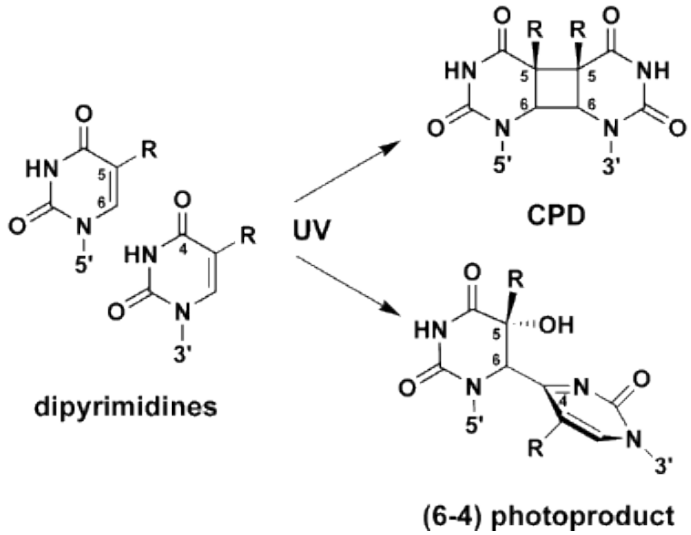

Figure 1 | Cyclobutane pyrimidine dimers (CPDs) and pyrimidine pirimidone photoproduct [6-4]PPs formation following UV irradiation.

Exposure to ionizing radiation (IR) is known to cause many types of DNA damage; among these double-strand breaks (DSBs) are considered the most dangerous threat to genomic integrity (Ohnishi et al., 2009; Vilenchik et al., 2003). If unrepaired, DSBs can lead to permanent cell cycle arrest, induction of apoptosis, or mitotic cell death caused by loss of genomic material (Rothkamm et al., 2003); if repaired improperly, they can induce carcinogenesis through translocations, inversions, or deletions (Hoeijmakers, 2001; van Gent et al., 2001). High doses of ionizing radiation can also lead to complex DNA damage (Ward, 2010) consisting of DSBs associated with base damages as well as non-DSB clusters composed of base lesions, apyrimidinic or apurinic sites and single-strand breaks that can produce additional DSBs due to damage processing (Eccles et al., 2011).

Mammalian DNA Damage Response (DDR)

DNA damage response (DDR) is a complex process involving highly specialized systems which need to be efficiently and rapidly activated after DNA damage has been induced. Each of these signaling cascades and subsequent repair

mechanisms involve several unique, overlapping mechanisms generally classified as sensors, mediators, transducers, and effectors whose activation ultimately leads to the spatio-temporal assembly of multi-protein complexes in the region of the damaged DNA (Collis et al., 2007) (Figure 2). DNA damage activates a checkpoint signalling system triggering the phosphoinositol-3-kinase-related kinases, ATM and ATR. These are activated in response to different types of DNA lesions: for the former, double-strand breaks and regions of ssDNA normally associated with stalled and/or collapsed replication forks, and for the latter, by lesion processing. It is now known, however, that there is some overlapping of functions and cross-talk between these pathways (Cuadrado et al., 2006; Collis et al., 2007). Activation of ATM and ATR is dependent upon the respective DNA-binding properties of the MRE11-RAD50-NBS1 (MRN; recruits ATM) complex and replication protein A (RPA; recruits ATR via its binding partner ATRIP), which are responsible for the recruitment and subsequent activation of ATM and ATR to the sites of DNA damage (Bartek et al. 2004; Harrison and Haber 2006; Collis et al., 2007). Activation of ATM and ATR triggers a signalling cascade through the phosphorylation of many downstream proteins, which ultimately leads to rapid alterations in the expression profiles of proteins involved in the transition of cell cycle phases (such as Chk1 and Chk2), recruitment of effectors of DNA repair, or in the regulation of cell survival (p53). The functional importance of DDR integrity is highlighted by its conservation throughout eukaryotes. DDR defects in human cells can, in fact, lead to genomic instability, mutagenesis, chromosomal abnormalities and an increased risk of cancer induction and progression (Chen et al., 2004; Zhou et al., 2000).

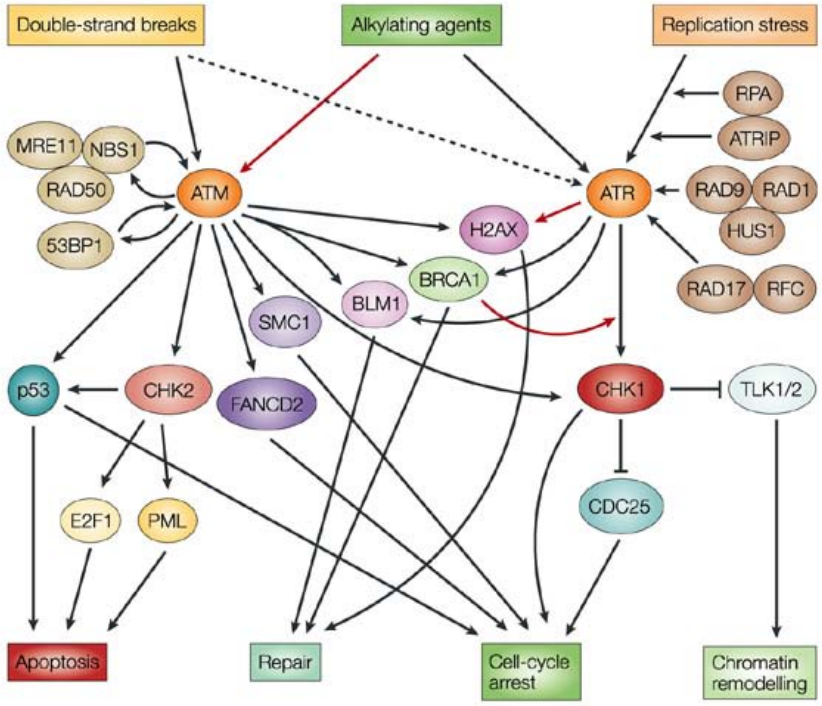

Figure 2 | The DNA damage response (DDR). DNA damage induced by different genotoxic stresses triggers a cascade of signals and subsequent repair mechanisms involving several unique and overlapping factors (Zhou et al., 2004).

DNA Double-Strand Break Repair

Following DNA double-strand break formation (DSBs), protein kinase ATM is activated and relocated through interaction with the Rad50/Mre11/NBS1 (MRN) complex (Lavin et al., 2008). ATM is a 370 kDa protein that, in the form of inactive dimer, is localized mainly in the nucleus. Following exposure to even low doses of ionizing radiation, a rapid autophosphorylation occurs at serine 1981 of ATM, leading to the dissociation of the dimer and the formation of active monomers (Kurz et al., 2004). Activated ATM has been shown to phosphorylate hundreds of proteins (Matsuoka et al., 2007), including those involved in checkpoint activation (e.g., p53 and Chk2) and in DNA-repair, such as Brca1 and 53BP1. A critical target of ATM is phosphorylation of the Ser-139 in the C terminus of the histone variant H2AX (γ-H2AX). Phosphorylation of H2AX by

ATM spreads away from the DSB, creating a γ-H2AX domain that extends for about two megabases along the chromatin from the DSB (Rogakou et al., 1999).

Eukaryotic cells rely on two highly regulated DSB repair pathways: the non-homologous end joining (NHEJ) and homologous recombination (HR) (Figure 3|A and 3|B, respectively). The former, which rejoins DNA ends without requiring sequence homologies, is carried out by the DNA-dependent protein kinase (DNA-PK) holoenzyme, consisting of the heterodimer KU70/KU80 and the DNA-PK catalytic subunit (DNA-PKcs) and by the DNA LIG4-XLF (Cernunnos)- XRCC4 complex. The process starts with binding of the Ku70-Ku80 complex on both ends of the damaged DNA, creating the scaffold for the assembly of other NHEJ enzymes. In the early repair stages, the DNA-Ku70/80 scaffold attracts the DNA-dependent protein kinase catalytic subunit (DNA-PKcs). DNA-PK holoenzyme plays multiple roles in DSBs repair, including the formation of a synaptic complex that holds the two DNA ends together. Damaged extremities, in fact, must often be processed by multiple enzymes, primarily nucleases and polymerases, which add or remove sequences to make them compatible for joining. This process can result in the occasional loss of nucleotides, which makes NHEJ an error-prone repairing system. Finally, the XRCC4 ligase IV complex catalyzes the ligation of the filaments carrying out the DNA repair.

Homologous recombination, instead, uses long homologous sequences from the undamaged sister chromatid or the homologous chromosomes as the template to faithfully restore the DNA strands at the broken site. HR's central activity is coordinated by RAD51 protein, associated with RAD52 and RPA, which catalyze the strand capture and invasion of broken ends of DSBs into intact homologous DNA sequences. Finally, the homologous sequence guides the synthesis and resolution of the two strands, which complete the repair process without introducing any errors (error-free system) (Lisby et al., 2009; Shrivastav et al., 2005; Shrivastav et al., 2009; Tracker et al., 2005). As the two chromatids are identical, genomic stability should be ensured. A potential risk is represented, however, by recombination between different chromatids or between homologous

sequences dispersed in the other chromosomes. The close proximity and structural cohesion promote, however, the use of sister chromatids as templates for HR repair of DSBs (Fabre, et al., 1984; Johnson, et al., 2000).

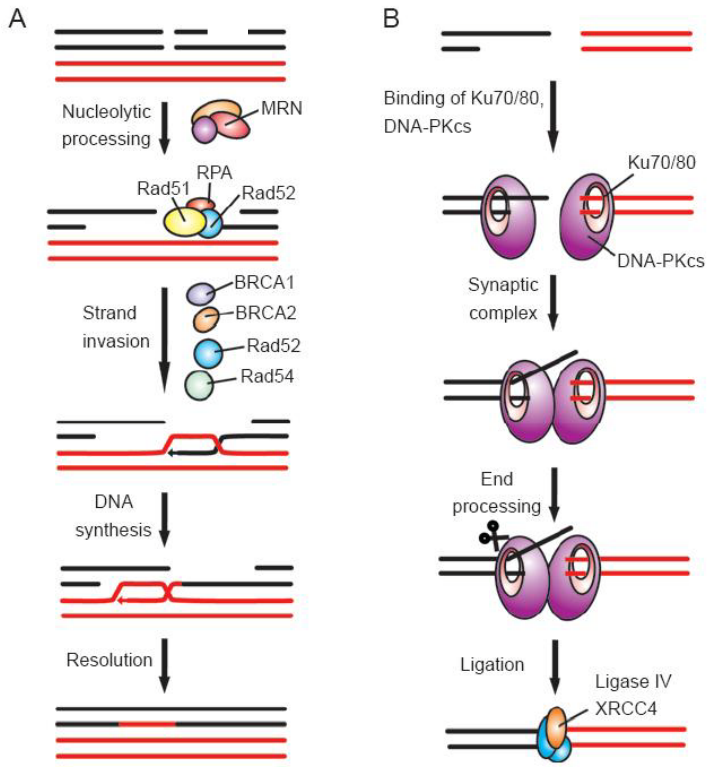

Figure 3 | DNA double-strand break repair systems. (A) A simplified overview of homologous recombination (HR) and **(B)** non-homologous end-joining (NHEJ).

UV-Induced DNA Repair: The Nucleotide Excision Repair system

Nucleotide excision repair (NER) is a universal, versatile repair system that corrects all types of lesions to DNA bases. In many organisms including humans it is, moreover, the only system that corrects DNA adducts such as cyclobutane pyrimidine dimers (CPDs) and pyrimidine-pirimidone photoproducts ([6-4]PPs) (Sancar et al., 2010). Defects in NER, in fact, underlie genetic disorders featuring genomic instability and segmental progeria. Mutations in NER proteins are responsible for severe genetic disorders, such as Xeroderma pigmentosum (XP), Cockayne syndrome (CS) and Trichothiodystrophy (TTD). Patients suffering from these disorders are predisposed to sun-induced skin cancer

incidence by more than a thousand-fold with respect to wild type controls, and show skin hypersensitivity to sunlight, a high frequency of internal tumors, accelerated neurodegeneration and developmental abnormalities.

The system can be broadly divided into two major pathways: the first sub-pathway, the global genome NER (GG-NER), is able to repair lesions throughout the entire genome through recognition of the reduced DNA rigidity resulting from the helix distortion. The second sub-pathway, transcription-coupled NER (TC-NER), specifically repairs DNA lesions in genes that block the actively transcribing RNA polymerases II (RNAPII) (Figure 4|A). The two mechanisms differ only in the initial recognition of DNA damage. The GG-NER initially requires the XPC-HR23B and DDB1-DDB2 (DNA damage binding protein 1 and 2) complexes to recognize the lesion. In TC-NER, instead, the RNA polymerase is itself involved in damage recognition and in the subsequent recruitment of CSA and CSB proteins which replace it. After this phase, the two mechanisms proceed along the same steps (Figure 4|B): the DNA double helix is unwound by the TFIIH complex in a reaction that requires ATP-dependent helicase activity of the subunits XPB (3'-5' strand) and XPD (5'- 3' strand). The resulting single-stranded DNA is stabilized by XPA and RPA proteins (replication protein A). Then the XPG and ERCC1-XPF nucleases proceed by cutting a segment of 27-30 nucleotides around the damaged site. Finally, the gap created is filled by a process that requires DNA polymerases δ or ε, as well as the accessory replication proteins and a correctly balanced pool of dNTPs (Palomera-Sanchez et al., 2010; Pontarin et al., 2012).

It has recently been demonstrated that repair is dependent on the type of lesion: apart from the different amount, [6-4]PPs are repaired five-fold faster than CPDs, probably due to the affinity of the damage sensor XPC for this type of lesion or its higher accessibility to DNA, facilitating in both cases the recruitment of other proteins involved in the repair process. The repair of transcriptionally active genes takes place, moreover, more rapidly with respect to transcriptionally silent DNA regions (Rastogi et al., 2010).

A

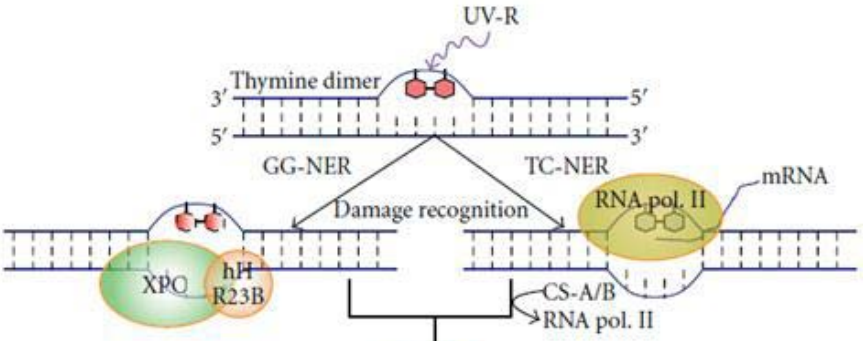

B

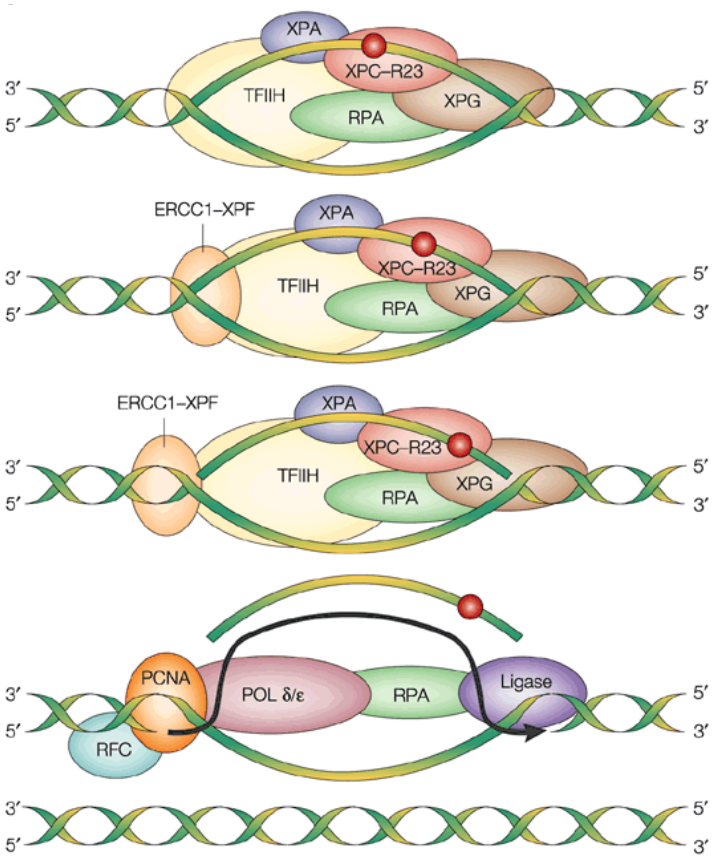

Figure 4 | The nucleotide excision repair system. (A) Thymidine dimer recognition by global genome repair (GGR), responsible for repairing lesions in the wide genome, and transcription-coupled repair (TCR), responsible for repairing damage in transcriptionally active genes **(B)** The repair is carried out by cutting a 27-30 nucleotide segment around the damaged site followed by repair synthesis and ligation (Friedberg et al., 2001).

This difference could depend on stalling of RNA polII at the DNA lesion that acts as a damage recognition signal in TC-NER, without requiring recognition of helix distortion by the XPC-RAD23B and DDB complexes (Mellon, 2005).

The Circadian Clock

The circadian clock is the molecular system that confers rhythmicity to daily physiological functions. From an evolutionary point of view, it is a form of adaptation on the part of organisms to the regular cycles of the Earth's rotation on its axis in a 24-hour solar day. The system's major function is to synchronize internal metabolic processes with daily and seasonal environmental variations/signals in order to ensure optimal performance of the different organs. In mammals, the control of circadian rhythmicity is localized in the central nervous system, in a region of the anterior hypothalamus called the suprachiasmatic nucleus (SCN), whose primary function is to synchronize the activity of the peripheral clocks which operate in almost every cell and tissue. The basic molecular architecture of the SCN clock is the same as those of the peripheral clocks; the SCN, however, has the capability of signaling to, and thus synchronizing, the peripheral clocks with itself and with one another (Sancar et al., 2010). The master clock is influenced by several stimuli, among which the light-dark cycle that plays a predominant role. The retina of the eye contains photoreceptors that absorb sunlight and send nervous signals to the brain which modulates the circadian clock's molecular machinery allowing it to control the organisms' physiological activities through the synchronization of the peripheral clocks. The regulation of the 'peripheral' organs' circadian rhythms occurs through the release of hormones, such as glucocorticoids, which are secreted, under the control of the central nervous system, in a rhythmic pattern by the adrenal glands. Glucocorticoids bind to intracellular receptors, causing a conformational change that leads to the translocation of the receptors into the nucleus where, by binding to glucocorticoid response elements (gRES), they

modulate the expression of circadian clock genes, such as Per1 (Yamamoto et al., 2005) and Rev-erbα (Torra et al., 2000).

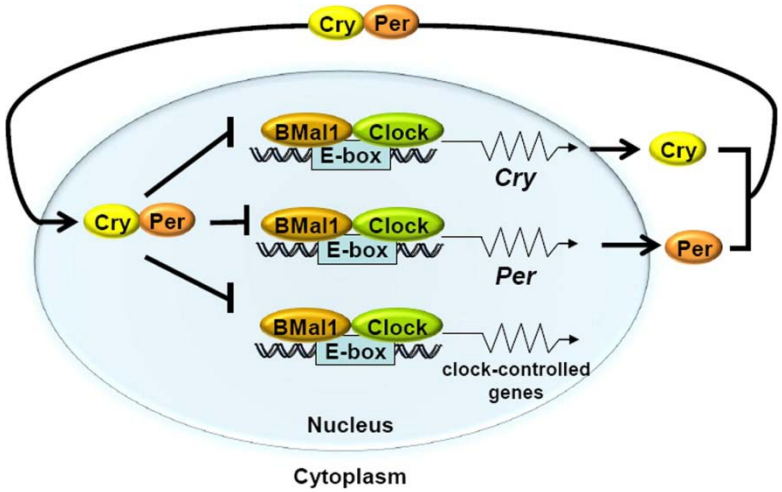

Figure 5 | The mammalian circadian clock. The transcription factors CLOCK and BMAL1 bind to the E-box motifs of Per and Cry gene promoters activating their transcription. The CRY and PER proteins make heterodimers which, after a delay, enter the nucleus and inhibit CLOCK-BMAL1-activated transcription (Antoch et al., 2010).

The circadian clock's molecular mechanisms consist of a small group of genes/proteins, which operate in such a way as to generate transcription-translation feedback loops (TTFLs) (Figure 5). The positive components of the loop are the basic helix-loop-helix-PAS domain (bHLH-PAS domain) transcription factors CLOCK and BMAL1. In the form of a heterodimer in the nucleus, they drive the rhythmic expression of numerous genes through the E-box elements (CACGTG) in their promoter regions. Among the transcriptional targets of the CLOCK/BMAL1 complex are the Period (Per1 and Per2) and Cryptochrome (Cry1 and Cry2) genes. PER and CRY proteins function as negative components of the circadian loop by inhibiting CLOCK/BMAL1-mediated trans-activation. The Bmal1 gene is also regulated by two of its transcriptional targets, the nuclear receptors REV-ERBα and RORα (retinoic acid receptor–related orphan receptor α), which function, respectively, as the repressor and activator of Bmal1 transcription by competing for the RORE (RORα response

element, (A/T rich)$_6$GGTCA) in its promoter (Antoch et al., 2010). Clock-BMal1 also controls the transcription of about 10% of the genes in a given cell, causing rhythmic expression of these so-called clock-controlled genes (CCG) (Hughes et al., 2007).

Cell Cycle Control of DNA Repair

Cell cycle regulation involves processes crucial to cell survival, including the detection and repair of genetic damages as well as the prevention of uncontrolled cell division. Progression through cell cycle phases requires the successive activation of different cyclin-dependent protein kinases (CDKs). These enzymes are controlled by transient associations with cyclin regulatory subunits, binding of inhibitory polypeptides, and reversible phosphorylation reactions. To promote progression towards DNA replication (S-phase), CDK/cyclin complex phosphorylate proteins required for the activation of genes involved in DNA synthesis, as well as components of the DNA replication machinery (Nigg, 1995). Following detection of DNA damage, a rapid phosphorylation-driven signaling cascade results in immediate inhibition of Cdk/cyclin complexes and in a delayed transcriptional response that promotes a prolonged cell cycle arrest through the induction of Cdk inhibitors, such as p21 (Boucas et al., 2012). Besides controlling cell cycle progression, Cdk/cyclin complexes represent the core of the Homologous Recombination system in DNA double-strand break repair. Although both NHEJ and HR contribute to DSB rejoining, their involvement varies during the different cell cycle phases as NHEJ is active throughout all cell cycles while HR is active only during the S- and G2- phases when the sister chromatids are available (Figure 6). The key regulator of HR is represented by the phosphorylation on S3291 of the Breast Cancer Type 2 susceptibility protein (BRCA2), which is crucial for modulating the activity of the essential recombination protein RAD51. Phosphorylation of S3291 in the C-terminal region of BRCA2 increased throughout G2/M during the cell cycle and was reduced in G1, respectively allowing or inhibiting RAD51 activity (Esashi et al., 2005).

As the two repair systems (NHEJ and HR) can be operating at the same time in the G2-cell cycle phase with respect to G1-phase during which only NHEJ can operate, it has been hypothesized that the efficiency of DSBs repair could be different. Some authors have, however, identified HR as part of a "slow component" in DSBs repair as it requires the recruitment of ATM and the endonuclease Artemis in order to process the damaged DNA extremities (Beucher et al., 2009). Consistent with this hypothesis, the majority of IR-induced DSBs (approx 80%) are repaired by NHEJ with fast kinetics in the G1- and in G2-phases. Other researchers have reported that HR is involved even during the first hours following IR, demonstrating that within 5 min of irradiation, homologous chromosomes make contact at the sites of DSBs induced by ionizing radiation (Gandhi et al., 2013). The question if NHEJ and HR are two competitive repair systems or cooperate to enhance the efficiency of DSBs repair in the S- and G2-phases is as yet unanswered.

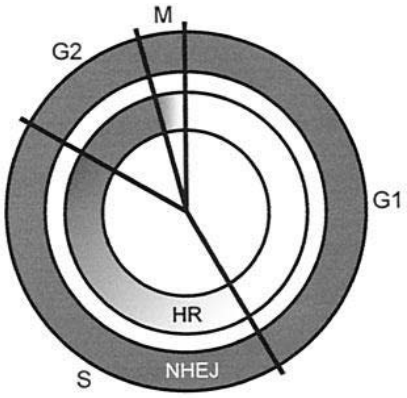

Figure 6 | The different contributions of Non-homologous End Joining and Homologous Recombination systems during cell cycle progression.

Recent works have, moreover, reported that there are differences, during cell cycle progression, even in Nucleotide Excision Repair efficiency (Li et al., 2011; Li et al., 2013). They demonstrated that NER efficiency is regulated by the ATR/p53 checkpoint via modulation of importin-α4-mediated XPA nuclear import in cell cycle synchronized cells. As this regulation occurs in a cell cycle-

dependent manner, the removal of cyclobutane pyrimidine dimers (CPDs) has been found to be more efficient in the S- phase with respect to G1- phase cells.

The Circadian Clock, DNA Damage Response, and Cancer

The role of the circadian clock in cancer development and progression is intimately linked to the role of the circadian system in the genotoxic stress response of an organism (Kang et al., 2009). Results of several epidemiological studies involving employees working the night shift have shown that abnormal work schedules are correlated with a higher risk of developing different types of carcinomas, including breast and prostate cancer. These findings are consistent with an interconnection between functional defects in the circadian system and carcinogenesis. Experiments carried out on mice have revealed, in fact, that interruption of normal rhythmicity due to surgical removal of the suprachiasmatic nucleus or due to chronic exposure to frequent changes in the light-dark cycle resulted in an accelerated growth of implanted tumors (Figure 7) (Antoch et al., 2010). In agreement with an interconnection between functional defects in the circadian system and carcinogenesis, cancer prognosis has, moreover, been found to be less favorable in patients with an altered with respect to a normal circadian rhythm (Sahar et al., 2009).

Several key cancer-related genes and signalling pathways have been found to be potential targets for the circadian clock. It has been hypothesized that potential molecular mechanisms underlying the link between the circadian clock and cancer development include several DNA damage response components, such as cell cycle progression control, DNA repair and apoptosis (Kondratov, 2012). Recent studies have suggested that the principal mechanism involved in UV-induced DNA repair, the Nucleotide Excision Repair (NER), is strictly controlled by the circadian clock (Kang et al., 2009). Those authors analyzed the expression of the main proteins involved in DNA repair of UV-induced damage over a 24 h period. Their results showed that, unlike all other proteins of the Nucleotide Excision Repair, XPA, the protein involved of the recognition of DNA dimers and signal transduction, exhibits a circadian expression pattern. Other investigators

found a decreased latency and about a five-fold increased multiplicity of skin cancer (invasive squamous cell carcinoma) in mice exposed to repeated UV irradiation at CT 4:00 AM (XPA Nadir) with respect to mice exposed to UV at 4:00 PM (XPA Zenith) (Gaddameedhi et al., 2011). Those authors recently reported, however, that cells derived from mutant mice are indistinguishable from the wild-type mice in their response to UV radiation and they concluded that the majority of DDR is not controlled by the circadian clock and even if that kind of control exists at the organism level, it is masked in cell culture by the homeostatic control mechanism (Gaddameedhi et al., 2012). These contradictions underline that data connecting DNA repair with the circadian clock are not entirely consistent and have led to the "case" being reopened.

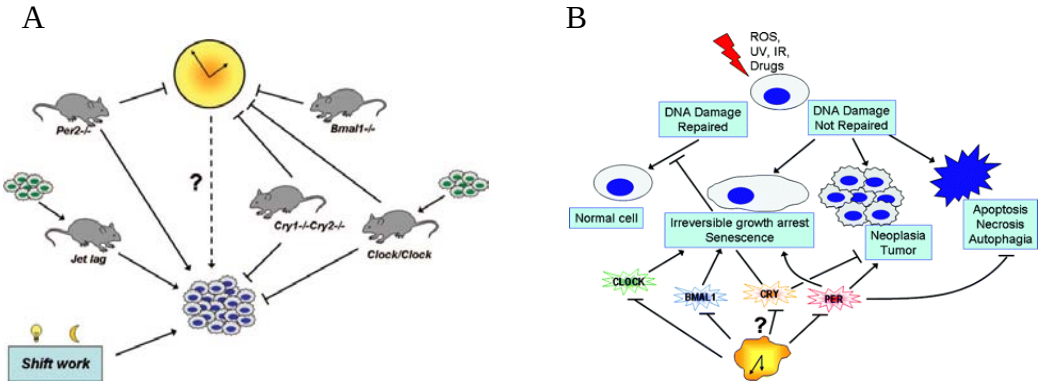

Figure 7 | Correlations between the circadian clock and carcinogenesis. (A) Shift work and mutations in some clock genes increase the risk of tumor development. **(B)** The correlation between circadian proteins and the regulation of the cellular response to genotoxic stress (Antoch et al., 2010).

The Circadian Clock and the Cell Cycle

At the molecular level, cell life is marked by rhythmic events resulting from the two major oscillatory systems: the circadian clock and the cell cycle, which share some striking similarities. Both consist of interlocked auto-regulatory loops and both rely on chromatin remodeling events that produce sequential transcription, translation, post-translational modification and degradation phases. Several findings indicate that progression through the cell cycle occurs at specific

times of the day/night cycle and suggest that this process is controlled by the circadian clock. Analysis of microarrays have revealed that many of the key components of the cell cycle (such as cyclin D1, cyclin B1, cyclin E, cyclin A, Wee1 and c -myc) have circadian expression. The three main components of cell cycle network, p21, c-Myc and Wee1, were found to be regulated by the clock proteins (Figure 8). The p21 gene, responsible for the G1-S-phase transition, is under the control of RORα and REV-ERBα, which, in turn, respectively induce and repress its transcription. The oncogene c-Myc, which plays a key role in cell proliferation, is inhibited by the Per1 and Per2 genes, while Wee1, which regulates the transition G2-M, is activated by the CLOCK-BMAL1 heterodimer and repressed by CRYs proteins (Borgs et al., 2009). It has recently been hypothesized that the RNA-binding protein NONO (p54nrb) is a synchronizing factor between the circadian clock and the cell cycle (Kowalska et al., 2012). This hypothesis is based on observations that NONO disruption completely abrogates circadian gating of the cell cycle in fibroblasts without severely disrupting either the circadian clock or the cell cycle. NONO, moreover, was found to be necessary for correct dermal wound healing, and when this control was lacking there was a loss of circadian cell cycle gating *in vitro* and tissue over-proliferation *in vivo*.

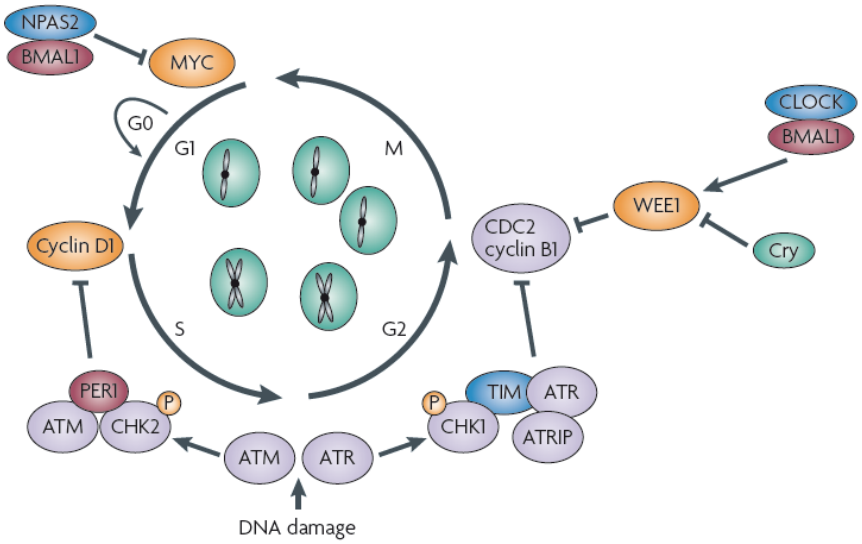

Figure 8 | Regulation of the cell cycle by the circadian clock. (Sahar et al., 2009)

The Circadian Clock and Chromatin remodeling

It has become increasingly clear that chromatin remodeling is one of the processes through which the circadian clock regulates the transcription of genes controlled by it (Sahar et al., 2013). The transcription process requires a rhythmic assembly and recruitment of specific multiprotein complexes in the appropriate sites of chromatin. This event is accompanied by modifications of clock proteins and chromatin components, such as acetylation, deacetylation and methylation of histones. Histone acetylation is a marker for transcription activation which is achieved by remodeling the chromatin to make it more accessible to the transcription machinery (Jenuwein and Allis, 2001). Histone methylation, on the other hand, acts as a signal for recruitment of chromatin remodeling factors which can either activate or repress transcription (Sahar et al., 2013). The key of this epigenetic control of gene expression is CLOCK, a central component of the circadian pacemaker, recently found to have histone acetyltransferase (HAT) activity, essential for circadian clock-controlled gene expression. CLOCK is able to acetylate the lysines 9 and 14 of histone H3 (H3K9 and H3K14), stimulating the opening of the chromatin and promoting gene transcription. BMAL1, the heterodimerization partner of CLOCK, seems to be involved in enhancing the HAT function (Doi et al., 2006). The histone deacetylase sirtuin 1 (SIRT1) was, moreover, found to regulate circadian rhythms by counteracting the HAT activity of CLOCK (Nakahata et al., 2008). SIRT1 operates, thus, as a rheostat of the circadian machinery, modulating the amplitude and "tightness" of CLOCK-mediated acetylation and the consequent transcription cycles in metabolic tissues. The prominent role of SIRT1 in longevity provides another interesting link between the circadian clock and ageing. Perturbations in the expression or activities of these regulators (CLOCK and SIRT1) could contribute to cancer development by causing higher proliferation and defects in the metabolic pathways (Sahar et al., 2013). Some investigators have recently reported that the most pervasive circadian regulation observed on a genome scale are rhythms in H3K4me3, H3K9ac (responsible for chromatin relaxation), H3K27ac, and RNAPII recruitment and transcription initiation, which occur at thousands of

expressed genes regardless of whether RNA cycling was detectable (Koike et al., 2012). This demonstrates that gene expression *per se* exhibits circadian rhythms with temporally separated activation and repression phases (Figure 9).

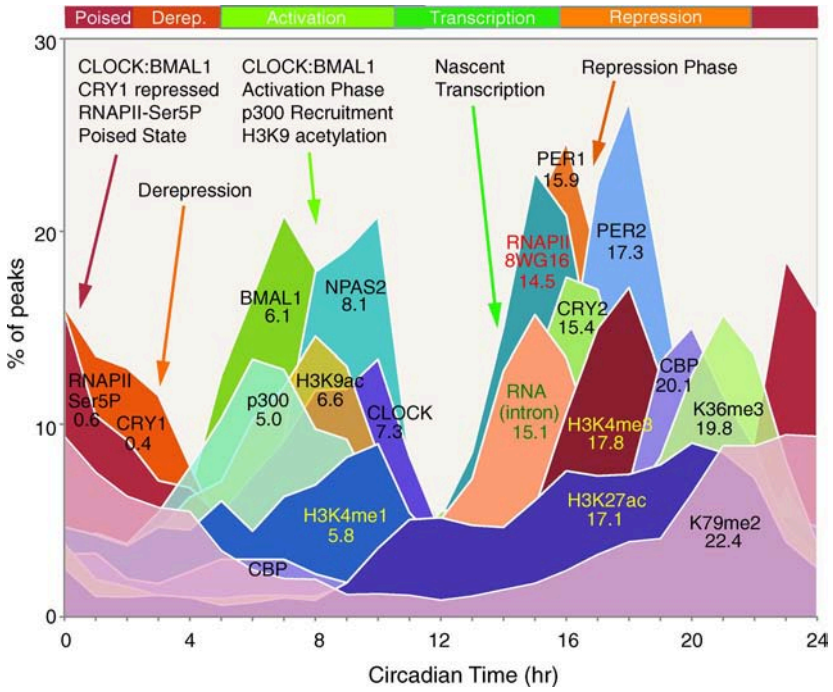

Figure 9 | Phase distributions of circadian transcriptional regulators, intron cycling RNA transcripts, and histone modifications (Koike et al., 2012).

Access to genomic DNA for events such as DNA repair must be facilitated by processes that directly alter chromatin structure leading to increased DNA accessibility. Since different conformational states of chromatin could affect both DNA damage incidence and repair processes, it is possible that the circadian clock regulates DNA damage response by transcription-coupled chromatin remodeling.

Aim of the Study

The overall aim of this study was to investigate whether the rhythmic progression of events resulting from the two major oscillatory systems, the cell cycle and the circadian clock, affect the efficiency of DNA repair following genotoxic stress induction. Specifically we planned the following objectives:

1. To analyze in human fibroblasts irradiated with γ-rays (a) the involvement and the efficiency of the two main repair systems during the phases of cell cycle and (b) the timing of HR recruitment during the repair incubation.
2. To investigate whether the impairment of NHEJ affects the efficiency of HR to rejoin DSBs in G2 phase cells.
3. To develop a system to maintain cell culture in a long-term quiescence status and to validate a set of techniques which allow to accurately quantify the kinetics of UV-induced DNA damage repair.
4. To synchronize human cell cultures and induce the circadian expression of various genes which oscillate in living animals.
5. To investigate whether the effectiveness of DDR is affected by the circadian time at which the cells are irradiated.

PAPER I

PLoS One
2013 Jul 11
8(7):e69061

Leonardo Bee[1*], Sonia Fabris[1*], Roberto Cherubini[2], Maddalena Mognato[1], and Lucia Celotti[1,2]

[1] Dipartimento di Biologia, Università di Padova, Padova, Italy.

[2] Laboratori Nazionali di Legnaro, Istituto Nazionale di Fisica Nucleare, Padova, Italy.

[*]Equally contributing authors.

[THE EFFICIENCY OF HOMOLOGOUS RECOMBINATION AND NON-HOMOLOGOUS END JOINING SYSTEMS IN REPAIRING DOUBLE-STRAND BREAKS DURING CELL CYCLE PROGRESSION]

Abstract

This study investigated the efficiency of Non-Homologous End Joining (NHEJ) and Homologous Recombination (HR) repair systems in rejoining DNA double-strand breaks (DSB) induced in CCD-34Lu cells by different γ-ray doses. The kinetics of DNA repair was assessed by analyzing the fluorescence decrease of γ-H2AX foci measured by SOID (Sum Of Integrated Density) parameter and counting foci number in the time-interval 0.5-24 hours after irradiation. Comparison of the two methods showed that the SOID parameter was useful in determining the amount and the persistence of DNA damage signal after exposure to high or low doses of ionizing radiation. The efficiency of DSB rejoining during the cell cycle was assessed by distinguishing G1, S, and G2 phase cells on the basis of nuclear fluorescence of the CENP-F protein. Six hours after irradiation, γ-H2AX foci resolution was higher in G2 compared to G1 cells in which both NHEJ and HR can cooperate. The rejoining of γ-H2AX foci in G2 phase cells was, moreover, decreased by RI-1, the chemical inhibitor of HR, demonstrating that homologous recombination is at work early after irradiation. The relevance of HR in DSB repair was assessed in DNA-PK-deficient M059J cells and in CCD-34Lu treated with the DNA-PKcs inhibitor, NU7026. In both conditions, the kinetics of γ-H2AX demonstrated that DSBs repair was markedly affected when NHEJ was absent or impaired, even in G2 phase cells in which HR should be at work. The recruitment of RAD51 at DSB sites was, moreover, delayed in M059J and in NU7026 treated-CCD-34Lu, with respect to DNA-PKcs proficient cells and continued for 24 hours despite the decrease in DNA repair. The impairment of NHEJ affected the efficiency of the HR system and significantly decreased cell survival after ionizing radiation, confirming that DSB rejoining is strictly dependent on the integrity of the NHEJ repair system.

Introduction

It is known that exposure to ionizing radiation (IR) causes many types of DNA damage, and, among these, double-strand breaks (DSBs) are considered the most dangerous threat to genomic integrity [1, 2]. Radio-induced DSBs can have a different complexity with respect to the ionization density of radiation. It has been demonstrated that high-LET radiation induces clusters of DNA lesions along the particle track while low-LET radiation causes sparse ionizations. When administered at high doses, low-LET radiation can also, nevertheless, lead to complex DNA damage [3] consisting of DSBs associated with base damages as well as non-DSB damage clusters comprised of base lesions, apyrimidinic or apurinic sites and single-strand breaks that can produce additional DSBs due to damage processing [4].

The efficiency of DNA repair after exposure to IR depends on the complexity of the radio-induced damage [5]. The presence of DSBs, whatever their origin may be, elicits a complex DNA-Damage Response (DDR) consisting of a cascade of events, involving damage sensing, signal transduction to the effectors of DNA repair, cell cycle arrest, and induction of apoptosis [6]. After exposure to IR, the extensive phosphorylation of histone H2AX at Ser139 results in the formation of discrete γ-H2AX foci which can be easily identified by immunostaining, a valuable tool highlighting the presence of DSBs [7, 8]. Since phosphorylation of H2AX at Ser 139 is abundant, fast, and correlates well with each DSB, it is the most sensitive marker that can be used to examine DNA damage and subsequent lesion repair [9]. Apart from γ-H2AX, numerous additional proteins that participate in DDR form Ionizing Radiation Induced Foci (IRIF) through their recruitment and accumulation at DNA damaged sites and often closely overlap with the relatively large γ-H2AX foci. One of these, the tumor suppressor p53-binding protein 1 (53BP1) rapidly localizes at DSB sites and activates p53 along with specific kinases. The number of 53BP1 foci has a linear relationship with the irradiation dose, and the time course of 53BP1 foci formation and disappearance is similar to that of γ-H2AX foci [10-14]. Another, smaller type of foci restricted to stretches of single-stranded (ss) DNA produced

from DSB end resection is formed by the components of the homologous recombination (HR) repair pathway, including Rad51 and RPA proteins. RPA binds to ssDNA during the initial phase of homologous recombination. Just as in DNA replication, this keeps ssDNA from binding to itself, in such a way that the resulting nucleoprotein filament can then be bound by Rad51 and its cofactors [15]. Broadly similar to the γ-H2AX foci detection, these additional foci provide convenient surrogate markers useful for monitoring the presence of DNA DSBs or the recruitment of HR repair proteins.

Eukaryotic cells rely on two highly regulated DSB repair pathways: the non-homologous end joining (NHEJ) and homologous recombination (HR). The former, which rejoins the DNA ends without requiring sequence homologies, is carried out by the DNA-dependent protein kinase (DNA-PK) holoenzyme, consisting of the heterodimer KU70/KU80 and the DNA-PK catalytic subunit (DNA-PKcs) and by the DNA LIG4-XLF (Cernunnos)-XRCC4 complex. HR's central activity is coordinated by RAD51 protein, which catalyzes the strand capture and invasion of broken ends of DSBs into intact homologous DNA sequences, which are the sister chromatid or the homologous chromosome, to ensure the fidelity of the repair process [16-19]. Although both NHEJ and HR contribute to DSB rejoining, their involvement varies during the different cell cycle phases as NHEJ is active throughout all cell cycle while HR is active during the S and G2 phases when sister chromatids are available. Some authors observed that the cell cycle control of DSB pathway choice can be bypassed in IR-exposed cells, thus promoting a preferential repair by HR [20-22].

The involvement and efficiency of NHEJ and HR repair systems during cell cycle phases in normal human CCD-34Lu fibroblasts exposed to different γ-ray doses were analyzed here. The study aimed, moreover, to determine if the impairment of DNA-PKcs protein by NU7026, a chemical inhibitor, or due to a frameshift mutation in M059J cells, alters RAD51 protein activity during the repair of γ-ray-induced DSBs. In order to analyze DSB repair at different stages of the cell cycle, G1and G2 phases were distinguished on the basis of the nuclear fluorescence intensity of CENP-F protein, whose expression and localization are cell cycle-dependent. CENP-F is a protein of the nuclear matrix that gradually

accumulates during the cell cycle until it reaches peak levels in G2 and M phase cells and is rapidly degraded after mitosis is complete [23]. It is thus detectable by *in situ* immunofluorescence throughout the late S, G2, and M phases of the cell cycle, but it is absent in the G1 one [24].

We used different methods based on quantifying foci fluorescence as an indicator of DNA damage and repair to study the kinetics of DNA DSB rejoining during the cell cycle. From our experiments, the Sum Of Integrated Density (SOID) parameter [25] results a valuable tool which takes into account the number and the size of IR-induced foci, allowing to accurately quantify DNA damage signal after exposure to high or low doses of ionizing radiation [26].

Our data indicated that the NHEJ and HR repair systems cooperate in G2 phase cells in DSB rejoining not only long after irradiation, but also during the first hours of post-irradiation incubation. We also noted that besides decreasing the general efficiency of DNA repair, the impairment of NHEJ in CCD-34Lu treated with the DNA-PKcs inhibitor, NU7026, as well as in DNA-PKcs deficient M059J cells likewise affected RAD51 recruitment to DSB sites.

Materials and Methods

Cell lines

Normal human neonatal lung fibroblasts CCD-34Lu (ATCC N. CRL-1491^{TM}) were grown in high glucose (4.5 g/l) Dulbecco's Modified Eagle Medium (DMEM) containing GlutaMAX (Gibco, Life Technologies), supplemented with 10% heat-inactivated fetal calf serum (FCS, Biochrom KG, Seromed), HEPES 20 mM (Sigma-Aldrich), 1% MEM non-essential amino acids (Gibco, Life Technologies). At the time the experiments were carried out the cells were at 27 to 40 population doublings and actively proliferating, as confirmed by flow cytometry analysis. Human malignant M059J glioblastoma cells were purchased from ATCC (CRL-2366™), while M059K cells were kindly provided by Professor S.C. West (Cancer Research UK London Research Institute, Clare Hall Laboratories, South Mimms, UK). Both cell lines were grown in a 1:1 mixture of DMEM and Ham's F-12 medium (DMEM/F-12, Gibco, Life Technologies), HEPES 20mM, 1% of MEM non-essential amino acids and 10% of heat-inactivated FCS.

Cell irradiation

Gamma irradiation was performed at the Department of Oncological and Surgical Sciences of the University Padova Medical Center with a ^{137}Cs source (dose rate of 2.8Gy/min). Cells (0.4x 10^6) were seeded 48h before the experiment and irradiated on Petri dishes (60x15mm), with or without coverslips, kept on ice before and after irradiation, and cultured at 37°C in fresh medium for different repair times. Except for irradiation, the control cells were subjected to the same experimental conditions.

Immunofluorescence staining

The cells were fixed at 0.5, 2, 6 and 24h after irradiation for Fluorescence Intensity (FI) analyses. Non-irradiated and irradiated cells were rinsed once with cold Phosphate Buffered Saline (PBS) and fixed with a 4% solution of formaldehyde (Sigma-Aldrich) at 37°C for 15 min and washed three times with PBS. The cells were permeabilized with 0.5% Triton X-100 in PBS at 37°C for 10

min and non-specific binding sites were masked with goat serum (10% in PBS) at room temperature for 1h. The cells were incubated for 2h at room temperature with anti-53BP1 (Bethyl Laboratories, 1:100), anti- γ-H2AX (Ser139) (Abcam or Millipore Chemicon Upstate Clone JBW301, 1:100), anti-RAD51 (Santa Cruz Biotechnology, H-92: sc-8349, lot. G0811, 1:100), anti–CENP-F (BD Bioscience, 610768, Clone 11, 1:100 or Abcam, ab5, lot. GR73067-3, 1:300) primary antibodies followed by three washings in PBS and once in PBS + 0.1% Triton X-100. The cells were subsequently incubated at room temperature for 1h with Alexa Fluor 488 goat anti-mouse secondary antibodies and Alexa Fluor 594 donkey anti-rabbit antibodies (Life Technologies, 1:250 and 1:350, respectively) and washed, as described above. Immunofluorescent staining for RPA and R2 were performed using the MAX-Stain™ reagents (Active Motif) according to the manufacturer's instructions. Briefly, fixed cells were incubated for 1h at 37°C with MAX-Block™ Blocking medium, washed 10 min with PBS, and incubated for 1h at 37°C with primary anti-R2 (Santa Cruz, N-18 sc:10844, lot. K061, 1:200) and anti-RPA32/RPA2 antibodies (Abcam, 9H8 lot. GR92538-1, ab2175, 1:200) diluted in MAX-Bind™ staining medium. The cells were then washed three times in PBS + 0.05% Tween-20, incubated for 1h at 37°C with secondary antibodies diluted in MAX-Bind™ staining medium, and washed, as described above. Cover slips were then mounted on glass slides with Vectashield mounting medium (Vector Laboratories) containing DAPI 0.2 µg/ml.

Images of 53BP1, γ-H2AX and RAD51 and *RPA* foci were taken using a Leica TCS SP5 confocal microscope (Leica Microsystems) with 40X or 63X oil immersion objectives. All images were acquired under the same laser intensity, PMC voltage, pinhole aperture, and 8-bit intensity value conditions. Z-plane stack scanning (500 nm thickness) was performed using sequential scanning to prevent crosstalk due to overlap of the emission spectra from the various fluorophores. Manual counts of γ-H2AX and 53BP1 foci were performed using the maximum intensity projection (MIP) images. The red and green images were superimposed by ImageJ software (NIH) to obtain merged images. The number of γ-H2AX and 53BP1 foci was determined for each time point on an average of 100 nuclei in

three independent experiments and listed in the figures after the number of foci in the non-irradiated cells was subtracted.

Nocodazole treatment

We added the spindle poison nocodazole (Sigma-Aldrich) to CCD-34Lu to arrest cell cycle progression during the M phase 1h before irradiation at 5 and 10 Gy at the final concentration of 50ng/mL. After irradiation the cells were maintained for 2h in the drug's presence and then analyzed by immunofluorescence for the presence of CENP-F nuclear protein and RAD51 foci.

Quantification of nuclear fluorescence

The images acquired with the confocal microscope were processed and analyzed with ImageJ software, using a specifically designed Macro to enable automated analysis of a larger number of nuclei (average of 200 nuclei) for each time point. All the images were processed to remove the background. The nuclear area for each image was determined by 4', 6-Diamidino-2-phyenylindole (DAPI) fluorescent signal and saved as a list of coordinates for subsequent analyses. Nuclear fluorescence was calculated as the mean intensity of all the pixels included in the nuclear area. In accordance with Mistrik et al. [25] and Ishikawa et al. [26], the SOID parameter was calculated for each nucleus as the product of the sum of the area of the foci and the mean fluorescence intensity. An intensity threshold was set to calculate the SOID so that only foci were included in the analysis.

The nuclear fluorescence intensity (FI) of CENP-F protein was used to discriminate the γ-H2AX and RAD51 SOID signal in the G2 and G1 cells. We also assigned the specific range of CENP-F FI values to G1, S, and G2 cells correlating CENP-F nuclear FI with the DNA replication phase using the EdU (5-ethynyl-2-deoxyuridine, Life Technologies) staining method described by Salic et al. and Buck et al. [27, 28], with minor modifications. Non-irradiated cells were seeded on Petri dishes with glass coverslips 48h before labeling for EdU assay. The cells were then incubated with EdU (30 μM) for 1h, rinsed three times with PBS and fixed with 4% of formaldehyde for 15 min at 37°C. The cells were

washed again before the "Click" stain reaction was performed and permeabilized with Triton X-100 0.5% in TBS for 5 min at RT. The "Click" reaction was performed incubating the cells for 30 min with a freshly prepared mix of 50 mM Tris-HCl pH 7.3, 2 mM $CuSO_4$, 5 µl/ml fluorescent 647-azide, 10 mM ascorbic acid and used immediately after ascorbate was added. EdU-stained coverslips were immunostained with CENP-F antibody, as described. Double stained slides were acquired using a Leica TCS SP5 confocal microscope and nuclear fluorescence was quantified. The range of CENP-F FI associated with the 95% of EdU positive cells identifying S-phase cells was calculated while the CENP-F FI values associated with EdU negative nuclei were assigned to the G1 cells. Finally, the values of CENP-F FI associated with EdU negative nuclei but higher than the maximum value of S-phase cells were assigned to the G2 cells. Throughout the different cell cycle phases during analyses of DNA repair we excluded nuclei with CENP-F intensity values within the confidence interval of S-phase, estimated as the mean CENP-F values ± S.D.

Due to the incompatibility between CENP-F and RPA antibodies, we used the presence of cytosolic RPA fluorescence of the ribonucleotide reductase R2 subunit as a marker of G1 and G2 phases [29]. R2 positive cells (S-G2) were discriminated by the presence of cytosolic fluorescence.

FACS analyses

The cell cycle distribution of irradiated and non-irradiated control cells was assessed by flow cytometry analysis of DNA content following staining with 50 µg/µl of propidium iodide (PI, Sigma-Aldrich), as previously described [30].

To analyze CENP-F content throughout the cell cycle, the cells were fixed in 70% cold ethanol, rinsed twice in PBS, centrifuged at 200 g for 10 min at 4 °C, and permeabilized in PBS with 0.1% TritonX-100 and 4% goat serum for 10 min on ice. After centrifugation, the cells were incubated over night with primary antibody diluted in permeabilization solution (mouse anti-CENP-F, 1:100). Then the cells were rinsed three times in PBS with 2% of goat serum and incubated at room temperature for 1h with agitation with secondary antibody (Alexa Fluor 488 goat anti-mouse) diluted in permeabilization solution. After three washings in

PBS with 2% goat serum, the cells were stained with at 37 °C for 1h. FACS analysis of total γ-H2AX content was carried out in a similar way, using a rabbit anti-γ-H2AX (1:500) as the primary antibody and Alexa Fluor 488 goat anti-mouse as the secondary one.

Data concerning FI were collected from $10x10^3$-$25x10^3$ cells/sample using a BD FACSCanto™ II flow cytometer (Becton Dickinson, BD Biosciences) and analyzed using the ModFit LT software (Verity Software House).

NU7026 and RI-I treatments

To specifically inhibit NHEJ or HR, 24h before irradiation CCD-34Lu cells were incubated with 10 μM NU7026 (DNA-PKcs inhibitor, Sigma-Aldrich) or 10 μM of RI-1 (RAD-51 inhibitor, CALBIOCHEM), both diluted in DMSO. After irradiation, the medium was replaced with a fresh one containing the inhibitor, and the cells were incubated for the fixed repair times. Non-irradiated cells were treated with DMSO only, NU7026 only, or RI-1 only to exclude any potential toxicity from contributing to the effects of radiation; no differences were detected in the various treatment conditions.

Cell viability

Cell viability was determined by a clonogenic assay in non-irradiated and irradiated CCD-34Lu, incubated with or without NU7026, the DNA-PKcs inhibitor, in M059K and M059J cells. After irradiation, 200 viable CCD34-Lu cells were seeded together with feeder layer cells (IMR90, $15x10^5$ cells/plate), previously irradiated with 40 Gy of γ-rays in complete medium supplemented with 15% serum in 10 cm diameter Petri dishes. When CCD-34Lu cells were treated with NU7026 they were maintained for 24h with the inhibitor and then the medium was replaced with a fresh one without the inhibitor. During clonogenic assay, 500 viable M059K and M059J cells were seeded in complete medium, without a feeder layer. Culture plates were scored for colony formation 14 days later by staining cells with crystal violet 0.4%. Only colonies containing at least 50 cells were considered positive. Cell survival was calculated as the percentage of cloning efficiency of treated cells over that of control cells.

Statistical Analysis

Data from at least three separate experiments are presented as means ± standard deviation (S.D.). All comparisons, with the exception of the cell survival experiments, were calculated using Student's *t*-test, in which case the *P* values are based on a two-way ANOVA analysis. Differences with a <0.05 *P*-value are considered significant.

Results

Kinetics of the formation and repair of DNA double-strand breaks

The formation and rejoining of DNA DSBs were analyzed by determining the number of ionizing radiation induced foci (IRIF) of γ-H2AX and 53BP1 proteins in CCD-34Lu cells irradiated with 0.5 Gy of γ-rays. Our data indicated that the kinetics of DSB rejoining is characterized by a complete resolution of IRIF within 24h of irradiation and the almost complete co-localization of γ-H2AX and 53BP1 foci (Figure 1A, B). Although the number of foci is correlated with the number of DNA DBSs [9], this parameter alone cannot precisely quantify the amount of DNA damage signal, which is linked to the size and persistence of foci during DNA-repair kinetics. The SOID parameter, which accounts for the number, the size, and the fluorescence density of ionizing radiation-induced foci, was thus utilized to accurately quantify the DNA damage. The results obtained, indicated in the text and in the figures as foci fluorescence intensity (FI), showed that the resolution of foci in cells irradiated with 0.5 and 5 Gy occurred with similar kinetics for both doses, even if with different values, according to the dose-related intensity of DNA damage signal (Figure 1C). By comparing the results of γ-H2AX kinetics obtained on the same samples of irradiated cells by manual foci counting and SOID parameter, we observed that in 0.5 Gy irradiated cells the kinetics of DNA damage signal (SOID parameter) and the DSB resolution (foci number) were rather similar, as both methods showed a complete DBS resolution in the 0.5-24h time-interval (Figure 1D). Following irradiation with 5 Gy, it was impossible to count the foci manually as shortly after irradiation the foci number was too high for reliable eye resolution. As a result we could not compare the kinetics obtained using the two methods. We were, however, able to observe that the decrease in the fluorescence of the foci detected by SOID proceeded in a slower manner with respect to the decrease in the number of foci, as demonstrated by the higher SOID values 2 and 6 hours after irradiation, mainly due to the increase over time of the size of the foci (Figure S1). We also measured the kinetics of γ-H2AX fluorescence using flow cytometry**,** which is a convenient

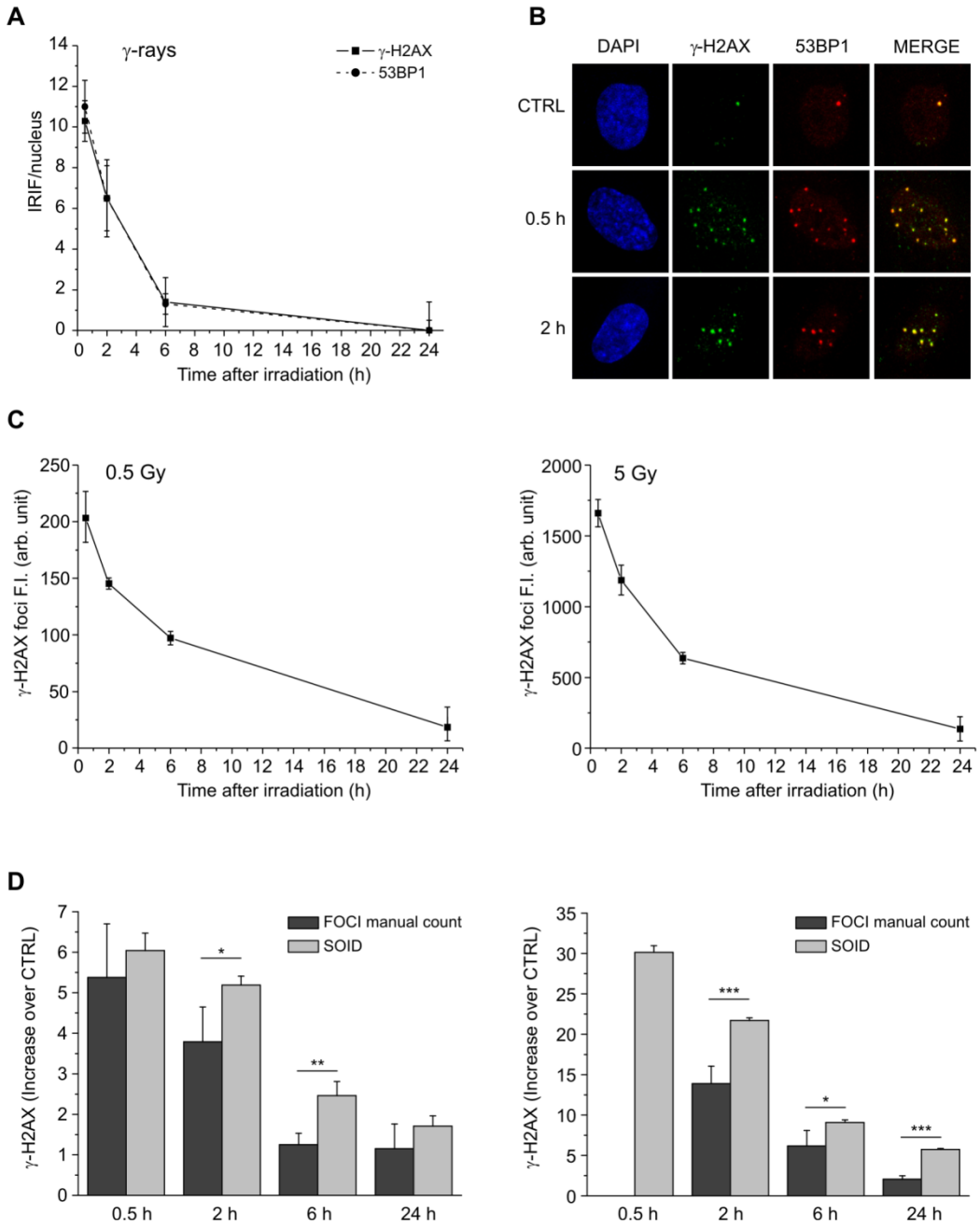

Figure 1. **Kinetics of DSB rejoining in cells irradiated with γ-rays plotted against 24h of the repair time.** (A) DBS rejoining was measured by manual counting of γ-H2AX and 53BP1 foci induced by irradiation with 0.5 Gy. (B) Representative pictures of γ-H2AX (green) and 53BP1 foci (red) in nuclei (blue) at 0.5 and 2 h from γ-irradiation, showing the almost complete co-localization of γ-H2AX and 53BP1 foci. (C) Fluorescence intensity (FI) of γ-H2AX foci has been determined by SOID parameter in cells irradiated with 0.5 Gy and 5 Gy of γ-rays. (D) Comparison

of FI of γ-H2AX foci, induced by irradiation with 0.5 Gy and 5 Gy, analyzed by manual counting and SOID parameter, expressed as increase over control. Error bars represent standard deviation of the mean calculated from 3-4 experiments (**P*<0.05, ***P*<0.01, ****P*<0.001, SOID vs. foci number, Student's *t*-test).

method to analyze a high number of cells. In our experiments the method did not, however, prove to be sensitive enough to detect differences in γ-H2AX FI at the different time-points after irradiation with the lower IR dose (Figure S2). On the basis of our experiments, we concluded that the SOID parameter was the most useful method to evaluate both high and low values of γ-H2AX FI, reflecting the amount and the persistence of DNA damage signal.

To evaluate the efficiency of DSB rejoining in the different cell cycle phases, we used nuclear fluorescence intensity of CENP-F protein, whose expression is cell cycle-dependent, to discriminate G1, S and G2 cells. By staining the cells with CENP-F antibody, positive G2 cells can be easily distinguished from negative G1 cells, but weakly stained cells, probably in the late S-phase, cannot be reliably identified by this method (Figure 2B). To overcome this difficulty, we determined the range of CENP-F fluorescence intensity of G1, S, and G2 cells by labeling the S-phase of non-irradiated cells with EdU staining (Figure 3). Cell distribution through cell cycle phases determined with CENP-F fluorescence by confocal microscopy has been confirmed by propidium iodide FACS analysis (Figure S3). By using SOID parameter, we were thus able to monitor the kinetics of DSB resolution, based on the disappearance of damage signaling, in G1, S, and G2 cells irradiated with 0.5 and 5 Gy of γ-rays. Our results showed that the majority of IR-induced DSBs were repaired within the first 6 hours of irradiation in all cell

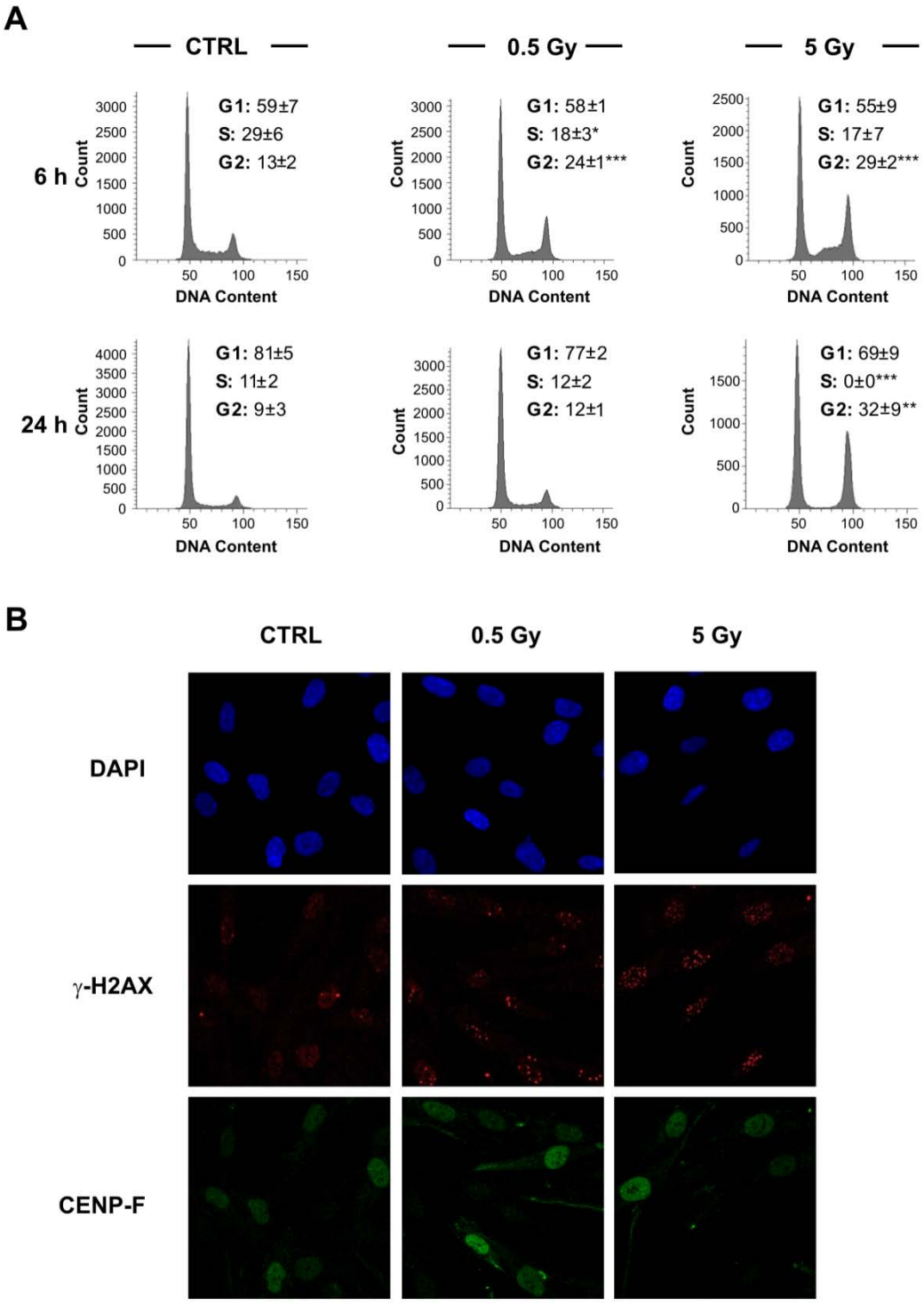

Figure 2. Cell cycle distribution of CCD-34Lu cells at 6 and 24h from irradiation with 0.5 and 5 Gy of γ-rays. (A) X axis, DNA content; Y axis, number of cells.*P<0.05; **P<0.01; ***P<0.001 (Student's t-test). (B) Pictures of γ-H2AX foci (red) in nuclei counterstained with

DAPI (blue) in CENP-F positive (green) and negative cells at 2h from irradiation with 0.5 and 5 Gy of γ-rays.

cycle phases (Figure 4A). Moreover, at 6 hours following irradiation, the decrease in fluorescence intensity in γ-H2AX foci induced by both IR doses was higher in the G2-phase with respect to the G1-phase cells. In the subsequent post-irradiation period (6-24h), FI disappearance was similar in the G1 and G2 cells after irradiation with 0.5 Gy, but it was higher in G2 cells after irradiation with 5 Gy (Figure 4B). As shown in Figure S1A, the foci size increased similarly over time in both G1 and G2 cells, while the intensity of foci fluorescence increased over time only in the G2 cells, probably due to the persistence of some unrepaired DSBs that were formed in previous cell cycle phases (Figure S1B). These data were confirmed by FACS analyses carried out in cells irradiated with 5 Gy in which FI disappearance in the 0.5-6h time-window was higher in the G2- with respect to the G1-phase cells (P<0.001, G2 vs. G1; Figure S4).

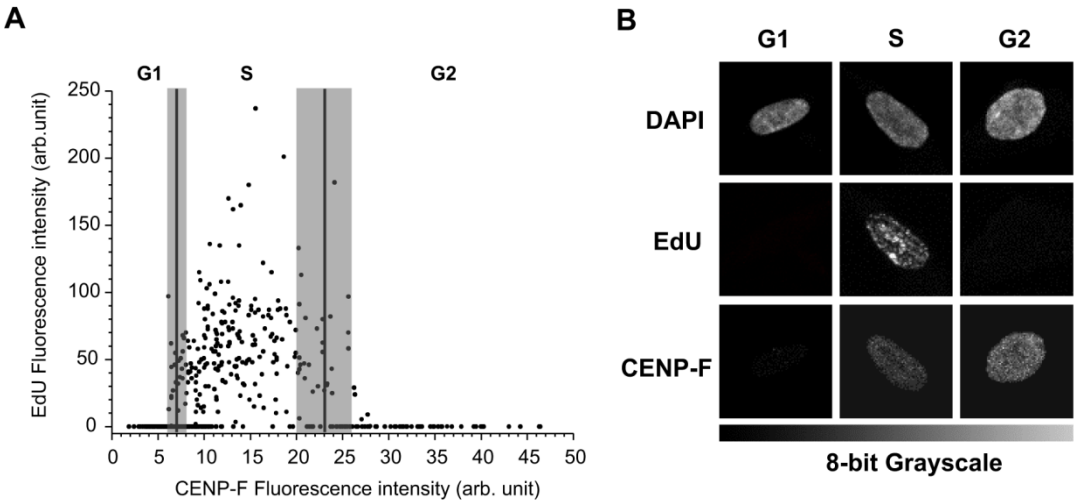

Figure 3. Fluorescence intensity (FI) of CENP-F protein plotted against FI of EdU. (A) CENP-F FI < 6.7 ± 0.5 has been assigned to G1 cells, CENP-F FI > 22.7 ± 2.5 to G2 cells. FI within the range 6.7-22.7 has been assigned to S phase cells. Cells with CENP-F intensity values within the confidence interval of S-phase, estimated as mean values of CENP-F ± S.D, have been excluded from the analyses (shaded area). (B) Representative pictures of EDU negative, CENP-F negative G1 cells; EDU positive, CENP-F weakly positive S-phase cells; EDU negative, CENP-F positive G2 cells.

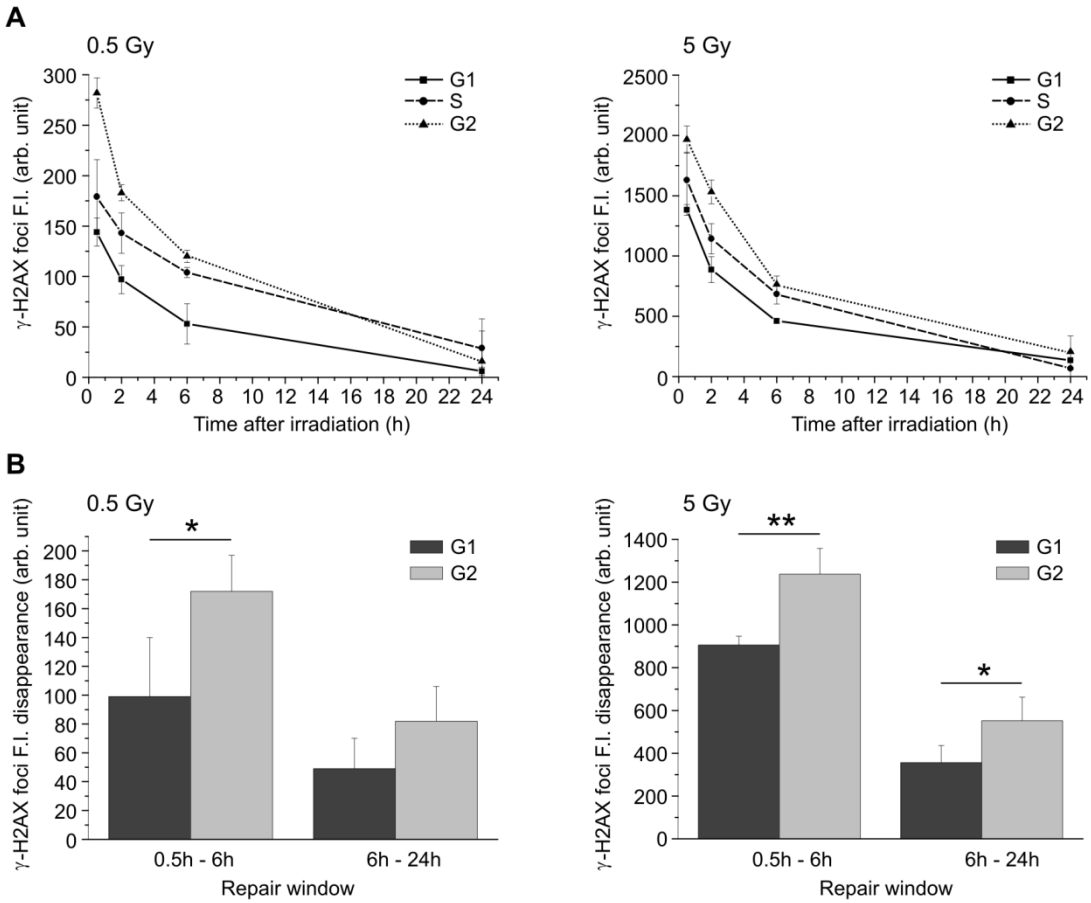

Figure 4. Kinetics of γ-H2AX foci in G1, S and G2 cells irradiated with γ-rays. (A) Values of γ-H2AX foci FI are mean ± S.D. from SOID determinations carried out in at least four independent experiments in cells irradiated with 0.5 and 5Gy. (B) Disappearance of γ-H2AX foci FI in G1- and G2-phases cells calculated in the 0.5-6h and 6-24h time-windows after irradiation (**P*<0.05, ***P*<0.01, G2 cells vs. G1 cells, *t*-test).

Since our results suggest that DSBs are repaired faster in the G2-phase cells during the first time-window after irradiation (0.5-6h), we analyzed the kinetics of RAD51 and RPA foci formation, representative of HR repair system involvement, in CCD-34Lu cells irradiated with 5 Gy (Figure 5). RAD51 foci were clearly visible beginning 2 hours after irradiation, they peaked at 6h, and at 24h they were mostly disassembled. Foci of RPA displayed similar kinetics, with fluorescence intensity values lower than those of RAD51. We can thus conclude that some HR proteins are recruited at DSB sites during the first hours after irradiation.

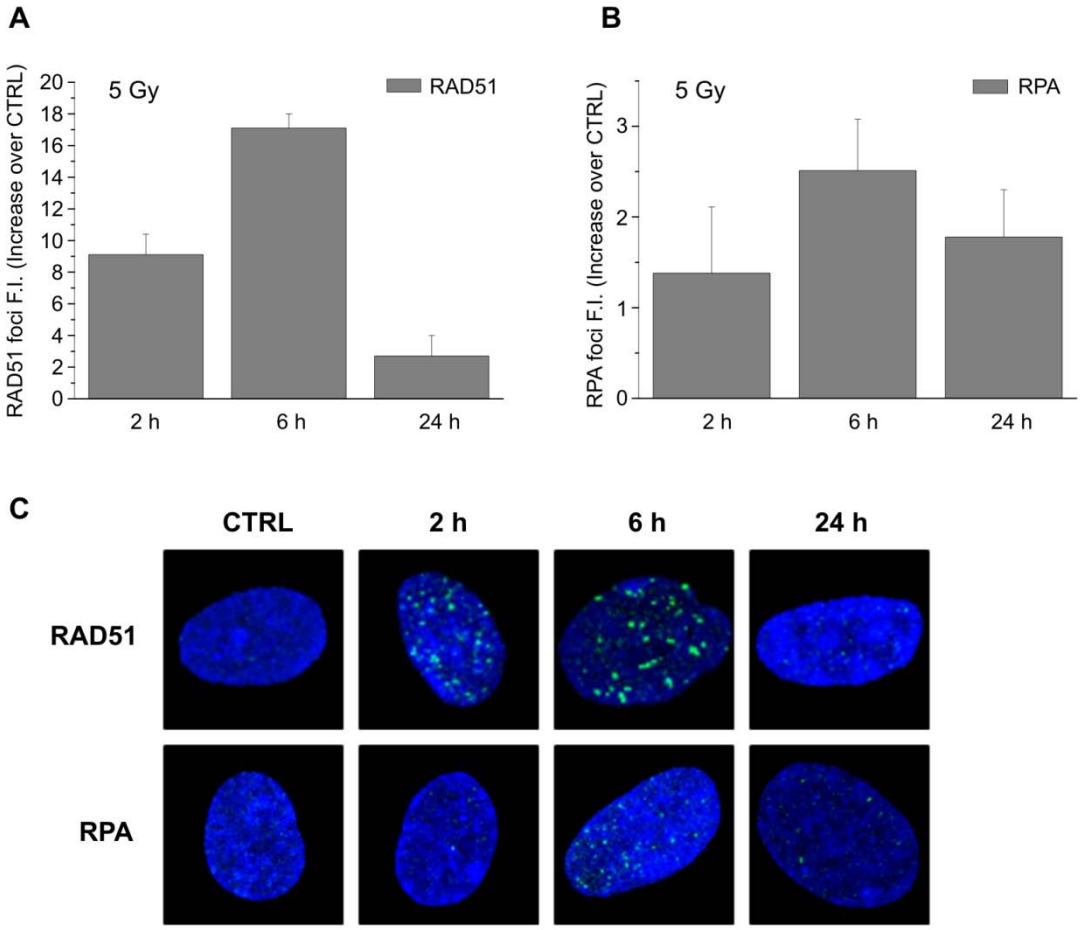

Figure 5. Analysis of RAD51 and RPA recruitment in CCD-34Lu cells irradiated with γ-rays. Fluorescence intensity (FI) of foci was determined at 2, 6 and 24h after irradiation with 5Gy. Values of FI are mean ± S.D. from SOID determinations carried out in at least three independent experiments and plotted as increase over controls.

We then evaluated the contribution of HR and NHEJ in rejoining IR-induced DSBs in G1- and G2-phase cells by quantifying γ-H2AX foci FI in CCD-34Lu treated with NHEJ and HR inhibitors, NU7026 and RI-1, before irradiation with 5Gy. As previously shown, the majority of DSBs (~60%) in untreated CCD-34Lu cells were repaired during the first 6 hours after irradiation both in the G1- and G2- phases (Figure 4), while HR- and NHEJ-inhibited cells showed a delay in DSB resolution in both phases (Figure 6A). In particular, six hours after irradiation the remaining FI in G1-phase cells was significantly higher in the

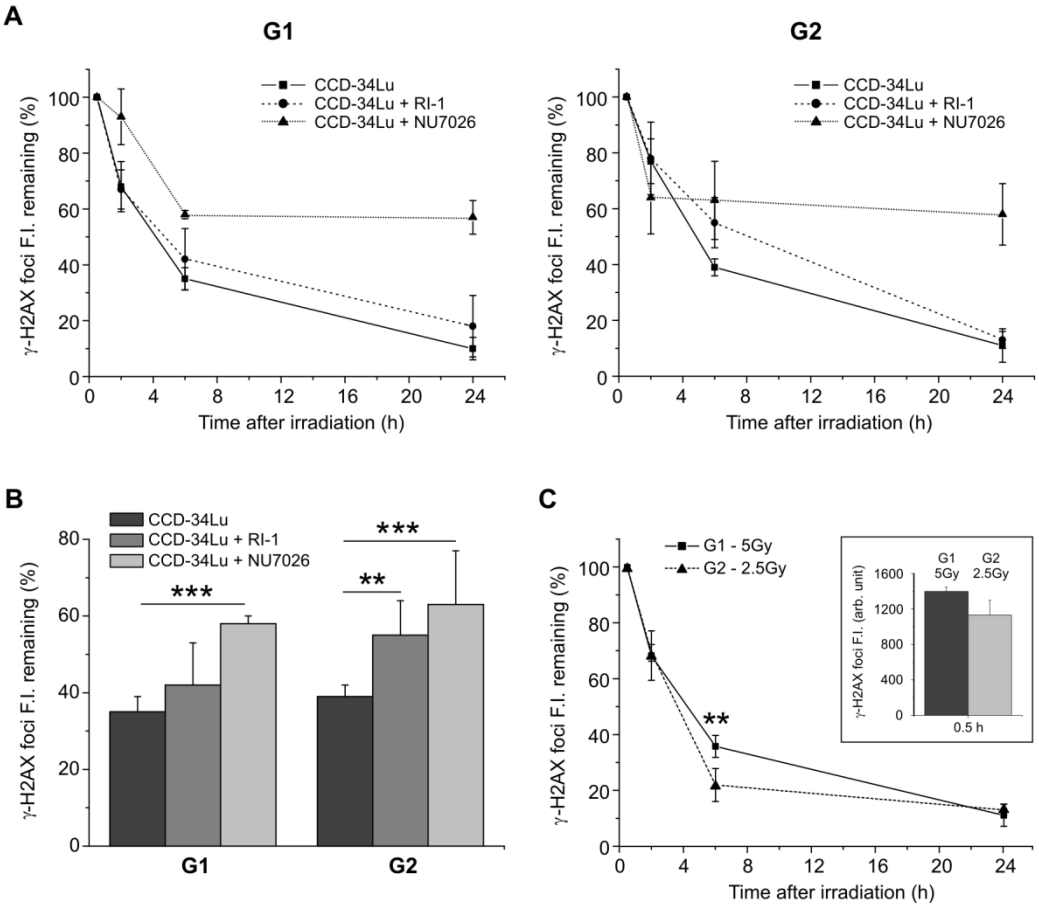

Figure 6. Contribution of HR and NHEJ pathways to DSB repair in G1- and G2-phases. (A) The quantification of γ-H2AX FI induced by 5 Gy was performed by SOID parameter in untreated CCD-34Lu and in NHEJ- and HR-inhibited cells, incubated respectively with the inhibitor of DNA-PKcs, NU7026, and the inhibitor of RAD51, RI-1. (B) In G1 cells the remaining FI at 6h after irradiation with 5 Gy increased in NHEJ-inhibited cells with respect to untreated cells (58% vs. 35%, ****P*<0.001, *t*-test). In G2 cells both inhibitors significantly increased the remaining FI at 6h after irradiation with respect to untreated cells (in NU7026-treèated cells FI was 63% vs. 39% in untreated cells and 55% in RI-1 treated cells, ***P*<0.01, *t*-test). (C) Disappearance of γ-H2AX foci FI in G1- and G2-phase of cells with similar initial SOID values obtained by irradiating the cells respectively with 5 and 2.5 Gy. The values of FI at 0.5h after irradiation were 1132 ± 166 in G2 cells irradiated with 2.5 Gy and 1450 ± 45 in G1 cells irradiated with 5Gy (see the box on the right). At 6h after irradiation the remaining γ-H2AX foci FI was significantly higher in G2 cells (***P*<0.01, *t*-test).

NU7026-treated cells compared to the untreated ones (P<0.001, Figure 6B). After treatment with RI-1 inhibitor, instead, the percentage of remaining γ-H2AX FI was similar to that in the untreated cells. Both inhibitors significantly affected the repair of DSBs in G2-phase cells by increasing the fraction of remaining γ-H2AX FI (P<0.01, Figure 6B). Since DSB repair kinetics have been analyzed in cells that probably have different amounts of initial DNA damage, we analyzed DSB rejoining of γ-H2AX foci in G1 cells irradiated with 5 Gy and in G2 cells irradiated with 2.5 Gy. The initial values of SOID parameter for γ-H2AX foci in G1 and G2-phase cells were very similar in these experimental conditions: 1450 ± 45 for G1 cells and 1132 ± 166 for G2 cells. The results outlined in Figure 6C confirmed that the decrease of γ-H2AX foci FI was slightly but significantly higher in the G2 cells compared to the G1 cells (P<0.01).

DSB rejoining in DNA-PKcs-deficient cells

After we verified that the chemical inhibition of DNA-PKcs in CCD-34Lu cells affected the rejoining of DSBs in the G1 and G2 cell cycle phases, we analyzed the DNA repair kinetics in the DNA-PKcs-deficient M059J cells, and, for comparison, in the isogenic DNA-PKcs proficient M059K cell line. As reported in the literature [31] and detected in our experiments (not shown), both cell lines are G1/ S checkpoint deficient. By contrast, and differently from M059K cells, M059J retained the G2/M checkpoint, as shown by the significant increase in G2-phase cells 24 hours after irradiation with 5 Gy (Figure S5). Figure 7 shows that M059K cells rejoined almost completely the DSBs induced by 0.5 and 5 Gy during the 24h of post-irradiation incubation, as was similarly observed in CCD-34Lu (Figure 6A). In M059J cells, both in G1- and G2-phases, almost 60% of γ-H2AX foci fluorescence persisted 24 hours after irradiation with 0.5 Gy, but there was no fluorescence decrease after irradiation with 5Gy.

We analyzed the kinetics of RAD51 foci in CCD-34Lu cells incubated with the DNA-PKcs inhibitor and in M059J cells to verify if the impairment of NHEJ can alter the recruitment of HR proteins at DSB sites (Figure 8). In cells proficient for DNA-PKcs (i.e. untreated CCD-34Lu cells and M059K cells) the fluorescence intensity of RAD51 foci after irradiation with 5 Gy peaked at 6h and

then fell at 24h in both the G1 and G2 cells. On the contrary, in NU7026-treated CCD-34Lu and in M059J cells the formation of RAD51 foci in the G2-phase was strongly affected by the absence of DNA-PKcs activity, with an initial delay in the RAD51 recruitment, followed by a progressive increase in foci FI up to 24h. The kinetics of RAD51 foci was similar in NU7026-treated and untreated CCD-34Lu cells in G1-phase, while it was very different in M059J and M059K cells, which was true also in the G2-phase (Figure 8A).

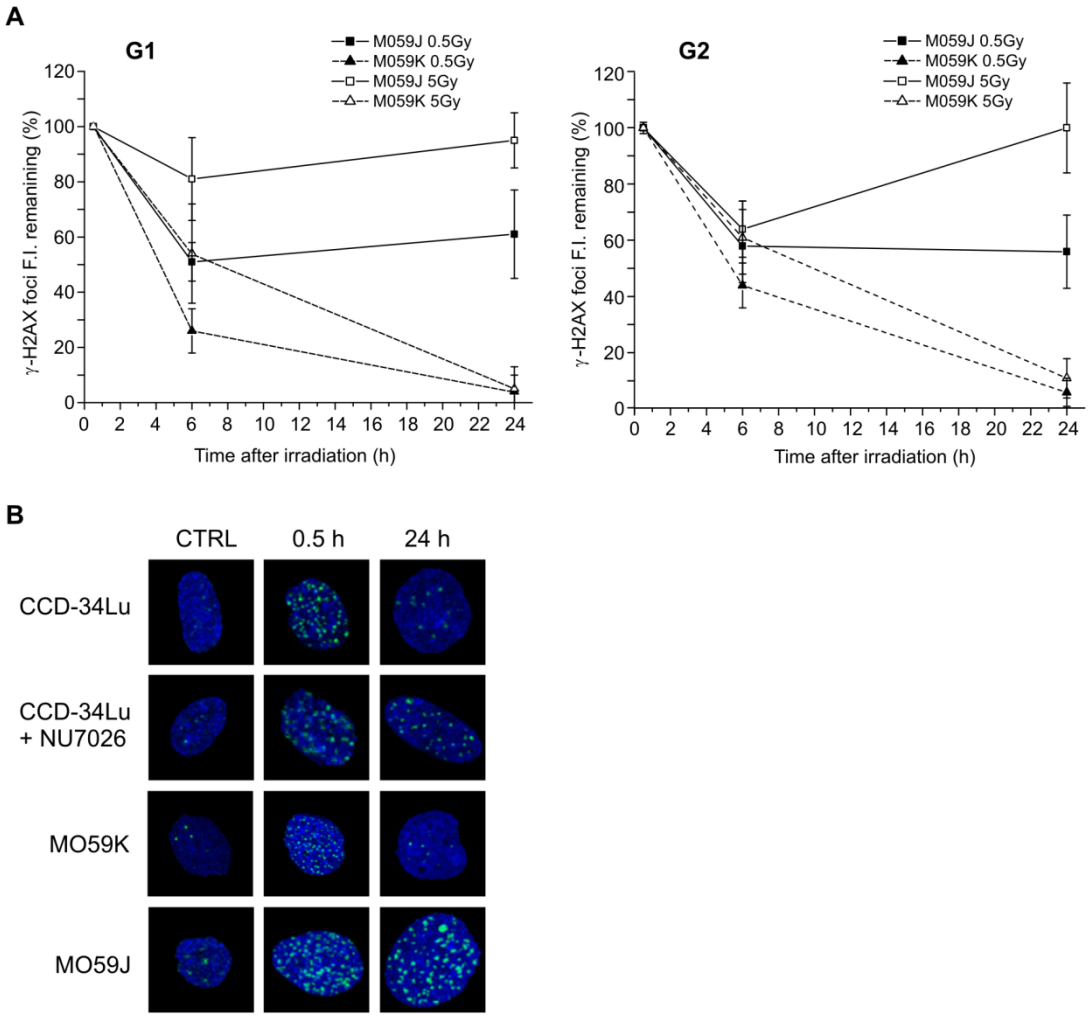

Figure 7. DSB repair in cells with DNA-PKcs inhibited or absent. (A) Fluorescence intensity (FI) of the remaining γ-H2AX foci was measured in G1- and G2-phase of M059K and M059J cells irradiated with 0.5 and 5 Gy of γ-rays. (B) Representative pictures of γ-H2AX foci in CCD-34Lu cells, with and without inhibitor, and in M059K and M059J cells at 0.5h and 24h after irradiation with 0.5Gy.

We also evaluated if the radiation dose alters regulation of the choice between NHEJ and HR repair systems during cell cycle progression. FI of RAD51 foci was quantified two hours after CCD-34Lu cells were irradiated with increasing doses of γ-rays. We chose to quantify the foci at that time point because, as described by other investigators and indicated by our previous observations (our unpublished results and 22, 32, 33), a peak in RAD51 foci induction was noted between one to 4 hours following irradiation.

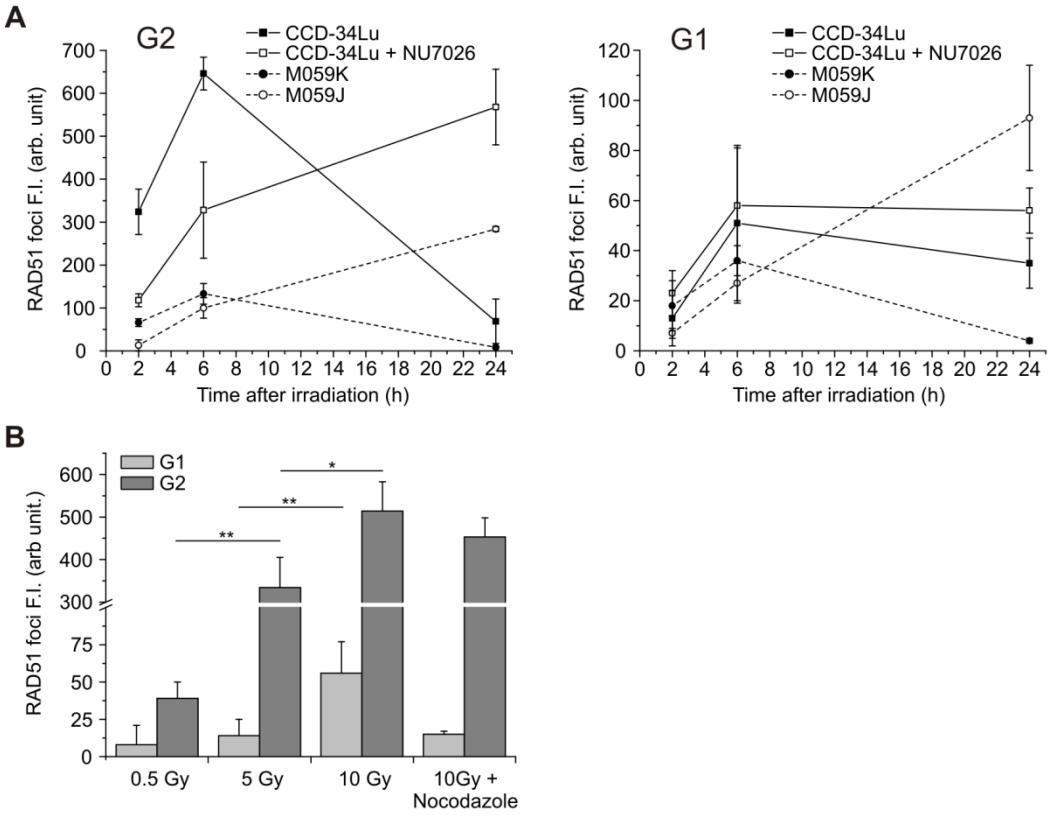

Figure 8. Kinetics of RAD51 foci in G1- and G2-phase. (A) RAD51 foci fluorescence intensity (FI) in CCD-34Lu, CCD-34Lu + NU7026, M059K and M059J cells irradiated with 5 Gy of γ-rays cells. (B) RAD51 foci FI in CCD-34Lu cells at 2 h after irradiation with 0.5, 5 and 10 Gy; in G2 cells RAD51 recruitment significantly increases with dose (**P*<0.05, ***P*<0.01), in G1 cells at 10 Gy RAD51 recruitment significantly increases respect to 5 Gy (***P*<0.01, *t*-test). In cells treated with nocodazole before irradiation with 10 Gy no G1 cells with RAD51 foci were detected.

As expected, the recruitment of RAD51 at the sites of DSBs significantly increased with the γ-ray dose in the G2 cells as well as after irradiation with 10 Gy, also in G1 cells (Figure 8B). The quantification of RPA foci FI was in agreement with that of RAD51 in G2 cells, while there was a negative or very scanty recruitment of RPA in G1 cells irradiated with 5-10 Gy (data not shown). To check the origin of RAD51 loaded at the DBS sites of G1 cells irradiated with 10 Gy, we blocked cell-cycle progression from G2/M to G1-phase using nocodazole, the inhibitor of the mitotic spindle. Under these experimental conditions, no G1 cells with RAD51 foci were detected, indicating that the foci previously observed were probably due to the persistence of unrepaired DSBs formed in the G2-phase of cells that 2h later passed to G1-phase.

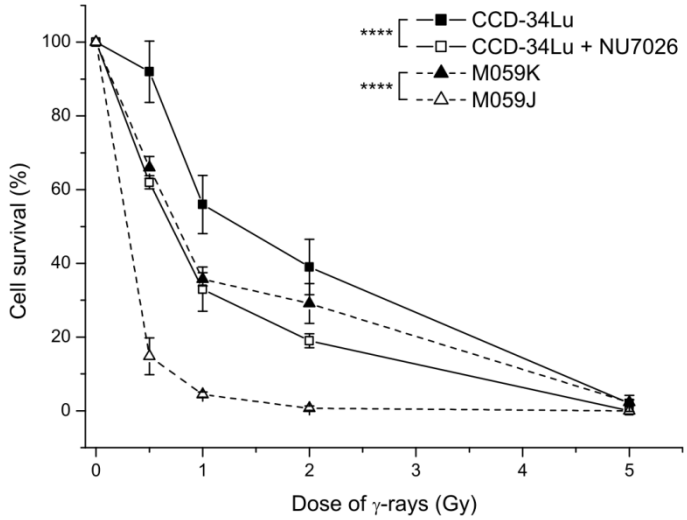

Figure 9. Cell survival after irradiation with increasing doses of γ-rays. Cells impaired for NHEJ repair pathway showed a significant lower survival at 0.5, 1 and 2 Gy respect to their proper control cells (CCD-34Lu+NU7026 vs. CCD-34Lu cells and M059J vs. M059K cells, ****$P<$ 0.0001, two-way ANOVA). Data are means ± S.D. of 3-5 independent experiments.

The decrease in DNA repair efficiency in DNA-PKcs-inhibited CCD-43Lu and in DNA-PKcs-deficient M059J cells markedly affected cell viability after irradiation with increasing IR doses (Figure 9). Cell survival of NU7026-treated CCD-34Lu

was significantly lower than that of the untreated cells for all the doses ($P<0.0001$). Similar results were observed in the M059J with respect to the DNA-PK proficient M059K cells ($P<0.0001$). At the lowest dose of γ-rays (0.5 Gy), the viability of untreated CCD-34Lu was slightly affected, while it was significantly lower than that in non-irradiated cells when incubated with the NU7026 inhibitor (62% vs. 92%). The same γ-ray dose reduced the survival of M059K to 65% and that of M059J to 15% with respect to the non-irradiated cells.

Discussion

Increasing doses of γ-rays were utilized to investigate if DNA damage of different structural complexities affects DSB signaling and repair. The questions of whether and to what extent HR or NHEJ are involved in repairing radio-induced DSBs were also addressed. The shift from NHEJ toward HR as the cell cycle progresses from G1 to S/G2 is regulated by CDK activity. It has been seen that during homologous recombination repair process CDK-mediated phosphorylation at ser3291 of BRCA2 blocks its interaction with the RAD51 protein required for homology searching and strand invasion. HR is, thus, blocked when ssDNA resection is prevented by CDK1 inhibition and early during G1-phase when CDK1 is inactive. Some investigators have reported that in cells exposed to IR cell cycle checkpoint control can be bypassed, leading to a rapid decrease in ser3291 phosphorylation and an increased association of BRCA2 with RAD51 to promote DSB repair by HR [18, 34, 35].

In agreement with previous data demonstrating that the time course of 53BP1 foci formation and disappearance is similar to that of γ-H2AX foci, our results in human fibroblasts irradiated with 0.5 Gy of γ-rays indicate that the kinetics of γ-H2AX and 53BP1 foci is very similar (Figure 1) [10-14]. To verify whether DSB repair efficiency was dose-related, the kinetics of γ-H2AX cellular content after irradiation with increasing doses of γ-rays was assessed using different methods : manual counting of nuclear foci, fluorescence intensity of foci measured by the SOID parameter and flow cytometry. In agreement with Ishikawa et al.'s findings, our results indicated that the SOID parameter is an accurate method to quantify even slight variations of γ-H2AX fluorescence [26]. By contrast, γ-H2AX kinetics after 5 Gy irradiation could not be evaluated by manual foci counting since the number of foci induced by that dose was too high for a reliable determination; nor does the method take into account the increase in foci size detected at later times after irradiation. When the kinetics of DSB rejoining was analyzed by means of the SOID parameter, it was possible to quantify not only the number of the remaining foci but also the total fluorescence of DDR proteins still associated to DSBs. In particular, the size increase of γ-

H2AX foci over time markedly influences the SOID parameter value, highlighting the persistence of some DSBs difficult to repair during the post-irradiation incubation.

By comparing the efficiency in rejoining radiation-induced DSBs during cell cycle progression, we found that in G2-phase cells, whose frequency significantly increased after irradiation (Figure 2A), DNA repair proceeded very efficiently, both during the first period of repair-incubation (0.5-6h) and at later times (6-24h, Figure 4). Previous studies reported that the kinetics of IR-induced DSB repair in the G1-phase exhibit fast as well as slow components [36, 37]. The former removes the majority of DSBs within the first 2 h, while the latter represents a sub-pathway of the NHEJ pathway [38, 39]. Just as in G1, DSB-repair kinetics are biphasic in G2-phase with the fast component representing NHEJ and accounting for the majority of DSB-repair events, while the slow component represents HR and accounts for 15-20% of DSB-repair events [22]. We analyzed the kinetics of γ-H2AX foci in the G1- and G2-phases of HR-inhibited cells to evaluate the contribution of HR in rejoining DNA DSBs during cell cycle progression. According to our results, G2-phase cells treated with the HR inhibitor (RI-1) exhibited a higher level of unrepaired DSBs 6 hours after irradiation (Figure 6). By comparing the repair rate in G1 and G2 phase cells having a similar amount of initial DNA damage, we were able to confirm that the HR repair system contributed to rejoining DSBs also during the first hours following irradiation (Figure 6C), differently from what reported by Beucher et al. [22]. The differences between our and Beucher's findings could be explained by the two different methods adopted to measure the decreased level of γ-H2AX: counting the number of foci used by Beucher [22] and the SOID parameter used during our experiments. The hypothesis that HR is involved in the first hours after IR is, moreover, supported by recent observations by Gandhi et al., [40] who demonstrated that within 5 min of irradiation, homologous chromosomes make contact at the sites of DSBs induced by ionizing radiation in human G0-G1 cells.

Proteins that mediate the recruitment of HR and NHEJ are generally distinct, but in some cases they are implicated in both pathways. Among those proteins, DNA-PK primarily regulates DSB repair by NHEJ, but it can also

influence HR. Several studies have reported that when DNA-PKcs is absent and NHEJ is compromised, HR repair is enhanced [41]. Other authors have, instead, reported that HR involvement is reduced during DNA repair of cells in which DNA-PKcs is physically present but functionally compromised [42]. It would seem then that functionally compromised DNA-PKcs has more severe consequences than the enzyme's complete absence, probably blocking its auto-phosphorylation that allows the NHEJ pathway to proceed [37]. Experiments on CCD34-Lu cell line in which DNA-PKcs was impaired through chemical inhibition (NU7026) and DNA-PK deficient M059J cells as a consequence of a nonsense frame-shift mutation [43] were carried out to evaluate contribution of HR in DSB repair. The presence of DNA-PKcs inhibitor significantly decreased the efficiency of DSB rejoining in irradiated CCD-34Lu cells, both in G1- and G2-phase, as well as in M059J cells (Figures 6 and 7). Moreover, when NHEJ was compromised, the recruitment of RAD51 at DSB sites in both NU7026-treated CCD-34Lu and M059J cells was low early after irradiation and continued up to 24h in both G1 and G2 cells (Figure 8). In M059J cells, DSBs present in the G2-phase were partially caused by lesions induced in this phase of the cell cycle as well as by unrepaired lesions that occurred in the G1-phase and accumulated 24h later in the G2-phase due to the lack of a G1/S checkpoint. However, despite the extensive recruitment of RAD51 at DSB sites 24h after irradiation, the HR pathway, which should be fully functional in those cells, is unable to compensate for the impairment of NHEJ, as evidenced by the persistence of γ-H2AX phosphorylation and the low level of cell survival, even after irradiation with low doses of ionizing radiation.

As we analyzed if radiation dosage alters the choice between the NHEJ and the HR repair systems during cell cycle progression, we observed that RAD51 was recruited at DSB sites even in G1 cells irradiated with the highest dose. Although in accordance with data outlined by Kim et al. [33] and by Rapp and Greulich [44] showing the presence of RAD51 foci in the G1-phase of irradiated cells, these observations can be more accurately interpreted by blocking the transition of cells from the G2/M- to the G1-phase. Indeed, cells irradiated with high doses of IR in the G2-phase could be able to progress to the G1-phase with

unrepaired DSBs. By blocking the progression of G2 cells with unrepaired DSBs, we demonstrated that the presence of G1 cells positive for RAD51 foci can be explained by the advancement of cells with RAD51 foci formed in the S-G2 phases.

Our data generally agree with the model that NHEJ is the major pathway for IR-induced DSBs repair. They also demonstrate that RAD51, the main protein in the HR pathway, participates, together with NHEJ, in DSB rejoining even during the first hours after irradiation. RAD51 recruitment and activity at DSB sites appears, however, to be strictly dependent on the integrity of NHEJ components, highlighting the dominant role that DNA-PKcs play in regulating the cell response to DNA damage throughout cell cycle progression.

Acknowledgements

We gratefully acknowledge Vito Barbieri for cell irradiation with γ-rays, and Prof. S.C. West (Cancer Research, UK London Research Institute, Clare Hall Laboratories, South Mimms) for providing M059K cells. We would also like to thank Chiara Romualdi for statistical analysis and helpful discussion, Giovanna Pontarin for assistance with R2 immunostaining, Antonella Russo for providing experimental protocols for nocodazole treatment, Cristina Girardi for foci counting, and Renzo Mazzaro for help with graphics.

Author Contributions

Conceived and designed the experiments: LC LB MM SF. Performed the experiments: LB SF MM. Analyzed the data: LC LB MM RC. Wrote the paper: LC MM LB SF.

References

1. Ohnishi T, Mori E, Takahashi A (2009) DNA double-strand breaks: Their production, recognition, and repair in eukaryotes. Mutat Res 66: 8-12.

2. Vilenchik MM, Knudson AG (2003) Endogenous DNA double-strand breaks: production, fidelity of repair, and induction of cancer. Proc Natl Acad Sci USA 100: 12871-876.

3. Ward JF (2000) Complexity of damage produced by ionizing radiation. Cold Spring Harb Symp Quant Biol 65: 377-382.

4. Eccles LJ, O'Neill P, Lomax ME (2011) Delayed repair of radiation induced clustered DNA damage: friend or foe? Mutat Res 711: 134-141.

5. Nikjoo H, O'Neill P, Wilson WE, Goodhead DT (2001) Computational approach for determining the spectrum of DNA damage induced by ionizing radiation. Radiat Res 156: 577-583.

6. Bassing CH, Alt WF (2004) The cellular response to general and programmed DNA double strand breaks. DNA Repair (Amst) 3: 781-796.

7. Fernandez-Capetillo O, Lee A, Nussenzweig M, Nussenzweig A (2004) H2AX: the histone guardian of the genome. DNA Repair (Amst) 3: 959-967.

8. Svetlova MP, Solovjeva LV, Tomilin NV (2010) Mechanism of elimination of phosphorylated histone H2AX from chromatin after repair of DNA double-strand breaks. Mutat Res 685: 54-60.

9. Sharma A, Singh K, Almasan A (2012) Histone H2AX Phosphorylation: A Marker for DNA Damage. Methods in Molecular Biology 920:613-626.

10. Ward IM, Minn K, Jorda KG, Chen J (2003) Accumulation of checkpoint protein 53BP1 at DNA breaks involves its binding to phosphorylated histone H2AX. J Biol

Chem 278: 19579-582.

11. Schultz LB, Chehab NH, Malikzay A, Halazonetis TD (2000) p53 binding protein 1 (53BP1) is an early participant in the cellular response to DNA double-strand breaks. J Cell Biol 151: 1381-390.

12. Rappold I, Iwabuchi K, Date T, Chen J (2001) Tumor suppressor p53 binding protein 1 (53BP1) is involved in DNA damage-signaling pathways. J Cell Biol 153: 613-620.

13. Anderson L, Henderson C, Adachi Y (2001) Phosphorylation and rapid relocalization of 53BP1 to nuclear foci upon DNA damage. Mol Cell Biol 21: 1719-729.

14. Asaithamby A, Chen DJ (2009) Cellular responses to DNA double-strand breaks after low-dose gamma-irradiation. Nucleic Acids Res 37: 3912-923.

15. Wold MS (1997). "Replication protein A: heterotrimeric, single-stranded DNA-binding protein required for eukaryotic DNA metabolism". Annual Review of Biochemistry 66 (1): 61–92.

16. Lisby M, Rothstein R (2009) Choreography of recombination proteins during the DNA damage response. DNA Repair 8: 1068-076.

17. Shrivastav M, De Haro LP, Nickoloff JA (2005) Regulation of DNA double-strand break repair pathway choice. Cell Res 18: 134-147.

18. Shrivastav M, Miller CA, De Haro LP, Durant ST, Chen BPC, et al. (2009) DNA-PKcs and ATM co-regulate DNA double-strand break repair. DNA Repair 8: 920-929.

19. Tracker J (2005) The RAD51 gene family, genetic instability and cancer. Cancer Lett 219: 125-135.

20. Sedelnikova OA, Rogakou EP, Panyutin IG, Bonner WM (2002) Quantitative detection of (125)IdU-induced DNA double-strand breaks with gamma-H2AX antibody. Radiat Res 4: 486-492.

21. Asaithamby A, Uematsu N, Chatterjee A, Story MD, Burma S, et al. (2008) Repair of HZE-particle-induced DNA double-strand breaks in normal human fibroblasts. Radiat Res 169: 437-446.

22. Beucher A, Birraux J, Tchouandong L, Barton O, Shibata A, et al. (2009) ATM and Artemis promote homologous recombination of radiation-induced DNA double-strand breaks in G2. EMBO J 28: 3413-427.

23. Liao H, Winkfein RJ, Mack G, Rattner JB, Yen TJ (1995) CENP-F is a protein of the nuclear matrix that assembles onto kinetochores at late G2 and is rapidly degraded after mitosis. J Cell Biol 130: 507-18.

24. Varis A, Salmela AL, Kallio MJ (2006) Cenp-F (mitosin) is more than a mitotic marker. Chromosoma 115**:** 288-295.

25. Mistrik M, Oplustilova L, Lukas J, Bartek J (2009) Low-dose DNA damage and replication stress responses quantified by optimized automated single-cell image analysis. Cell Cycle 8: 2592-599.

26. Ishikawa A, Yamauchi M, Suzuki K, Yamashita S (2010) Image-based quantitative determination of DNA damage signal reveals a threshold for G2 checkpoint activation in response to ionizing radiation. Genome Integr 1:10.

27. Salic A, Mitchison TJ (2008) A chemical method for fast and sensitive detection of DNA synthesis in vivo. Proc Natl Acad Sci USA 105: 2415-420.

28. Buck SB, Bradford J, Gee KR, Agnew BJ, Salic A (2008) Detection of S-phase cell cycle progression using 5-ethynyl-2'-deoxyuridine incorporation with click chemistry, an alternative to using 5-bromo-2'-deoxyuridine antibodies. Biotechniques 44: 927-929.

29. Pontarin G, Fijolek A, Pizzo P, Ferraro P, Rampazzo C, et al. (2008) Ribonucleotide reduction is a cytosolic process in mammalian cells independently of DNA damage. Proc Natl Acad Sci USA. 105: 17801–17806.

30. Canova S, Fiorasi F, Mognato M, Grifalconi M, Reddi E, et al. (2005) “Modeled microgravity" affects cell response to ionizing radiation and increases genomic damage. Radiat Res 163: 191-199.

31. Holgersson A, Heiden T, Castro J, Edgren MR, Lewensohn R, et al. (2005) Different G2/M accumulation in M059J and M059K cells after exposure to DNA double-strand break-inducing agents. Int J Radiat Oncol Biol Phys. 61(3):915-21.

32. Short SC, Giampieri S, Worku M, Alcaide-German M, Sioftanos G, et al. (2011) Rad51 inhibition is an effective means of targeting DNA repair in glioma models and CD133+ tumor-derived cells. Neuro Oncol 13: 487-99.

33. Kim JS, Krasieva TB, Kurumizaka H, Chen DJ, Taylor AM, et al. (2005) Independent and sequential recruitment of NHEJ and HR factors to DNA damage sites in mammalian cells. J Cell Biol 170(3):341-7.

34. Mao Z, Bozzella M, Seluanov A, Gorbunova V (2008) Comparison of non-homologous end joining and homologous recombination in human cells. DNA Repair 7: 1765-771.

35. Mukherjee B, Camacho CV, Tomimatsu N, Miller J, Burma S (2008) Modulation of the DNA-damage response to HZE particles by shielding. DNA Repair 7: 1717-730.

36. Löbrich M, Jeggo PA (2005) Harmonising the response to DSBs: a new string in the ATM

bow. DNA Rep (Amst) 4: 749–759.

37. Wu W, Wang M, Wu W, Singh SK, Mussfeldt T, et al. (2008) Repair of

radiation induced DNA double strand breaks by backup NHEJ is enhanced in G2. DNA Repair (Amst) 7: 329-338.

38. Rothkamm K, Krüger I, Thompson LH, Löbrich M (2003) Pathways of DNA double-strand
break repair during the mammalian cell cycle. Mol Cell Biol 23: 5706–5715.

39. Kühne M, Riballo E, Rief N, Rothkamm K, Jeggo PA, et al. (2004) A double-strand
break repair defect in ATM-deficient cells contributes to radiosensitivity. Cancer Res 64:
500–508.

40. Gandhi M, Evdokimova VN, Cuenco KT, Bakkenist CJ, Nikiforov YE (2013) Homologous chromosomes move and rapidly initiate contact at the sites of double-strand breaks in genes in G_0-phase human cells. Cell Cycle 12(4):547-52.

41. Allen C, Halbrook J, Nickoloff JA (2003) Interactive competition between homologous recombination and non-homologous end joining. Mol Cancer Res 1: 913-920.

42. Convery E, Shin EK, Ding Q, Wang W, Douglas P, et al. (2005) Inhibition of homologous recombination by variants of the catalytic subunit of the DNA-dependent protein kinase (DNA-PKcs). Proc Natl Acad Sci USA 102: 1345-350.

43. Anderson CW, Allalunis-Turner MJ (2000) Human TP53 from the malignant glioma-derived cell lines M059J and M059K has a cancer-associated mutation in exon 8. Radiat Res 154: 473-476.

44. Rapp A, Greulich KO (2004) After double-strand break induction by UV-A, homologous recombination and non-homologous end joining cooperate at the same DSB if both systems are available. J Cell Sci. 117: 4935-45.

Supporting information

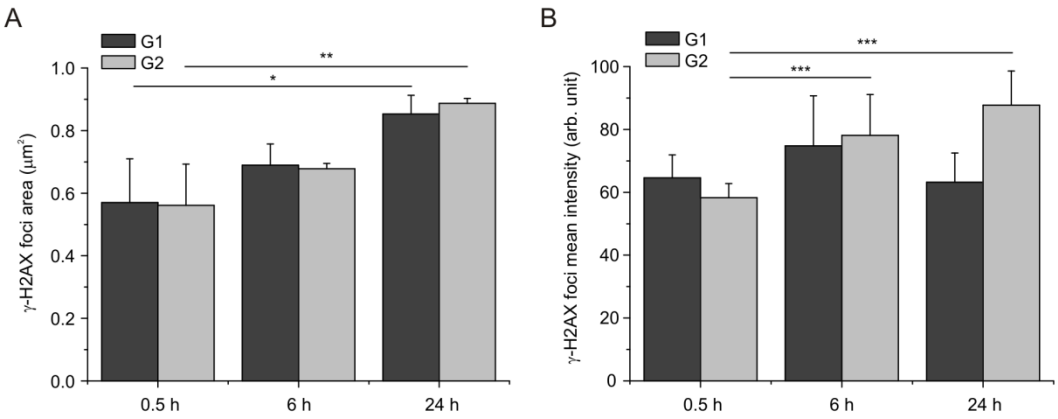

Figure S1. Analysis of γ-H2AX foci physical parameters in G1 and G2 cells after irradiation with 5 Gy of γ-rays. (A) γ-H2AX foci size increased significantly with time after irradiation in both G1 and G2 phases (*P<0.05, **P<0.01, t-test) without differences between the two phases. (B) Signal intensities of γ-H2AX foci were determined by SOID parameter in the same cells. The intensity of foci fluorescence increased with time only in G2 cells (****P*<0.001, *t*-test). The values are mean fluorescence intensity ± S.D. of single γ-H2AX foci determined from at least 30-50 nuclei for each time-point.

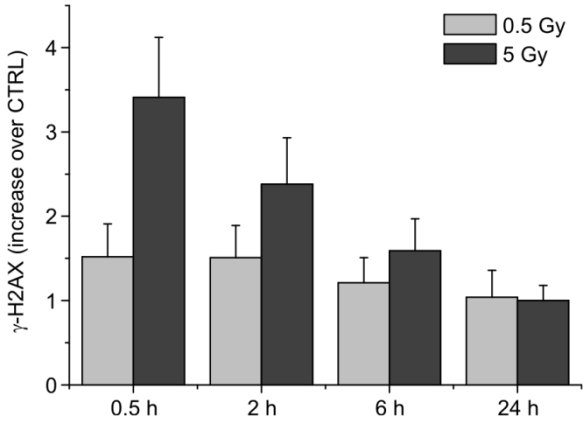

Figure S2. Kinetics of γ-H2AX total fluorescence determined by FACS analysis in cells irradiated with 0.5 and 5 Gy of γ-rays.

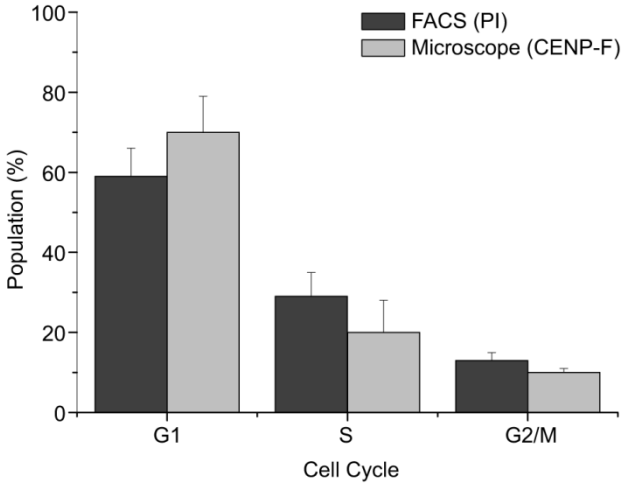

Figure S3. Comparison of data of cell distribution in cell cycle phases obtained from FACS analysis and from confocal microscopy of CENP-F F.I. in the same cell population.

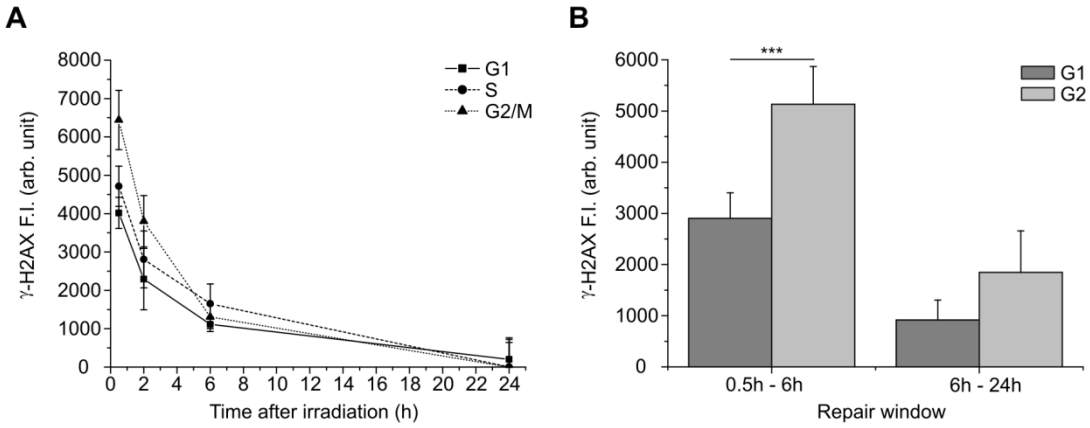

Figure S4. γ-H2AX total fluorescence determined by FACS analysis. Kinetics of γ-H2AX in G1, S and G2 cells irradiated with 5 Gy of γ-rays. (B) In the time-interval 0.5-6h, the γ-H2AX FI disappearance was significantly higher in G2 vs. G1 cells (P<0.001, G2 vs. G1).

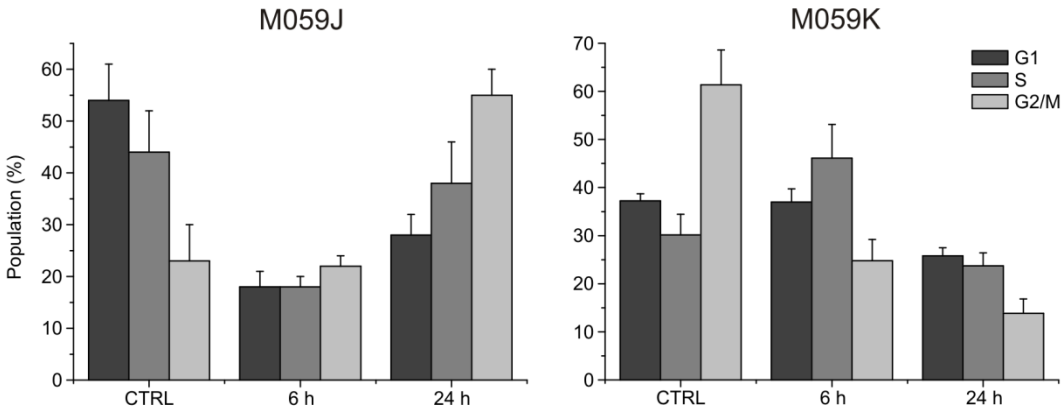

Figure S5. Cell cycle distribution in M059J and M059K cells after irradiation with 5Gy of γ-rays. In both cell lines γ-irradiation did not induce the G1/S checkpoint, whereas only in M059J cells the G2/M checkpoint was activated. Data are mean ± S.D. from three independent experiments.

PAPER II

Proc Natl Acad Sci USA
2012 Aug 14
109(33):13302-7

Giovanna Pontarin*, Paola Ferraro*, Leonardo Bee, Peter Reichard, and Vera Bianchi

Dipartimento di Biologia, Università di Padova, Padova, Italy.

*Equally contributing authors.

Author contributions: G.P., P.F., L.B., P.R., and V.B. designed research; G.P., P.F., and L.B. (Figure 7 and Figure S3) performed research; G.P., P.F., L.B. (Figure 7 and Figure S3), P.R., and V.B. analyzed data; and G.P., P.F., P.R., and V.B. wrote the paper.

[MAMMALIAN RIBONUCLEOTIDE REDUCTASE SUBUNIT P53R2 IS REQUIRED FOR MITOCHONDRIAL DNA REPLICATION AND DNA REPAIR IN QUIESCENT CELLS]

Abstract

In postmitotic mammalian cells, protein p53R2 substitutes for protein R2 as a subunit of ribonucleotide reductase. In human patients with mutations in RRM2B, the gene for p53R2, mitochondrial (mt) DNA synthesis is defective, and skeletal muscle presents severe mtDNA depletion. Skin fibroblasts isolated from a patient with a lethal homozygous missense mutation of p53R2 grow normally in culture with an unchanged complement of mtDNA. During active growth, the four dNTP pools do not differ in size from normal controls, whereas during quiescence, the dCTP and dGTP pools decrease to 50% of the control. We investigate the ability of these mutated fibroblasts to synthesize mtDNA and repair DNA after exposure to UV irradiation. Ethidium bromide depleted both mutant and normal cells of mtDNA. On withdrawal of the drug, mtDNA recovered equally well in cycling mutant and control cells, whereas during quiescence, the mutant fibroblasts remained deficient. Addition of deoxynucleosides to the medium increased intracellular dNTP pools and normalized mtDNA synthesis. Quiescent mutant fibroblasts were also deficient in the repair of UV-induced DNA damage, as indicated by delayed recovery of dsDNA analyzed by fluorometric analysis of DNA unwinding and the more extensive and prolonged phosphorylation of histone H2AX after irradiation. Supplementation by deoxynucleosides improved DNA repair. Our results show that in nontransformed cells only during quiescence, protein p53R2 is required for maintenance of mtDNA and for optimal DNA repair after UV damage.

Introduction

DNA replication and repair require the continued synthesis of the four dNTPs. They are synthesized by evolutionary-related ribonucleotide reductases operating with slightly different mechanisms in aerobic and anaerobic organisms (1). Each ribonucleotide reductase provides the required amounts of all four dNTPs. A similar allosteric mechanism, maintained throughout evolution, regulates both the enzyme's activity and its substrate specificity. Cells contain small dNTP pools of similar sizes, approximately 10-fold larger during DNA replication than during quiescence. Regulation of pool sizes by ribonucleotide reductases is of great importance for correct DNA replication, and changes in the actual sizes or in their balance lead to increased mutation rates (2). For mammalian cells, the induction of mutations by pool imbalances has been described in detail, along with possible mechanisms (3). In yeast, a recent elegant study (4) linked specific amino acid substitutions in the catalytic subunit of ribonucleotide reductase to defined pool imbalances, which result in increased mutation rates.

In mammalian cells, the canonical ribonucleotide reductase is a complex between two proteins: the large catalytic protein R1 that contains the allosteric sites and the smaller protein R2 that contributes a stable tyrosyl free radical during the reaction (1). Both proteins are transcriptionally activated during early S-phase (5) and are present in roughly equal amounts (6, 7) to deliver the dNTPs required for DNA replication. R2 is degraded during late mitosis (8); thus, postmitotic quiescent cells are essentially devoid of R2 but retain some R1. In the year 2000, a second radical-providing small subunit, termed p53R2, was discovered in mammalian cells (9). p53R2 has the same function as the homologous R2, but is not degraded in mitosis. Quiescent cells contain an undiminished amount of p53R2 (6, 7) but little or no R2. After DNA damage, p53R2 is transcriptionally activated by p53 and was reported to translocate into the nucleus (9). It was therefore thought to be primarily involved in DNA repair. However, with affinity-purified antibodies, we found p53R2, as well as R1 and R2, in the cytosol also after DNA damage (10). Moreover the concentrations of the three proteins at

different stages of the cell cycle speak against a specific requirement of p53R2 for DNA repair. During S-phase, murine or human fibroblasts contain roughly equimolar amounts of R1 and R2, whereas p53R2 amounts to only 3% of R2 and increases to 13% after DNA damage (6), indicating that the main catalytically active enzyme is an R1/R2 and not an R1/p53R2 complex. In a study of quiescent human fibroblasts, ribonucleotide reduction was catalyzed largely by an R1/p53R2 complex at a rate amounting to only 2–3% of that of cycling cells (7).

In 2007, Bourdon et al. (11) opened a new chapter in the history of p53R2 by reporting that in humans, genetic inactivation of p53R2 causes a severe mitochondrial disease characterized by profound depletion of mtDNA in differentiated cells and lethality shortly after birth. They found that skeletal muscle of patients with mutations in the RRM2B gene coding for p53R2 completely lacked mtDNA (11). Similar patients were described in later studies from several other laboratories (12–16). It is now clear that p53R2 activity is required for the stability of the mt genome in differentiated tissues, shifting the attention from DNA repair to mtDNA maintenance.

Less clear are the extent to which p53R2 is required for DNA repair and the extent to which it is required only in quiescent cells. Most experiments concerning p53R2's function have been carried out with transformed cell lines (9, 17–19), which are not suitable for addressing these questions. To investigate p53R2 in nontransformed cells, we recently examined in vitro the consequences of p53R2 inactivation with fibroblasts from a patient with a lethal homozygous missense mutation in the iron-binding center of p53R2 who had died at aged 3 mo with severe muscular mtDNA depletion (16, 20). Compared with age-matched controls, the mutant fibroblasts grew normally in culture and contained a normal complement of mtDNA (20); however, once they became quiescent, their ability to reduce ribonucleotides was strongly curtailed, resulting in smaller dCTP and dGTP pools. The profound changes in deoxyribonucleotide metabolism did not result in a depletion of mtDNA in vitro, unlike in the patient. We hypothesized that this ostensible paradox might be explained by the low copy number of

mtDNA in fibroblasts, only <5% of that in skeletal muscle cells, requiring much less dNTPs for its maintenance.

In the present work, we tested this hypothesis with cycling and quiescent fibroblasts. We induced mtDNA depletion by treating the cells with ethidium bromide (EtBr) (21), and followed the recovery of mtDNA after removal of the drug. In addition, we investigated the involvement of p53R2 in DNA repair by analyzing the ability of the mutated fibroblasts to repair DNA after UV damage. Our data demonstrate the importance of p53R2 for both mtDNA replication and DNA repair in quiescent cells that contain insufficient R2 for dNTP synthesis. The data indicate that correct pool balances are required not only for the fidelity of nuclear DNA replication, but also for optimal mtDNA synthesis and DNA repair after UV damage.

Materials and Methods

Cell culture

The fibroblasts from a patient with an inactivating mutation in the gene for p53R2 (16) were identical to those used in a previous study (20). G. Kollberg and E. Holme (Sahlgrenska University Hospital, Goteborg, Sweden) provided the original frozen cells (second passage) and suitable age-matched normal controls. Before use, both cell lines were immortalized with plasmid CMV-hTERT/PGK-Pura, as described previously (36). The cells for the experiments were seeded at 0.35 × 106 cells/10-cm dish and grown in MEM/10% FCS. Quiescent cultures were obtained by growing cells to confluence (usually for 7 d), changing the medium to MEM/0.1% dialyzed FCS, and keeping the cells in this medium until use in the experiments at different times, usually after 7 d. Cultures received fresh medium every third day. Where indicated, the medium was supplemented with 5 μM deoxynucleosides along with a medium change. To prevent degradation of individual deoxynucleosides, 0.5 μM immucillin (37) was added together with GdR and 10 μM erythro-9-2-hydroxy-3-nonyladenine (38) with AdR.

Materials

MEM and New Zealand FCS were obtained from Invitrogen. Erythro-9-2-hydroxy 3-nonyladenine was a gift from Staffan Eriksson (Swedish University of Agricultural Sciences, Uppsala, Sweden), and Immucillin H was a gift from Vern Schramm(Yeshiva University,NewYork, NY). Ethidium bromide (EtBr), deoxynucleosides, and deoxynucleotides were purchased from Sigma-Aldrich. The following mouse monoclonal antibodies were used: anti-cyclobutane pyrimidine dimers (CPDs) (clone TDM-2; CosmoBio), anti-(6,4) photoproducts (6-4PPs) (clone 64M-2; CosmoBio), and anti–phospho-histone H2AX (Ser139) (clone JBW301; Millipore).

Analytical Procedures

Intracellular concentrations of the four dNTPs were determined by an enzymatic assay (1) modified as described recently (2). The number of mtDNA copies was determined by real-time PCR (3) as described previously (4).

Depletion of mtDNA.

To deplete cells of mtDNA, EtBr (5) was added at a final concentration of either 20 or 50 ng/mL to medium supplemented with 1 mM sodium pyruvate and 50 μg/mL
of uridine. For cycling cells, cells were transplanted every third day in the EtBr-containing medium containing 10% FCS. To obtain quiescent mtDNA-depleted cultures, the cells were incubated in EtBr-containing medium with 10% FCS before they reached confluence, followed by a second 7-d incubation in EtBr medium with 0.1% dialyzed FCS. With both cycling and quiescent cells, treatment was stopped by removing the EtBr medium, washing the monolayer with warm PBS, and adding fresh medium without EtBr.

UV Irradiation of Cells

Cell monolayers were irradiated with a 254-nm UVS-11 mineral light lamp at a fluency rate of 2 J/m^2/sec. Then fresh medium was added, and the cells were returned to culture conditions.

Analysis of Photoproducts After UV Irradiation

Dot blot immunoassays (6) were performed to determine the relative amounts of CPDs and 6-4PPs in total genomic DNA from cells collected at different times after UV irradiation. Genomic DNA was isolated using the Puregene Core Kit B (Qiagen). After equal amounts of DNA were denatured from each sample by boiling for 5 min, the samples were placed on ice, and equal volumes of Tris-EDTA buffer and 20× sodium chloride-sodium phosphate-EDTA buffer were added. Using a dot-blot apparatus (BioRad), each sample was blotted in triplicate (10 ng DNA/dot for CPDs and 100 ng DNA/dot for 6-4PPs) onto

nitrocellulose membranes previously soaked in 6× SSC. DNA was fixed to the membranes by heating for 2 h at 80 °C, after which the membranes were blocked in PBS/ 0.2% Tween 20 containing 5% (wt/vol) blocking agent (GE Healthcare) for 1 h at room temperature. The membranes were then incubated with either the CPD-specific monoclonal antibody TDM-2 (dilution 1:6,000) or the 6-4PP–specific monoclonal antibody 64M-2 (dilution 1:6,000) overnight at 4 °C. After washing with PBS-Tween, the membranes were incubated with anti-mouse HRP-conjugated Ig (dilution 1:20,000) for 1 h at room temperature. After further washing, the signals were developed with the ECL Advanced Chemiluminescence Kit (GE Healthcare) in accordance with the manufacturer's instructions. The relative intensity of each signal was determined using a Kodak 440CF one dimensional imaging station.

Fluorometric Analysis of DNA Unwinding

Fluorometric analysis of DNA unwinding (FADU) (7) was performed using five different buffer solutions: solution B, composed of 0.25 M myoinositol, 1 mMMgCl2, and 10mMNa-phosphate buffer (pH 7.2); solution C, 9 M urea, 10 mM NaOH, 5 mM cyclohexanediaminetetraacetate, 0.1% SDS; solution D, 0.45 vol/vol solution C in 0.2 M NaOH; solution E, 0.40 vol/vol solution C in 0.2MNaOH; and solution F, 1 M glucose and 14 mM dithiotreitol. For FADU analyses, the cells were trypsinized at fixed time points after UV irradiation, counted, and washed twice with cold PBS. At each time point, the cells were suspended in solution B and divided (triplicate samples of 3.5 × 105 cells/0.1 mL of solution B) into each of three sets of tubes: B, blank samples, completely unwound DNA; T, total fluorescence of native DNA, and P, samples for determination of DNA unwinding rate. After addition of 0.1 mL of solution C, all samples were incubated on ice for 10 min. Samples T were neutralized with 0.2 mL of solution F with mixing. Then 0.05 mL of solution D and 0.05 mL of solution E were added very gently and without mixing to each triplicate sample B, P, and T. After a 30- min incubation on ice, samples B were sonicated for 15 min at 50 W in a Fisher 300 sonicator and then incubated for 1 h at room temperature.

Samples P were incubated in parallel for 1 h at 16 °C, and samples T were kept on ice for 1 h. Denaturation was stopped by adding 0.2 mL of solution F and chilling on ice. The percentage of dsDNA was estimated by staining with EtBr (0.5 μg/mL in 13.3 mM NaOH), which selectively binds to dsDNA. Fluorescence was read in a Jasko 821-FP spectrofluorimeter
(excitation, 520 nm; analyzer, 590 nm). The % dsDNA values (D) were calculated from the fluorescence of B, T, and P samples using the equation $D = (P - B)/(T - B)$.

γH2AX Determination by Flow Cytometry.

For flow cytometry analysis (8), cells that had been fixed in 70% ethanol and stored at 4 °C until analysis were washed in PBS, centrifuged, resuspended in 1 mL of cold PBS/4% FCS/0.1% Triton X-100 (T-PBS) and placed on ice for 10 min to rehydrate. They were then centrifuged, resuspended in 0.2 mL of mouse monoclonal anti-γH2AX antibody (1:500 in T-PBS), and incubated for 2 h at room temperature under shaking. After rinsing in T-PBS and centrifugation, cell pellets were resuspended in 0.2 mL of secondary antibody (donkey anti-mouse Alexa Fluor 488, 1:200 in T-PBS) and shaken for 1 h at room temperature. The cells were rinsed in T-PBS and counterstained with 50 μg/mL of propidium iodide in 1 mL of PBS containing RNase A (0.1 mg/mL) for 1 h at 37 °C. Samples of ~25,000 cells were analyzed with a BD dual-laser FACSCantoII flow cytometer. Data were analyzed using BD FACSDiva software.

γH2AX Determination by Immunofluorescence Microscopy.

Cells were grown in 35-mm thin-bottomed Petri dishes for high-end microscopy (Ibidi), fixed with 2% paraformaldehyde/0.3 M sucrose/ 0.5% Triton X for 20 min on ice, and blocked with MAXblock blocking medium (Active-Motif) for 1 h at 37 °C. The fixed cells were incubated with mouse monoclonal anti-γH2AX antibody (1:500) for 1 h at 37 °C. After three 10-min washes with PBS + 0.05% Tween 20, the cells were incubated with donkey antimouse Alexa Fluor 488 (1:500) for 1 h at 37 °C. The cells were counterstained with 20 ng/mL of DAPI for 20 min at room temperature, and after washing with PBS-Tween, the

coverslips were mounted for fluorescence microscopy. The immunostained cells were visualized using a Leica TCS SP5 confocal microscope equipped with a 63× oil immersion objective.

Results

Recovery of mtDNA After Depletion with EtBr.

Cells growing in the presence of EtBr lose their mtDNA (21). In preliminary experiments, p53R2 mutant and control fibroblasts cultured for 7 d in medium containing 10% FCS with either 20 or 50 ng EtBr/mL were rapidly depleted of mtDNA. When growth continued in the absence of EtBr, all cultures rapidly recovered mtDNA (Fig. S1A), with no clear difference between mutant and control cells. We repeated the experiment with quiescent cells. As before, we grew the fibroblasts with EtBr in 10% FCS for 7 d, but when the cultures became confluent we shifted them to 0.1% FCS + EtBr for 7 d longer. The cells reached quiescence, lost protein R2, and became dependent on p53R2. We then removed EtBr and followed the reappearance of mtDNA in low serum. Now only the control cells fully recovered their mtDNA (Fig S1B), suggesting that the cells with mutated p53R2 did not produce sufficient dNTPs for sustained mtDNA synthesis.

Previous studies have shown that quiescent mutant fibroblasts contain smaller dCTP and dGTP pools than controls, whereas dATP is unaffected and dTTP is slightly increased (20). If the inability of the mutant fibroblasts to reconstitute their mtDNA indeed depended on insufficient production of dNTPs, then it might be possible to compensate the deficiency by exploiting the salvage pathway of dNTP synthesis (22). Low micromolar amounts of deoxycytidine (CdR) and deoxyguanosine (GdR) added to the media of quiescent cultures increased the corresponding dNTP pools in both normal and mutant fibroblasts (Table 1). GdR alone diminished the dCTP pool of mutant cells in a concentration-dependent manner with a decrease to 50% after an 18-h incubation with 5 μM GdR (Table S1). The combination of the two deoxynucleosides increased both the dCTP and dGTP pools of mutant cells slightly above the pool sizes of the controls.

	dNTP, pmoles/10^6 cells							
	Control				Mutant			
Treatment	dCTP	dGTP	dTTP	dATP	dCTP	dGTP	dTTP	dATP
None	2.9 ± 0.63	0.5 ± 0.11	2.6 ± 0.89	2.4 ± 0.56	1.2 ± 0.25	0.2 ± 0.05	2.7 ± 0.79	1.4 ± 0.41
5 μM CdR + 5 μM GdR	4.5 ± 1.17	1.2 ± 0.28	2.9 ± 0.32	2.0 ± 0.67	3.8 ± 0.49	0.8 ± 0.16	3.4 ± 1.31	1.4 ± 0.76

Table 1. Effect of deoxynucleosides in the medium on dNTP pool sizes in quiescent control and p53R2 mutant fibroblasts. Summary of dNTP pools from between five and seven separate experiments with quiescent mutant and control cells. Pools were measured after an 18-h incubation with deoxynucleosides. Values are mean ± SD.

We next tested whether changes in intracellular dNTPs arising from the addition of deoxynucleosides to the medium affected the recovery of mtDNA in the quiescent mutant cells after depletion by EtBr. We found no clear increase in mtDNA after the addition of CdR and GdR either alone or in combination. However, when we also included deoxysadenosine (AdR), the restoration of EtBr-depleted mtDNA was almost complete at 7 d after removal of the drug (data not shown). Thus, in two independent time curves in quiescent fibroblasts, we compared the effects of AdR + CdR + GdR with those of CdR + GdR on the recovery of mtDNA depleted by 20 ng/mL EtBr (Fig. 1A) and 50 ng/mL EtBr (Fig. 1B). At both concentrations, control cells recovered a full complement of mtDNA independent of the presence of deoxynucleosides. In the mutant cells, in agreement with the preliminary results, mtDNA fully recovered only in the presence of all three deoxynucleosides, confirming the importance of AdR. Fig. 1C also shows the changes in dNTP concentrations induced by the two combinations of deoxynucleosides after removal of EtBr. We found no systematic differences in the concentrations at the various times of recovery, and thus report their average values here.

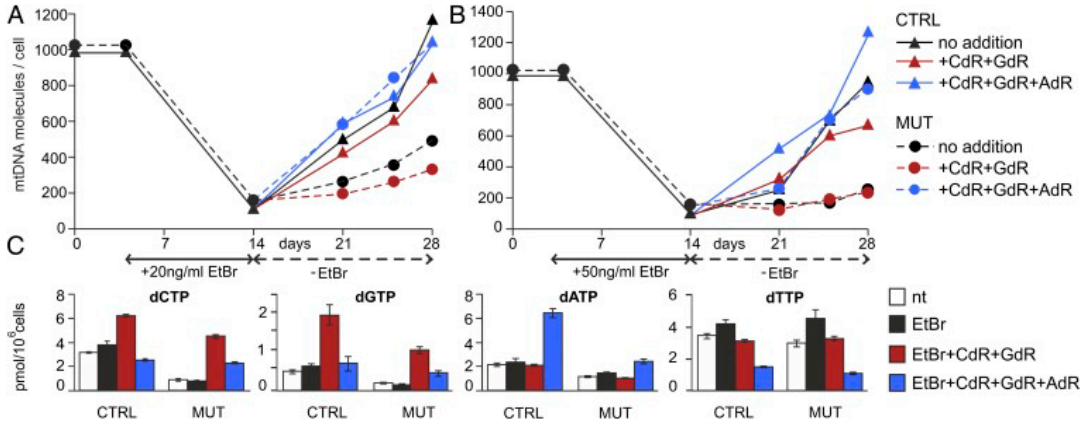

Fig. 1. Stimulation of mtDNA recovery in mutant cells by deoxynucleosides present in the medium. We depleted the mtDNA of quiescent mutant or control fibroblasts in 0.1% FCS with EtBr 20 ng/mL (A) or 50 ng/mL (B). After removal of the drug, the cultures were divided into three groups during a 2-wk recovery period. Group 1 (blue) was contained in a medium composed of 5 μM AdR, CdR, and GdR; group 2 (red) was in a medium composed of only CdR and GdR; and group 3 (black) served as control without deoxynucleosides. At the indicated time intervals, in cells from each group we determined the copy number of mtDNA by real-time PCR (A and B) and measured the sizes of the four dNTP pools (C). Pool sizes are mean ± SEM of the values measured at the three time points after removal of EtBr. nt (white), pool sizes in parallel cultures not treated with EtBr.

DNA Repair After UV Damage: dNTP Pools.

We first investigated whether and how UV irradiation affects the size of the four dNTP pools in quiescent mutant and control cells during a 3-h period after irradiation. In the control fibroblasts, the pools did not change, but in the mutant cells, the dCTP pool (originally 50% of the control pool) decreased further to 25% after irradiation. UV irradiation had no clear effect on the very small dGTP pool (Fig. 2A). Neither dATP nor dTTP was affected (data not shown).

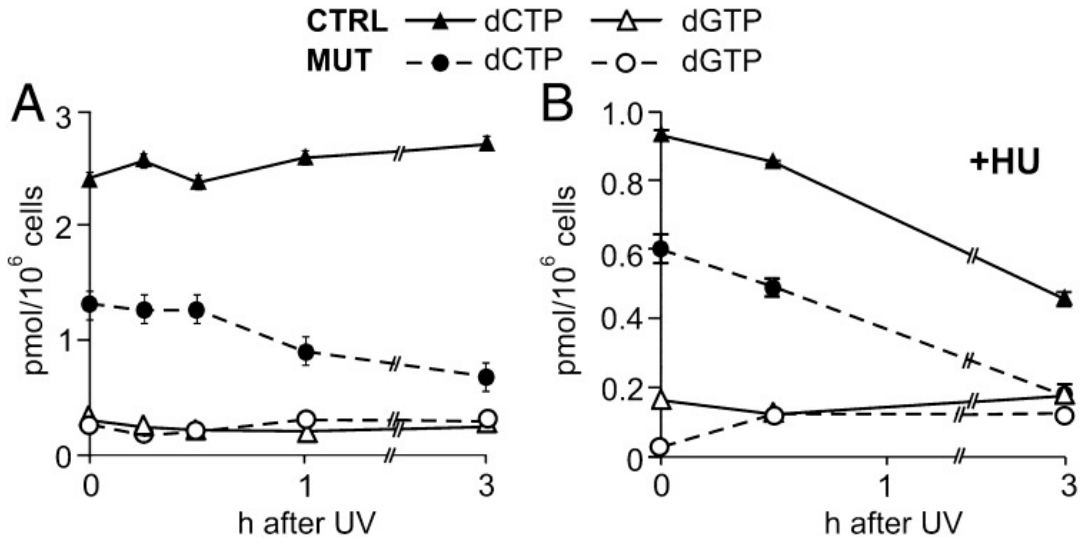

Fig. 2. Effects of UV irradiation and hydroxyurea on dCTP and GTP pools. (A) Pool changes after irradiation. We irradiated quiescent mutant or control fibroblasts with UV (24 J/m2) and measured the size of the dCTP and dGTP pools during a 3-h repair period. (B) Effect of hydroxyurea. The same experiment as in A was run but with 2 mM hydroxyurea (HU) in the medium starting at 30 min before irradiation and during repair. Bars indicate SEM. In most cases, the values were too low to be visible in the figure.

Does a remaining activity of ribonucleotide reductase support the dNTP pools in the mutant cells? The addition of 2 mM hydroxyurea to the incubation medium at 30 min before irradiation and during the subsequent 3 h decreased the size of the dCTP pool in both mutant and control cells (Fig. 2B). Hydroxyurea inactivates ribonucleotide reductase by sequestering the free tyrosyl radical of R2 (23). Its inhibitory effect on the dCTP pool of both types of cells indicates that in the mutated fibroblasts, ribonucleotide reduction was responsible for maintenance of the dCTP pool, implying either that p53R2 was not completely inactivated by the mutation or that the quiescent cells retained some R2 activity.

DNA Repair After UV Damage: Disappearance of Primary Damage.

The primary UV-induced damage involves mainly two types of cross-links in the DNA structure (24): cyclobutane pyrimidine dimers (CPDs) and a smaller

number of 6-4 pyrimidone photoproducts (6-4PPs). Early during nucleotide excision repair (NER), specific proteins recognize the DNA damages and remove the cross-links, with 6-4PPs disappearing rapidly during the first 6 h after irradiation and CPDs possibly persisting longer (24).

Using specific antibodies, we determined the time-dependent disappearance of the two types of DNA damage in quiescent mutant and control cells after exposure to UV irradiation (Fig. 3). The 6-4PPs were gone after 6 h, whereas CPD removal took considerably longer. In both instances, we found no clear difference between mutant and control cells, indicating that the mutant cells were not deficient in the early recognition and removal of the damaged sites.

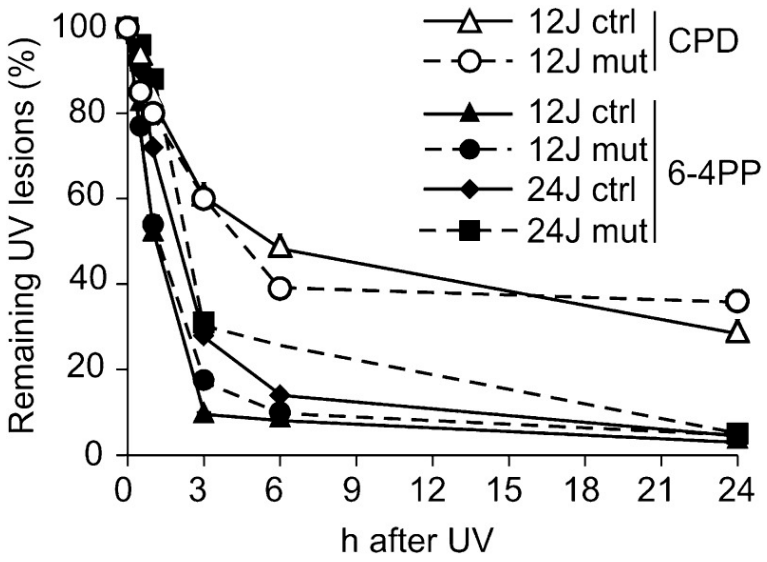

Fig. 3. Disappearance of primary DNA damage in mutant and control fibroblasts. We treated quiescent mutant or control cells with UV (12 or 24 J/m2) and used specific monoclonal antibodies to identify the disappearance of the two main types of DNA damage products (CPDs and 6-4PPs) over the subsequent 24 h.

dNTPs are required during NER to fill the gaps arising from excision of the UV-induced photoproducts. At the end of the process, the nicks are sealed by ligases, restoring the original dsDNA. Before the ligation step, alkali treatment of

the nicked DNA produces single-stranded regions at the sites of the initial damage. Thus, the extent of DNA double-strandedness provides a measure of the ongoing but still incomplete repair (25, 26). This can be quantified by fluorometric analysis of DNA unwinding (FADU) (27) from the fluorescence of DNA-bound EtBr. Immediately after the damage occurs, fluorescence of the DNA-bound EtBr shows a rapid drop in alkali. When the nicks are sealed after resynthesis with fresh dNTPs, the ensuing recovery of fluorescence reflects completion of the gap-filling process.

In a series of experiments, we used FADU to evaluate UV-induced DNA repair in cultures of the two cell lines maintained in low serum for various time periods. We irradiated cells with 24 J/m2 UV after 0 d (confluent cultures), 3 d, 7 d, or 14 d in 0.1% FCS, and determined the percentage of dsDNA at 3 h after irradiation (Fig. 4A). At all time points, the mutant contained less dsDNA than the control, suggesting a greater residual damage caused by slower repair. We next investigated the time course of DNA repair after UV irradiation with 12 or 24 J/m2 immediately after serum change (Fig. 4B1) or after 7 d in low serum (Fig. 4B2). In both instances, the fluorescence dropped to low values immediately after irradiation, indicating the rapid loss of dsDNA, followed over the next 6 h by a slow recovery that was almost complete after 24 h. There were some quantitatively distinct features, however; the drop in fluorescence was larger in cells irradiated with the higher UV dose, after incubation in low serum, and in mutant cells. These data suggest that the timing of fluorescence recovery is related to the efficiency of DNA repair. Such a relationship is also supported by the effects of hydroxyurea (23) and aphidicolin (28), two inhibitors of DNA synthesis (Fig. 4C). Neither drug affected the immediate loss of fluorescence after UV irradiation, but both drugs completely abolished the recovery phase in both cell lines. In fact, at the first time point after irradiation (i.e., 30 min), fluorescence was already higher in the cultures without inhibitors than in those with the inhibitors. The difference was particularly marked in the controls, reflecting the efficiency of repair synthesis.

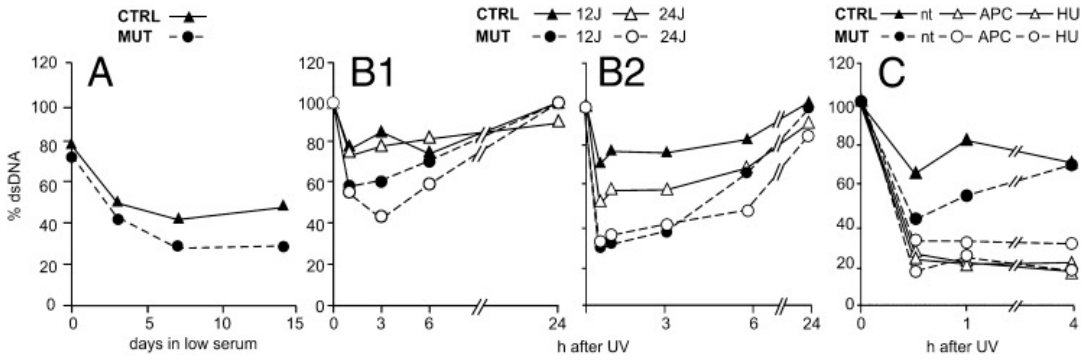

Fig. 4. Repair of UV-damaged DNA analyzed by FADU, which measures the fraction of dsDNA from the fluorescence of EtBr bound to alkali-treated DNA. (A) Mutant and control fibroblasts were maintained for up to 14 d in low-serum medium, as indicated on the abscissa, before irradiation with UV (24 J/m2). The percentage dsDNA was determined after 3 h of repair. (B) Time course of DNA repair in mutant and control cells after irradiation with UV (12 or 24 J/m2) after 0 (B1) or 7 (B2) days in low serum. (C) Inhibition of DNA repair by 2 mM hydroxyurea (HU) or 2 μM aphidicolin (APC) in quiescent mutant or control cells maintained for 7 d in low serum before UV irradiation (24 J/m2). The drugs were present 30 min before and for 4 h after irradiation. nt, not drug-treated.

CdR and GdR were converted to their triphosphates, and in the mutant fibroblasts, their combination "cured" the dCTP and dGTP pool deficiencies (Table 1). In a FADU experiment with mutant cells, the two deoxynucleosides did not affect the initial decay of DNA fluorescence (Fig. 5A), suggesting that they do not affect the detection and removal of DNA cross-links, that is, the early steps of NER that do not require dNTPs. However, after 3 h, DNA fluorescence was already higher in the presence of deoxynucleosides than in the absence of deoxynucleosides and continued to increase until the end of the experiment, indicating faster repair. GdR alone had the opposite effect (Fig. 5A), reducing the recovery of fluorescence. This suggests that a deficiency of dCTP delays repair (Fig. 5B and Table S1).

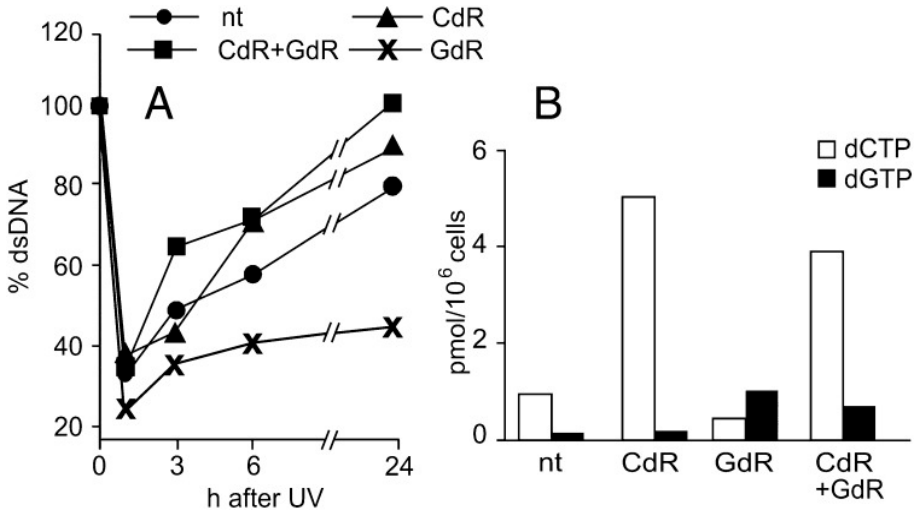

Fig. 5. Effects of CdR and/or GdR on UV-induced DNA repair in quiescent mutant fibroblasts. After 7 d in low serum, we irradiated mutant cells with UV (12 J/m2). The indicated deoxynucleosides were added at final concentrations of 5 μM 18 h before irradiation and during DNA repair. (A) Fraction of dsDNA determined by FADU at various time points after irradiation. (B) dCTP and dGTP pool sizes at the time of irradiation. nt, cells not treated with deoxynucleosides.

We conducted three additional FADU experiments, comparing results from mutant and control cells kept in low serum for 4, 7, or 11 d before irradiation, to substantiate a connection between dNTP pools and DNA repair (Fig. S2). In all cases, mutant cells showed delayed DNA repair, with progressively more marked effects with increasing quiescence time. The addition of CdR + GdR counteracted the delay. The combined FADU data strongly suggest that the p53R2 mutation reduces the cells' ability to repair UV-induced DNA damage because of limitations in the supply of dNTPs.

DNA Repair in Mutant Fibroblasts: Histone H2AX Phosphorylation.

The phosphorylation of histone H2AX on Ser-139 (γH2AX) is considered a marker of repair of double-strand breaks induced by ionizing radiation (29, 30). DNA damage by UV also induces γH2AX in both proliferating and quiescent

cells (31, 32), but its relevance to this connection is unclear. Thus, it was proposed that γH2AX might act as a biomarker of UV damage rather than as a participant in repair (33). During NER, the presence of γH2AX signals a persistence of DNA gaps created by excision of the UV-induced damage, and its disappearance signals filling of the gaps by dNTP polymerization. A comparison of γH2AX kinetics in mutant and control fibroblasts after UV irradiation further illuminates the importance of dNTPs and the p53R2 mutation for DNA repair.

We analyzed the γH2AX content in quiescent mutant and control cells at different times after UV irradiation by flow cytometry and confocal fluorescence microscopy. In cells maintained in low-serum medium, flow cytometry showed that G1/G0 cells accounted for 95% or more of the total cell population; thus, we limited our analysis to these phases of the cell cycle. In cycling cultures, the intensity of the γH2AX signal remained almost unchanged after irradiation, with no differences between mutant and control fibroblasts (Fig. 6). In contrast, in quiescent cultures, the γH2AX signal increased in the irradiated cells and reached higher values in the mutant fibroblasts compared with the control fibroblasts. This difference increased with the time of quiescence (Fig. 6).

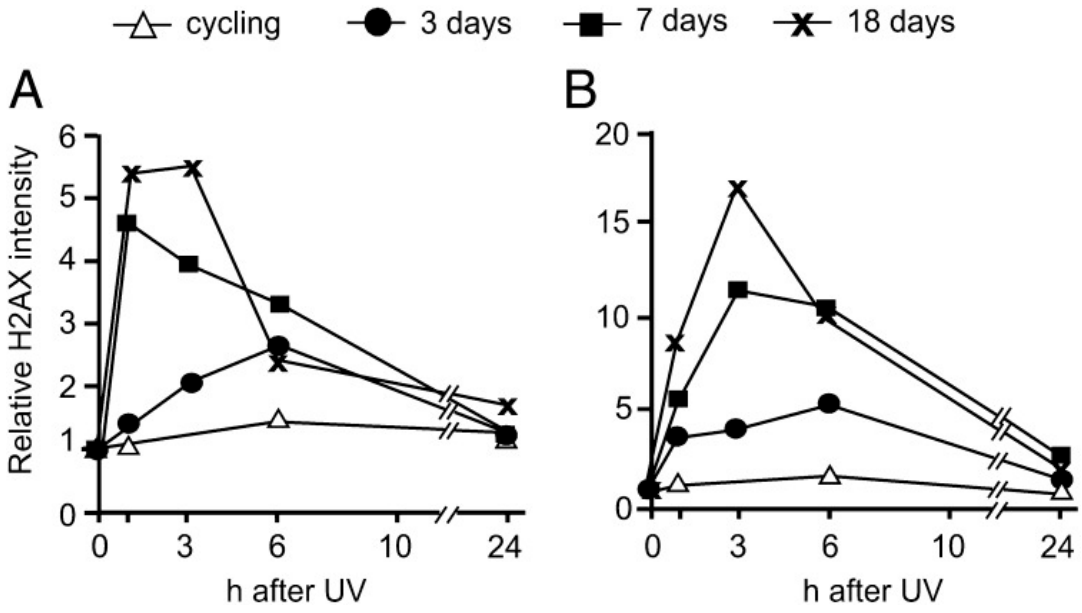

Fig. 6. Histone H2AX phosphorylation after UV-induced DNA damage in cycling and quiescent mutant and control fibroblasts. Control (A) and mutant (B) cells were irradiated with UV (12

J/m2) during proliferation in 10% serum (cycling) or after 3, 7, or 18 d in 0.1% FCS medium. γH2AX was measured during a 24-h repair period by flow cytometry after staining with a specific monoclonal antibody. Note the difference in ordinates in the two panels.

We then examined the effects of deoxynucleosides on H2AX phosphorylation. Mutant and control fibroblasts were incubated with or without CdR + GdR for 7 d, from the shift to low serum to the time of UV irradiation, and during the 24 h after the irradiation. Parallel sets of cultures were maintained without added deoxynucleosides. Direct microscopic analysis of the accumulation and decay of γH2AX in irradiated mutant and control fibroblasts showed that addition of deoxynucleosides reduced the intensity and the persistence of the signal in the mutant cells, whereas it had no effect in the control cells (Fig S3).

In agreement with earlier observations (31, 33) immunofluorescence revealed that the cell distribution of γH2AX at each time point was not homogeneous (Fig S3). In a parallel experiment, flow cytometry demonstrated greater heterogeneity of the fluorescent signal in mutant fibroblasts than in control fibroblasts during the 24-h repair period (Fig. 7). In the control fibroblasts, the distribution of the γH2AX fluorescence was unimodal at all times after UV irradiation exception the 8-h time point. Peak fluorescence was already reached by 3 h and then shifted back to the original preirradiation value by 24 h. In the mutant fibroblasts, a bimodal pattern already began to appear by 1 h, with a high fluorescence peak that increased in intensity for up to 8 h postirradiation. The subpopulation with lower fluorescence expanded progressively, shifting toward lower signal intensities. The addition of deoxynucleosides enhanced expansion of the lower fluorescence subpopulation, suggesting that the distinctive heterogeneity of the γH2AX signal in the mutant fibroblasts is related to a limitation of DNA precursors during repair synthesis. Here again, deoxynucleosides had no effect on the behavior of the p53R2-proficient cells.

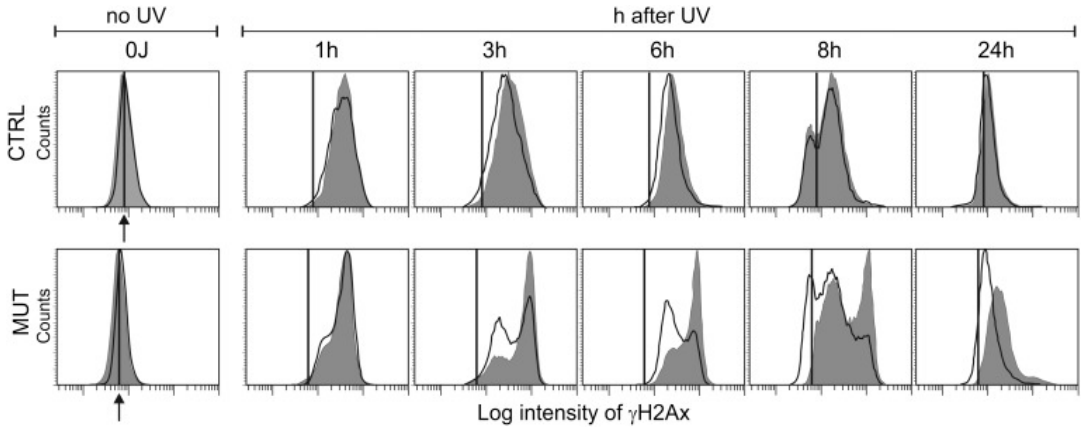

Fig. 7. Heterogeneity of the γH2AX signal after UV irradiaton of quiescent cells; effect of deoxynucleosides. Control and mutant cells were irradiated with UV (12 J/m2), and the distribution of γH2AX in the nuclei of G1/G0 cells during the subsequent 24 h was detected by flow cytometry after immunostaining. The gray histograms refer to cultures incubated without deoxynucleoside addition; the white histograms, to cultures incubated with 5 μM CdR + GdR for 7 d before and 24 h after irradiation. The vertical line indicates the median value of γH2AX fluorescence in nonirradiated cells, denoted by an arrow.

Discussion

Several levels of control regulate the intracellular concentrations of the four dNTPs required for DNA synthesis. Pool imbalances lead to mutations (2–4), and thus the supply of dNTPs is tightly controlled. The de novo synthesis of dNTPs is regulated by the sophisticated allosteric regulation of ribonucleotide reduction (1). In mammalian cells, their degradation to and resynthesis from deoxynucleosides in substrate cycles (34) provides further fine-tuning of pool sizes. Attesting to the importance of appropriate pool sizes are human genetic diseases caused by both deficiencies in and overproduction of dNTPs (35).

The p53R2 protein is a recent addition to this picture (9). This protein is a subunit of mammalian ribonucleotide reductase with the same radical-providing function as the canonical R2 protein. In postmitotic resting cells in which R2 has disappeared, only p53R2 can provide the free radical required for ribonucleotide reduction, acting as the functioning small subunit of mammalian ribonucleotide reductase (6, 7).

The results of our experiments with the mutant human fibroblasts reported here strongly support this concept. These cells carry a homozygous RR2MB mutation, resulting in the exchange of a highly conserved glycine residue located in the iron center of p53R2 with a valine (16). We found that the loss of p53R2 activity has no consequences for cycling cells containing a large excess of R2 over p53R2; however, in quiescent cells, when R2 function should be taken over by p53R2, mtDNA synthesis and DNA repair are disturbed. In our experiments, the final degradation of R2 occurred during maintenance of the cells in serum-depleted medium after they had reached confluency. At confluency, the cultures still contained a minor fraction of S-phase cells (20), yet the mutant already exhibited delayed repair (Fig. 4B1). After 1 wk in 0.1% FCS, the cells still contained a small amount of R2, along with small dNTP pools (20). Hydroxyurea, a known inhibitor of ribonucleotide reductase, blocked dNTP synthesis (Fig. 2B), demonstrating that the dNTPs are synthesized de novo. Additional evidence for some residual ribonucleotide reductase activity was the decrease in dCTP and dTTP pools after addition of GdR to the medium (Table S1). GdR increased the

intracellular dGTP pool, resulting in diminished size of the two pyrimidine dNTPs by allosteric regulation of the substrate specificity of a functioning ribonucleotide reductase, probably containing R2 (1). Despite the small remaining R2 activity in the mutant cells, the absence of p53R2 resulted in deficiencies of dCTP and dGTP, which were further accentuated by UV irradiation (Fig. 2A).

The mutant fibroblasts had been obtained from an individual completely lacking mtDNA in muscle cells. Nevertheless, they grew normally in culture and contained a normal amount of mtDNA even during prolonged quiescence (20). We hypothesized that the low mtDNA content in fibroblasts compared with muscle cells made the fibroblasts less sensitive to a deficiency of dNTPs. Thus, we set up conditions that forced the cells to renew all of their mtDNA during a relatively short period after depletion with EtBr. The R2-containing cycling fibroblasts efficiently resynthesized the mtDNA independent of their p53R2 status, whereas quiescent mutant fibroblasts were deficient (Fig. 1). In response to the increased demand for mtDNA precursors, the supply of dNTPs in the mutant cells was insufficient. This deficiency was cured by adding deoxynucleosides, which expanded the dNTP pools. The combination of CdR, GdR, and AdR was the most effective addition.

The mutant cells also exhibited defective repair of DNA damage after UV irradiation. Deoxynucleotides participate in NER only toward the end of the process, after excision of the damaged sites. The early steps involving recognition and removal of the cross-links in the damaged DNA functioned normally in the quiescent mutant cells (Fig. 3); however, the later steps requiring the participation of dNTPs were delayed, and the damage was more extensive and persistent. This delay was evident in the FADU experiments when the irradiated mutant cells contain more single-stranded DNA after alkaline treatment and required more time to reseal the nicked DNA. The addition of deoxynucleosides had a beneficial effect and favored repair. Particularly remarkable are the divergent results seen after the addition of GdR + CdR or GdR alone. The combination of the deoxynucleosides normalized the dCTP and dGTP pools (Table 1) and improved DNA repair. GdR alone increased the dGTP pool but decreased the dCTP pool,

resulting in delayed repair. Such a close correlation between the size of the dCTP pool and the cellular ability to repair DNA is strong evidence for a causal relation between the two parameters.

Surprisingly, the mutant cells required a different constellation of deoxynucleosides for mtDNA maintenance (AdR + CdR + GdR) and DNA repair (CdR + GdR). Given that the pool differences between mutant and control fibroblasts concern mainly dCTP and dGTP, we did not expect to see a requirement for AdR. However, considering that CdR is a precursor of both pyrimidine dNTPs via the conversion of dCMP to dTMP, whereas GdR feeds only the dGTP pool, we reasoned that adding AdR to the deoxynucleoside mix would create a condition favoring the synthesis of all four DNA precursors. The main effect of AdR was a twofold to threefold increase in dATP and concomitant similar decreases in the dCTP and dGTP pool expansions caused by the presence of CdR and GdR (Fig. 1C). The dTTP pool was also decreased by the addition of AdR. Thus, AdR provokes a large disturbance of the balance between dNTP pools. An important consideration in relation to the different requirements for deoxynucleosides to support mtDNA reexpansion and nuclear DNA repair is that different DNA polymerases are involved in the two processes.

The mutant cells also differed from the control cells in the level of phosphorylated histone H2AX. Kinetic flow cytometry analyses of UV-irradiated quiescent cells demonstrated larger amounts and a more extended persistence of γH2AX in the mutant fibroblasts than in the control fibroblasts. The distribution of γH2AX was not homogeneous and differed between the two cell populations. Confocal fluorescence microscopy yielded essentially similar results. The most important finding with both types of analysis was that the presence of CdR + GdR in the medium had little effect on the control cells, but shifted the behavior of the mutants toward that of the controls, again indicating that the defective DNA repair exhibited by the mutant fibroblasts in the absence of added deoxynucleosides depends on insufficient de novo synthesis of dNTPs.

Acknowledgments

We thank Dr. Arianna Calistri for advice and help with the immortalization of the fibroblasts. This work was supported by Italian Telethon Grant GGP09019 (to V.B.), Italian Association for Cancer Research (AIRC) Grant 1091 (to V.B.), the University of Padova, Strategic Project 2008 "Models of Mitochondrial Diseases," and the Cariparo Foundation.

References

1. Nordlund P, Reichard P. Ribonucleotide reductases. Annu Rev Biochem. 2006;75:681–706.

2. Niida H, Shimada M, Murakami H, Nakanishi M. Mechanisms of dNTP supply that play an essential role in maintaining genome integrity in eukaryotic cells. Cancer Sci. 2010;101:2505–2509.

3. Meuth M. The molecular basis of mutations induced by deoxyribonucleoside triphosphate pool imbalances in mammalian cells. Exp Cell Res. 1989;181:305–316.

4. Kumar D, et al. Mechanisms of mutagenesis in vivo due to imbalanced dNTP pools. Nucleic Acids Res. 2011;39:1360–1371.

5. Chabes AL, Björklund S, Thelander L. S phase-specific transcription of the mouse ribonucleotide reductase R2 gene requires both a proximal repressive E2F-binding site and an upstream promoter activating region. J Biol Chem. 2004;279:10796–10807.

6. Håkansson P, Hofer A, Thelander L. Regulation of mammalian ribonucleotide reduction and dNTP pools after DNA damage and in resting cells. J Biol Chem. 2006;281:7834–7841.

7. Pontarin G, et al. p53R2-dependent ribonucleotide reduction provides deoxyribonucleotides in quiescent human fibroblasts in the absence of induced DNA damage. J Biol Chem. 2007;282:16820–16828.

8. Chabes AL, Pfleger CM, Kirschner MW, Thelander L. Mouse ribonucleotide reductase R2 protein: A new target for anaphase-promoting complex Cdh1-mediated proteolysis. Proc Natl Acad Sci USA. 2003;100:3925–3929.

9. Tanaka H, et al. A ribonucleotide reductase gene involved in a p53-dependent cell-cycle checkpoint for DNA damage. Nature. 2000;404:42–49.

10. Pontarin G, et al. Ribonucleotide reduction is a cytosolic process in mammalian cells independently of DNA damage. Proc Natl Acad Sci USA. 2008;105:17801–17806.

11. Bourdon A, et al. Mutation of RRM2B, encoding p53-controlled ribonucleotide reductase (p53R2), causes severe mitochondrial DNA depletion. Nat Genet. 2007;39:776–780.

12. Bornstein B, et al. Mitochondrial DNA depletion syndrome due to mutations in the RRM2B gene. Neuromuscul Disord. 2008;18:453–459.

13. Acham-Roschitz B, et al. A novel mutation of the RRM2B gene in an infant with early fatal encephalomyopathy, central

hypomyelination, and tubulopathy. Mol Genet Metab. 2009;98:300–304.

14. Tyynismaa H, et al. A heterozygous truncating mutation in RRM2B causes autosomal-dominant progressive external ophthalmoplegia with multiple mtDNA deletions. Am J Hum Genet. 2009;85:290–295.

15. Shaibani A, et al. Mitochondrial neurogastrointestinal encephalopathy due to mutations in RRM2B. Arch Neurol. 2009;66:1028–1032.

16. Kollberg G, et al. A novel homozygous RRM2B missense mutation in association with severe mtDNA depletion. Neuromuscul Disord. 2009;19:147–150.

17. Devlin HL, et al. Impairment of the DNA repair and growth arrest pathways by p53R2 silencing enhances DNA damage-induced apoptosis in a p53-dependent manner in prostate cancer cells. Mol Cancer Res. 2008;6:808–818.

18. Kunos CA, et al. Ribonucleotide reductase inhibition enhances chemoradiosensitivity of human cervical cancers. Radiat Res. 2010;174:574–581.

19. Nakano K, Bálint E, Ashcroft M, Vousden KH. A ribonucleotide reductase gene is a transcriptional target of p53 and p73. Oncogene. 2000;19:4283–4289.

20. Pontarin G, et al. Deoxyribonucleotide metabolism in cycling and resting human fibroblasts with a missense mutation in p53R2, a subunit of ribonucleotide reductase. J Biol Chem. 2011;286:11132–11140.

21. King MP, Attardi G. Isolation of human cell lines lacking mitochondrial DNA. Methods Enzymol. 1996;264:304–313.

22. Arnér ES, Eriksson S. Mammalian deoxyribonucleoside kinases. Pharmacol Ther. 1995;67:155–186.

23. Krakoff IH, Brown NC, Reichard P. Inhibition of ribonucleoside diphosphate reductase by hydroxyurea. Cancer Res. 1968;28:1559–1565.

24. Friedberg E, et al. DNA Repair and Mutagenesis. Washington, DC: ASM Press; 2006.

25. Erixon K, Ahnström G. Single-strand breaks in DNA during repair of UV-induced damage in normal human and xeroderma pigmentosum cells as determined by alkaline DNA unwinding and hydroxylapatite chromatography: Effects of hydroxyurea, 5-fluorodeoxyuridine and 1-beta-D-arabinofuranosylcytosine on the kinetics of repair. Mutat Res. 1979;59:257–271.

26. Baumstark-Khan C, Hentschel U, Nikandrova Y, Krug J, Horneck G. Fluorometric analysis of DNA unwinding (FADU) as a method for detecting repair-induced DNA strand breaks in UV-irradiated mammalian cells. Photochem Photobiol. 2000;72:477–484.

27. Birnboim HC, Jevcak JJ. Fluorometric method for rapid detection of DNA strand breaks in human white blood cells produced by low doses of radiation. Cancer Res. 1981;41:1889–1892.

28. Huberman JA. New views of the biochemistry of eucaryotic DNA replication revealed by aphidicolin, an unusual inhibitor of DNA polymerase alpha. Cell. 1981;23:647–648.

29. Rogakou EP, Pilch DR, Orr AH, Ivanova VS, Bonner WM. DNA double-stranded breaks induce histone H2AX phosphorylation on serine 139. J Biol Chem. 1998;273:5858–5868.

30. Paull TT, et al. A critical role for histone H2AX in recruitment of repair factors to nuclear foci after DNA damage. Curr Biol. 2000;10:886–895.

31. Marti TM, Hefner E, Feeney L, Natale V, Cleaver JE. H2AX phosphorylation within the G1 phase after UV irradiation depends on nucleotide excision repair and not DNA double-strand breaks. Proc Natl Acad Sci USA. 2006;103:9891–9896.

32. Matsumoto M, et al. Perturbed gap-filling synthesis in nucleotide excision repair causes histone H2AX phosphorylation in human quiescent cells. J Cell Sci. 2007;120:1104–1112.

33. Cleaver JE. γH2Ax: Biomarker of damage or functional participant in DNA repair "all that glitters is not gold!" Photochem Photobiol. 2011;87:1230–1239.

34. Rampazzo C, et al. Regulation by degradation, a cellular defense against deoxyribonucleotide pool imbalances. Mutat Res. 2010;703:2–10.

35. Spinazzola A, et al. Clinical and molecular features of mitochondrial DNA depletion syndromes. J Inherit Metab Dis. 2009;32:143–158.

36. Chaouch S, et al. Immortalized skin fibroblasts expressing conditional MyoD as a renewable and reliable source of converted human muscle cells to assess therapeutic strategies for muscular dystrophies: Validation of an exon-skipping approach to restore dystrophin in Duchenne muscular dystrophy cells. Hum Gene Ther. 2009;20:784–790.

37. Schramm VL. Development of transition state analogues of purine nucleoside phosphorylase as anti–T-cell agents. Biochim Biophys Acta. 2002;1587:107–117.

38. Carson DA, Seegmiller JE. Effect of adenosine deaminase inhibition upon human lymphocyte blastogenesis. J Clin Invest. 1976;57:274–282.

Supporting information

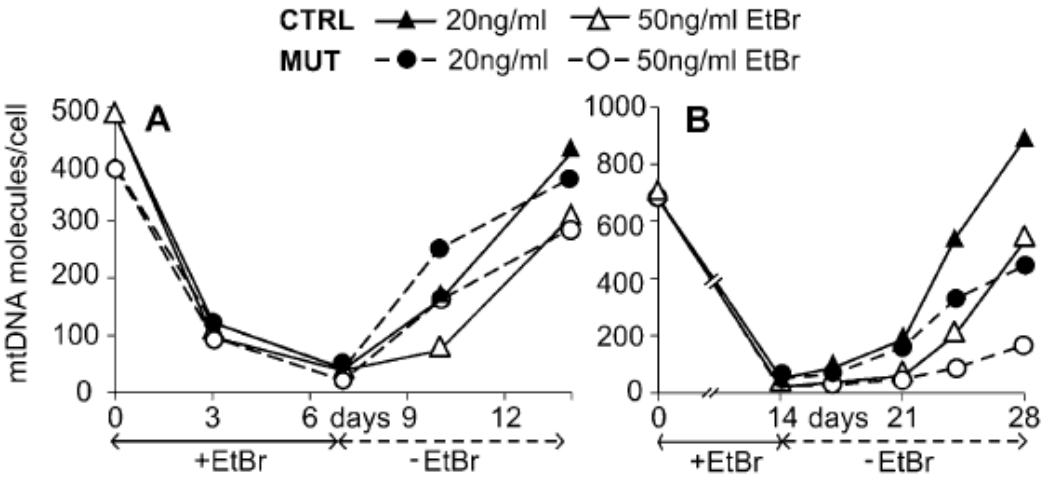

Fig. S1. Depletion and recovery of mtDNA in cycling and quiescent fibroblasts. Mutant and control fibroblasts were treated with EtBr 20 or 50 ng/mL for 7 d (cycling cells) or 14 d (quiescent cells), followed by a recovery period in the absence of the drug. The copy number of mtDNA (mtDNA molecules/cell) was determined at time intervals by real-time PCR. (A) Cycling cells, recovery period in 10% FCS. (B) Quiescent cells, recovery period in 0.1% FCS.

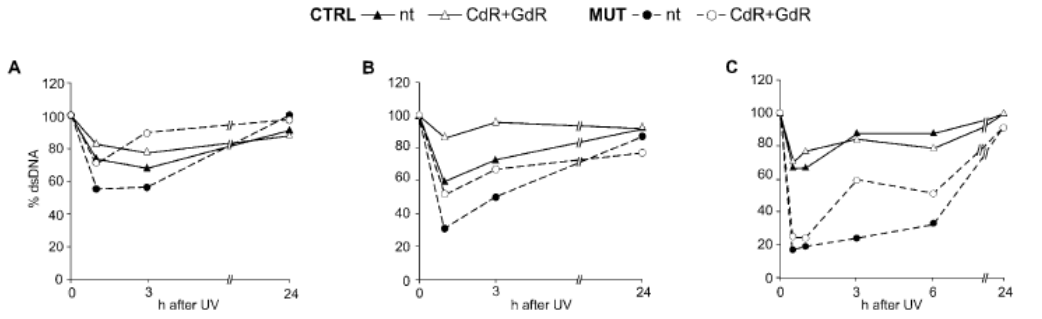

	dCTP		dGTP	
	nt	CdR+GdR	nt	CdR+GdR
CTRL	3.07	5.16	0.36	1.18
MUT	2.43	5.59	0.3	1.2

	dCTP		dGTP	
	nt	CdR+GdR	nt	CdR+GdR
CTRL	2.65	4.46	0.32	0.99
MUT	1.06	5.63	0.24	0.81

	dCTP		dGTP	
	nt	CdR+GdR	nt	CdR+GdR
CTRL	3.24	5.21	0.36	1.17
MUT	0.88	3.66	0.19	0.66

Fig. S2. FADU analysis of UV-induced DNA repair in quiescent mutant and control cells maintained for various periods in low serum; effects of deoxynucleosides. The cells were kept for 4 d (A), 7 d (B), or 11 d (C) in low serum before exposure to UV irradiation (12 J/m2). The time course of DNA repair was analyzed by FADU as recovery of dsDNA. In each experiment, half of the cultures received 5 μM CdR + GdR 18 h before UV irradiation and over the next 24 h. The tables show dCTP and dGTP pool sizes (pmol/106cells) measured at the time of irradiation. nt, cells not treated with deoxynucleosides.

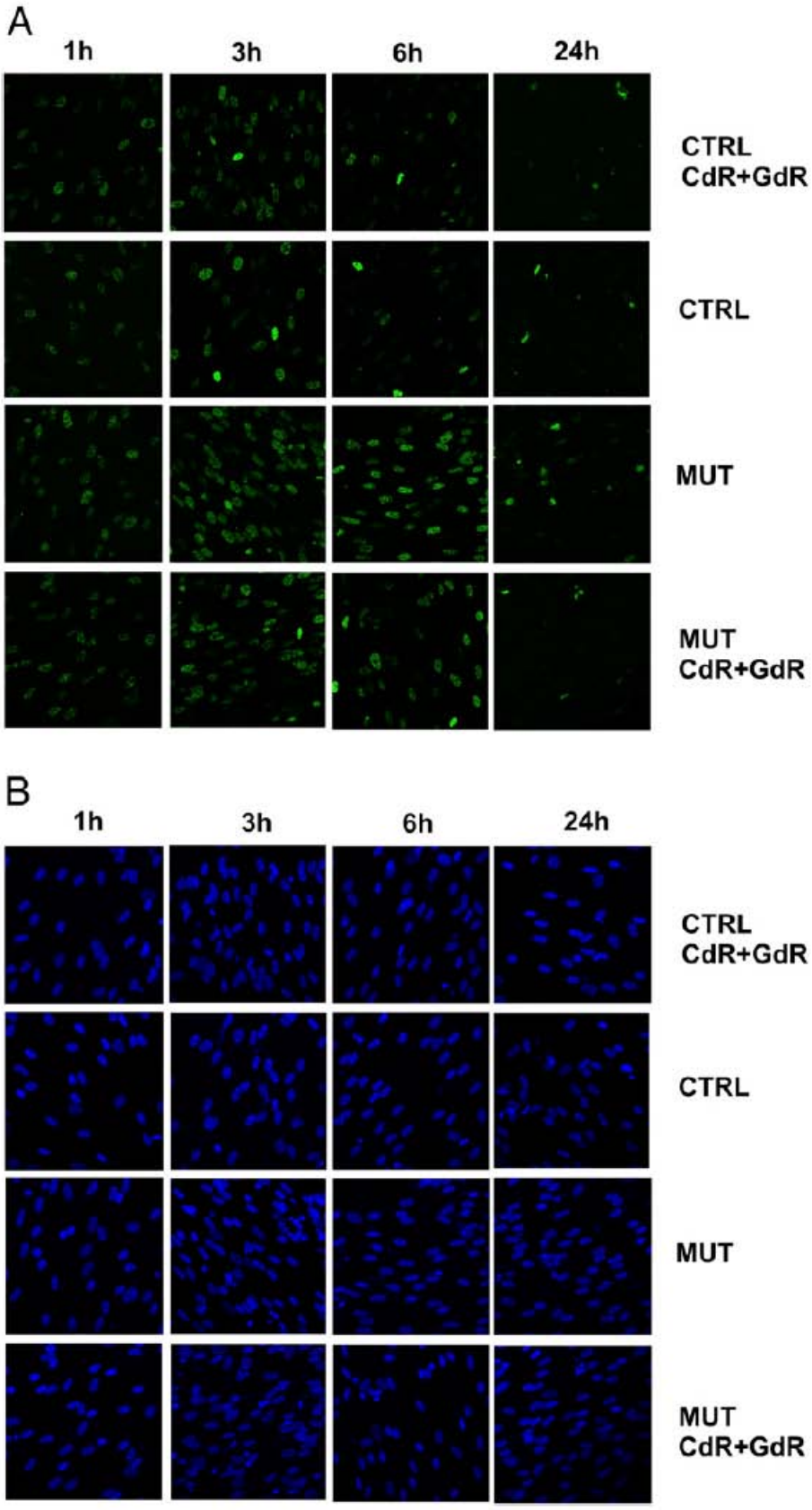

Fig. S3. Deoxynucleosides affect the heterogeneity of the UV-induced H2AX phosphorylation in quiescent mutant cells. We maintained control and mutant fibroblasts in the absence or presence of

CdR + GdR for 7 d in low serum and for 24 h after exposure to UV irradiation (12 J/m2). (A) γH2AX was detected by immunofluorescence analysis at the indicated times. (B) Nuclear DNA was counterstained with DAPI. In both cell lines, the γH2AX signal produced dim nuclear foci at 1 h after irradiation. After 3 h, most cells had brighter foci, and a few cells showed a far stronger pan-nuclear staining. After 6 h, the signal had declined in the control cells, whereas the mutant cells maintained the bright nuclear foci and the pan-nuclear staining. In both cell lines, the γH2AX signal virtually disappeared by 24 h. In the presence of deoxynucleosides, the γH2AX fluorescence pattern of mutant cells was closer to that of the control cells.

	dNTP pmoles/10^6 cells							
	Control				Mutant			
Treatment	dCTP	dGTP	dTTP	dATP	dCTP	dGTP	dTTP	dATP
None	1.8	0.4	2.0	2.3	1.3	0.3	2.5	1.4
5μM CdR	2.6	0.5	3.3	1.7	3.8	0.4	3.7	1.4
1μM GdR	1.3	0.7	1.6	1.6	0.9	0.7	1.8	1.1
5μM GdR	1.3	1.0	1.8	1.8	0.7	1.0	1.7	1.3
5μM CdR + 1μM GdR	2.5	0.7	3.1	1.6	2.9	0.7	3.1	1.3
5μM CdR + 5μM GdR	2.4	0.8	2.9	1.6	3.1	0.9	2.9	1.7

Table S1. Deoxynucleotide pools in quiescent mutant and control fibroblasts incubated with deoxynucleosides. Cells were maintained for 7 days in low serum and incubated for 18 h with deoxynucleosides before pool extraction.

Leonardo Bee[1], Selena Marini[1], Giovanna Pontarin[1], Paola Ferraro[1], Rodolfo Costa[1], Urs Albrecht[2], and Lucia Celotti[1]

[1]Department of Biology, University of Padova, Padova, Italy.

[1]Department of Biology, Unit for Biochemistry, University of Fribourg, Fribourg, Switzerland.

[THE CIRCADIAN CLOCK CONTROLS THE DNA SENSITIVITY TO UV-INDUCED DAMAGE AND REPAIR KINETICS]

Abstract

Several studies have recently indicated that the circadian clock, the molecular oscillatory system which confers rhythmicity to many biochemical processes, could have a role in regulating the cell response to DNA damages. In cultures of human quiescent fibroblasts we investigated whether the efficiency and kinetics of UV-induced DNA repair are affected by the circadian phase at which the cells are stressed. The cells were incubated with dexamethasone to induce rhythmic expression of the circadian clock genes and irradiated at two different circadian times corresponding at two opposite levels of clock gene expression, CT16 (PER2 nadir, BMAL1 zenith) and CT28 (PER2 zenith, BMAL1 nadir). Our results showed that the cells irradiated at CT 28 exhibited a slower repair kinetics with respect to CT16-irradiated cells, as suggested by the more extensive phosphorylation of histone H2AX and delayed recovery of double stranded DNA in this set of samples. By measuring the removal of pyrimidine pirimidone ([6-4]PP) photoproducts we found that the fibroblasts irradiated at PER2 zenith (CT28) exhibited a significantly slower kinetics of photoproduct removal with respect to those irradiated at CT16. In addition to the faster kinetics of photoproduct removal, fibroblasts irradiated at CT16 showed a significantly higher formation of both [6-4]PPs and cyclobutane pyrimidine dimers (CPDs). We evaluated whether in our cell system the XPA protein, the main limiting factor of nucleotide excision repair process, showed an oscillatory pattern as suggested by some authors. In contrast, we did not find any evidence of such oscillating pattern or direct connection between this protein and the circadian clock. Transfection of fibroblasts with siRNAs targeting BMAL1 gene expression confirmed that DNA damage formation and repair efficiency were strictly dependent to the circadian time of irradiation, although no direct involvement of some clock components has been detected.

Introduction

The efficient repair of DNA is crucial for the maintenance of genomic stability during dangerous environmental conditions such as exposure to the UV component of sunlight. Its exposure is responsible for the formation of two major classes of UV-induced DNA lesions: the cyclobutane pyrimidine dimer (CPD) and the pyrimidine-pirimidone photoproduct [6-4]PP, both of which play an important role in skin aging and wrinkling (photoaging) and skin cancer (Meeran et al., 2008; Gaddameedhi et al., 2011). Dimer formation triggers a complex process, the DNA damage response (DDR), which includes checkpoint activation, chromatin remodeling, DNA repair and/or apoptosis. In many organisms including humans, the Nucleotide excision repair (NER) system represents the only one that is able to repair a wide range of DNA adducts (Sancar et al., 2010). The system can be broadly divided into two major pathways: the global genome NER (GG-NER), which is responsible for repairing lesions throughout the entire genome, and the transcription-coupled NER (TC-NER), which specifically repairs DNA lesions in genes that block the actively transcribing RNA polymerases II (RNAPII) (Lagerwerf et al., 2011; Ray et al., 2013). Despite differences in recognizing photoproducts, removal of dimers proceeds in the same way through a dual incision of DNA around the damaged site and the consequent excision of a 27-30 nucleotide oligomer in a process carried out by six excision repair factors: RPA, xeroderma pigmentosum group A (XPA), XPC, TFIIH, XPG, and XPF-ERCC1 (Mu et al., 1995). In the end, the gap created is filled by a process that requires DNA polymerases δ or ε as well as the accessory replication proteins and a correctly balanced pool of dNTPs (Palomera-Sanchez et al., 2010; Pontarin et al., 2012).

A growing number of studies have recently indicated that the circadian clock, the molecular oscillatory system which confers rhythmicity to many biochemical processes, is also involved in the control of the DNA damage response. It has been reported, in fact, that circadian clock components such as BMAL1-CLOCK, PER1, PER2, PER3 and RORα are involved in controlling the

cellular response to genotoxic stresses (Kang et al., 2009; Im et al., 2010; Kim et al., 2011; Geyfman et al., 2012). Beyond the regulatory connection between the clock and UV-induced DNA damage repair, it has been reported that the NER system displays a circadian oscillation in mice, possibly through oscillations in the expression of Xeroderma pigmentosum group A protein (XPA), the DNA damage recognition protein for this pathway (Gaddameedhi et al., 2011). Since XPA is involved in the recognition of DNA dimers and represents the rate-limiting factor in excision repair, a time-dependent variation in its relative abundance results in an impaired DNA repair capability when UV-irradiation is performed in anti-phase with its expression (Kang et al., 2009; Gaddameedhi et al., 2011). Subsequent analysis revealed, however, that the response to UV radiation in cells derived from mice mutant in circadian clock proteins is indistinguishable from that in their wild-type counterparts, leading to the conclusion that the majority of DDR is not controlled by the circadian clock or that this control exists only at the organism level (Gaddameedhi et al., 2012), which of course complicates the picture.

We used cultures of human quiescent fibroblasts synchronized with dexamethasone to investigate if the effectiveness of UV-induced DNA repair is affected by the circadian phase at which cells are stressed. Our data demonstrated that despite indications that the NER system is not regulated by the circadian clock, both DNA sensitivity and repair efficiency are strictly correlated to the circadian time when cells are exposed to UV radiation.

Materials and methods

Cell cultures and Circadian clock synchronization

Primary human skin fibroblasts C63 and NIH-3T3 were grown in DMEM high glucose (Life Technologies) supplemented with 10% of heat-inactivated bovine serum (FBS, Biochrom), MEM Non-Essential Aminoacids and 100 U/ml of penicillin-streptomycin (25 mg/ml - 30 mg/ml), at 37°C and 5% CO_2 in a humidified incubator. Quiescent cultures were obtained by growing cells to confluence (usually for 7 d), changing the medium to DMEM-0.1% FBS, and keeping the cells in this medium for further 7-10 days. Cultures received fresh medium every 3-4 day. Quiescence was analyzed by flow cytometry after propidium iodide staining as previously described (Bee et al., 2013).

Circadian clock gene expression was synchronized by addition of DMEM containing 100 nM dexamethasone (Balsalobre et al. 2000). After 2 h the medium was removed and cells were washed two times with fresh medium w/o serum. After the dexamethasone shock quiescent C63 cells were incubated again with DMEM-0.1% FBS while NIH-3T3 were incubated in DMEM-5% FBS.

Transfection with siRNAs

C63 fibroblasts were seed and grown up to confluence in DMEM-10% FBS (usually 7 days). We then transfected the confluent cells with siRNA (30 nM final concentration, Life Technologies) in DMEM-0.1% FBS without antibiotics using RNAiMAX (Life Technologies), as reported by Franzolin et al. (2013). After three days medium was diluted 1:1 with fresh DMEM-0.1% FBS and cells were incubated for additional 3 days in presence of 15 nM siRNA. Fibroblasts were thus transfected a second time with 30 nM of siRNA in DMEM-0.1% FBS without antibiotics. After 24 h cells medium was exchanged with DMEM-0.1% FBS + 100 nm dexamethasone for 2 h, washed twice and incubated in the previous medium containing siRNA until UV irradiation.

RNA extraction, Reverse Transcription and Real-Time PCR

At specific circadian time (CT) after synchronization with dexamethasone, cells were harvested ($0.5x10^6$) and total RNAs extracted by using TRIzol reagent (Life Technologies). The quality and quantity of RNA were assessed by using NanoDrop 1000 spectrophotometer (Thermo Scientific) and by denaturing agarose gel electrophoresis with ethidium bromide staining. 1 µg of total RNA was transcribed to cDNAs using the ImProm-II™ Reverse Transcription System (Promega) and random hexamers (Life Technologies), according to the manufacturer's instructions. For quantitative real-time PCR 25 ng of cDNA was used and transcript levels of genes were detected by Sybr Green GoTaq® qPCR Master Mix (Promega). Reactions were performed in quadruplicate in 96-well optical plates with a 7500 real-time PCR system (Applied Biosystems). GAPDH and RPL32 were used as endogenous control for normalizations.

Nuclear Extracts and Western Blot

Pellets of 1-2 million cells were collected and washed 2 times in cold PBS. Nuclear protein extracts were obtained using the CelLytic™ NuCLEAR™ Extraction Kit (Sigma) according to manufacturer. Protein concentration were determinate by Bradford assay (Bio-Rad), and appropriate amounts (20-30 µg) were loaded and electrophoresed. Proteins were blotted on Hybond-C Extra nitrocellulose membrane (GE Healthcare). Membranes were washed 4 times in TBS-0.05% Tween-20 (TBS-T) and saturated with 2% ECL Prime Blocking Agent (GE Healthcare) in TBS-T for 1 h at room temperature. Membranes were, thus, incubated with the primary antibodies overnight at 4°C: anti-PER2 (1:200, Santa Cruz), anti-BMAL1 (1:1000, Abcam), anti-XPA (1:1000, Abcam), anti-GAPDH (1:10000, Millipore). After 4 washing with TBS-T for 10 min, membranes were incubated with the appropriate HRP-secondary antibodies (1:40000, GE Healthcare). After further 4 washing membranes were developed using the ECL Select chemiluminescence kit (GE Healthcare). The signal were detected on Kodak films and quantified with ImageJ software.

UV irradiation

Clock synchronized cells were irradiated with a 254-nm UVS-11 mineral light lamp at a fluency rate of 1.7 J/m^2/sec. Before irradiation medium was completely removed and subsequently fresh medium was added to cells.

Analysis of γ-H2AX

Flow cytometer analysis of γ-H2AX were performed as previously described (Bee et al., 2013). Briefly at 0, 0.5, 1, 2, 4, 6 and 24 h after irradiation, cells were fixed in 70% cold ethanol, rinsed twice in PBS and centrifuged at 200 g for 10 min at 4 °C. Samples were, thus, permeabilized for 10 min on ice with 0.1% Triton X-100 in PBS, supplemented with 4% goat serum. After centrifugation, the cells were incubated over night with primary antibody diluted in permeabilization solution (mouse anti-γ-H2AX, 1:500, Millipore). Cells were rinsed three times in PBS with 2% of goat serum and incubated at room temperature for 1 h with agitation with secondary antibody (Alexa Fluor 488 goat anti-mouse, 1:200, Life Technologies) diluted in permeabilization solution. After three washings in PBS with 2% goat serum, cells were resuspended in PBS and analyzed by FACS. Data concerning FI were collected from 20,000 cells/sample using a BD FACSCanto™ II flow cytometer (Becton Dickinson, BD Biosciences).

For immunofluorescence analysis of γ-H2AX, irradiated cells were rinsed once with cold PBS, fixed with 4% of formaldehyde (Sigma-Aldrich) at 37°C for 15 min and washed three times with PBS. The cells were permeabilized with 0.5% Triton X-100 in PBS at 37°C for 10 min and non-specific binding sites were masked with goat serum (10% in PBS) at room temperature for 1h. Samples were incubated for 2 h at room temperature with anti- γ-H2AX (Ser139) (Abcam or Millipore Chemicon Upstate Clone JBW301, 1:100), followed by three washings in PBS and once in PBS + 0.1% Triton X-100. Cells were subsequently incubated at room temperature for 1 h with Alexa Fluor 488 goat anti-mouse secondary antibodies (Life Technologies, 1:250) and washed, as described above. Cover slips were then mounted on glass slides with Vectashield mounting medium

(Vector Laboratories) containing DAPI 0.2 µg/ml. Images were taken using a Leica TCS SP5 confocal microscope (Leica Microsystems) with 40X oil immersion objective.

Analysis of [6-4]-PPs and CPDs after UV irradiation

Dot blot and ELISA immunoassays were performed to determine the relative amounts of CPDs and [6-4]PPs in total genomic DNA from cells collected at different times after UV irradiation (Pontarin et al., 2012). Genomic DNA was isolated using the Puregene Core Kit B (Qiagen). The quality and quantity of DNA were assessed by using NanoDrop 1000 spectrophotometer (Thermo Scientific) and by agarose gel electrophoresis with ethidium bromide staining.

For Dot-Blot analysis, DNA was denaturated by boiling it for 5 min followed by rapid chill in ice. Equal volumes of Tris-EDTA buffer and 20X sodium chloride-sodium phosphate-EDTA buffer were added to samples. Using a dot-blot apparatus (BioRad), each sample was blotted in triplicate (10 ng DNA/dot for CPDs and 100 ng DNA/dot for [6-4]PPs) onto nitrocellulose membranes previously soaked in 6X SSC. DNA was fixed to the membranes by heating for 2 h at 80°C, after which the membranes were blocked in PBS/0.2% Tween 20 containing 5% (wt/vol) blocking agent (GE Healthcare) for 1 h at room temperature. The membranes were then incubated with either the CPD-specific monoclonal antibody TDM-2 (1:12,000) or the 6-4PP–specific monoclonal antibody 64M-2 (1:12,000) overnight at 4°C. After washing with PBS-Tween, the membranes were incubated with anti-mouse HRP-conjugated IgG (1:20,000) for 1 h at room temperature. After further washing, the signals were developed with the ECL Select Chemiluminescence Kit (GE Healthcare) in accordance with the manufacturer's instructions. The relative intensity of each signal was determined using Amersham Hyperfilm ECL film, acquired by scanner and quantified using ImageJ software.

For ELISA assay DNA was denatured boiling samples at 100°C for 10 min and rapidly chilled in a ice bath for 15 min. 50 µl of/well of denatured DNA (4 ng/µl for [6-4]PPs and 0.2 ng/µl for CPDs) were distributed to protamine sulfate-

coated PVC microplates in quadruplicate and completely dried overnight at 37°C. Plates were thus washed 5 times with 150 µl/well of PBS-T (0.05% Tween-20 in PBS) and incubated 30 min at 37°C with 150 µl/well of 2% goat serum in PBS to prevent non-specific antibody binding. Plates were washed 5 times with 150 µl/well of PBS-T and incubated 30 min at 37°C with 100 µl/well of mouse anti-CPDs (TDM-2, 1:1000, CosmoBio) or mouse anti-6-6PPs (64M-2, 1:1500, CosmoBio) antibodies in PBS. Plates were washed 5 times with 150 µl/well of PBS-T and incubated 30 min at 37°C with 100 µl/well of Biotin-F(ab')2 fragment of goat anti-mouse IgG (H+L) secondary antibody (1:2000, Life Techonolgy) in PBS. Plates were washed 5 times with 150 µl/well of PBS-T and incubated 30 min at 37°C with 100 µl/well of Peroxidase-Streptavidin (1:10000, Life Technology) in PBS. Plates were washed 5 times with 150 µl/well of PBS-T and once with 150 µl/well of Citrate-phosphate buffer (Citric acid monohydrate 5.10 g, Na_2HPO_4 7.30 g, ddH_2O 1 l, pH 5.0). Buffer was thus thrown away and plates were incubated 30 min at 37°C with 100 µl/well of substrate solution (o-Phenylene diamine 8 mg, H_2O_2 30% 4.7 µl, citrate-phosphate buffer 20 ml). Enzyme reaction was stopped distributing 50 µl/well of 2 M H_2SO_4 and absorbance was read at 492 nm with a SynergyTM HT multi-mode 96-well plate reader (BioTek).

Flourometric Analysis of DNA Unwinding (FADU)

Fluorometric analysis of DNA unwinding (FADU) was performed according to Pontarin et al., 2012: Solution B (0.25 M myoinositol, 1 mM MgCl2, and 10 mM Na-phosphate buffer, pH 7.2), Solution C (9 M urea, 10 mM NaOH, 5 mM cyclohexane-diaminetetraacetate, 0.1% SDS), Solution D (0.45 vol/vol solution C in 0.2 M NaOH), Solution E (0.40 vol/vol solution C in 0.2 M NaOH) and Solution F (1 M glucose and 14 mM dithiotreitol).

For FADU analyses, the cells were trypsinized at fixed time points after UV irradiation, counted, and washed twice with cold PBS. At each time point, the cells were suspended in solution B and divided (triplicate samples of $3.5x10^5$ cells/0.1 mL of solution B) into each of three sets of tubes: B, blank samples, completely unwound DNA; T, total fluorescence of native DNA, and P, samples for determination of DNA unwinding rate. After addition of 0.1 mL of solution C,

all samples were incubated on ice for 10 min. Samples T were neutralized with 0.2 mL of solution F with mixing. Then 0.05 mL of solution D and 0.05 mL of solution E were added very gently and without mixing to each triplicate sample B, P, and T. After a 30-min incubation on ice, samples B were sonicated for 15 min at 50 W in a Fisher 300 sonicator and then incubated for 1 h at room temperature. Samples P were incubated in parallel for 1 h at 16 °C, and samples T were kept on ice for 1 h. Denaturation was stopped by adding 0.2 mL of solution F and chilling on ice. The percentage of dsDNA was estimated by staining with EtBr (0.5 μg/mL in 13.3 mM NaOH), which selectively binds to dsDNA. Fluorescence was read in a Jasko 821-FP spectrofluorimeter (excitation, 520 nm; analyzer, 590 nm). The % dsDNA values (D) were calculated from the fluorescence of B, T, and P samples using the equation $D = (P - B)/(T - B)$.

Trans-activation assay

For trans-activation assay, $0.3x10^6$ NIH-3T3 cells were seeded in 6-well plate and incubated in normal conditions for 24 h. Cells were transfected with 100 ng of pSCT1-lacZ, 500 ng of luciferase reporter constructs and the indicated amounts of expression vectors using JetPEI (Polyplus Transfection). Briefly, 10 μl lysate were added to 100 μl 1 mM ATP (Sigma), 10 mM MgAc, 0.1 mg/ml BSA in 250 mM Tris-HCl, pH 7.5. Samples were injected with 100 μl 200 μg coenzyme A, 30 μg/ml luciferine (Sigma) in 12.5 mM PIPES, pH 6.5. Light emission was measured after a delay of 0.3 seconds during a 10 second interval.

Transfection efficiency was normalized by β-galactosidase activity by incubating 5 μl of lysate in 140 μl of MUG reaction buffer (10 mg/ml 4-methylumbelliferone β-D-galactopyranoside in DMF, 100 mM Na_3PO_4, 2 mM $MgCl_2$, pH 8.0) for 30 min at 37°C protected from light. The reaction was stopped by addition of 100 μl of MUG reaction-stop buffer (300 mM Glycin, 15 mM EDTA, pH 11.5) and fluorescence was measured (360/460 nm, excitation/emission) with a Synergy™ HT multi-mode 96-well plate reader (BioTek).

Real-time Bioluminescence Monitoring

$0.3x10^6$ NIH-3T3 cells were seeded in 3.5 mm dishes and incubated in normal conditions for 24 h. Cells were transfected with 100 ng of pSCT1-SEAP and 1500 ng of luciferase reporter constructs using JetPEI (Polyplus Transfection). 24 h after transfection cells were synchronized with 100 nM dexamethasone, washed 2 times and incubated with red phenol-free medium supplemented with 5% FCS and 0.1 mM luciferin. Plates were thus loaded into the Lumicycle apparatus (Actimetrics) and bioluminescence was continuously recorded for 4-5 days. Transfection efficiency was normalized by quantification of secreted alkaline phosphatase (SEAP). From every sample, 20 µl of culture medium were collected before dexamethasone shock and processed by the chemiluminescence SEAP Reporter Gene Assay kit (Roche) according to the manufacturer. Light emission was measured during an interval of 1 sec using a MicroLumat Plus microplate luminometer (Berthold).

Unscheduled DNA Synthesis (UDS)

Immediately after irradiation, the medium of quiescent C63 cells was substituted with pre-wormed DMEM-0.1% FBS supplemented with 0.3 µM of [3H]-TdR (specific activity 20,000 CPM). At specific time-points cells were harvested, centrifuged at 4°C and washed twice with cold PBS. Pellets ($0.6x10^6$ cells) were thus dissolved in 150 ul of lyses buffer (10 mM Tris-HCl pH 7.4, 10 mM NaCl, 5% SDS and 10 mM EDTA). Lysates were spotted in glass microfiber GF/C filters and dried 10 min under infrared lamps. Filters were thus washed 5 times in trichloroacetic acid (TCA), 2 times in 100% ethanol and dried again under infrared lamps. Filters were placed inside scintillation tubes with 4 ml of scintillation liquid. Radioactivity of samples was measured for 10 min/sample and showed as count per minute/10^6 cells (CPM/10^6 cells).

Results

The Synchronization of Circadian Gene Expression in Quiescent Human Fibroblasts

Since our previous finding and literature data have shown that cell cycle can modulate DNA repair activity, we decided to explore the contribution of circadian clock alone in regulating DNA repair by carrying cells to a quiescent status (G0). Human primary skin fibroblasts (C63) were thus allowed to grow until confluence and then cultured in low-serum medium (0.1%) for 7 more days. Flow cytometer analysis of cell cycle distribution (Figure 1|A) confirmed that 98.6% of the fibroblasts were blocked in the G1-phase while 1.3% were in the S or G2/M phases (0.1%).

Quiescent C63 cells were then incubated for 2 h with dexamethasone, and mRNA was collected every 4 hours from the 12th to 44th hour of circadian time (CT). Relative amounts of BMAL1 and PER2 transcripts were analyzed by real-time PCR (Figure 1|B). Synchronization with dexamethasone induced a rythmic expression of BMAL1 and PER2 mRNAs in quiescent cells, as has been reported in cycling cells (Nagoshi et al., 2004). The time course of PER2 expression showed two negative peaks at CT 16 and CT 40 and a positive one at CT 28, with an overall period of about 24 h. BMAL1 mRNA exhibited two antiphase PER2 transcriptional oscillations showing a negative peak at CT 24-28 and a positive one at CT 36-40. The rhythmicity in qRT-PCR was confirmed by Western blot as BMAL1 and PER2 protein levels were quantified in the CT 12-48 window (Figure 1|C and |D). On the basis of these results, it was possible to identify two time points separated by a 12 h interval so that genotoxic stress by UV irradiation could be administered at two opposite ends of BMAL1 and PER2 expression. We decided to follow the PER2 protein concentration, which reached a nadir region corresponding to CT 16 and a zenith one corresponding to CT 28.

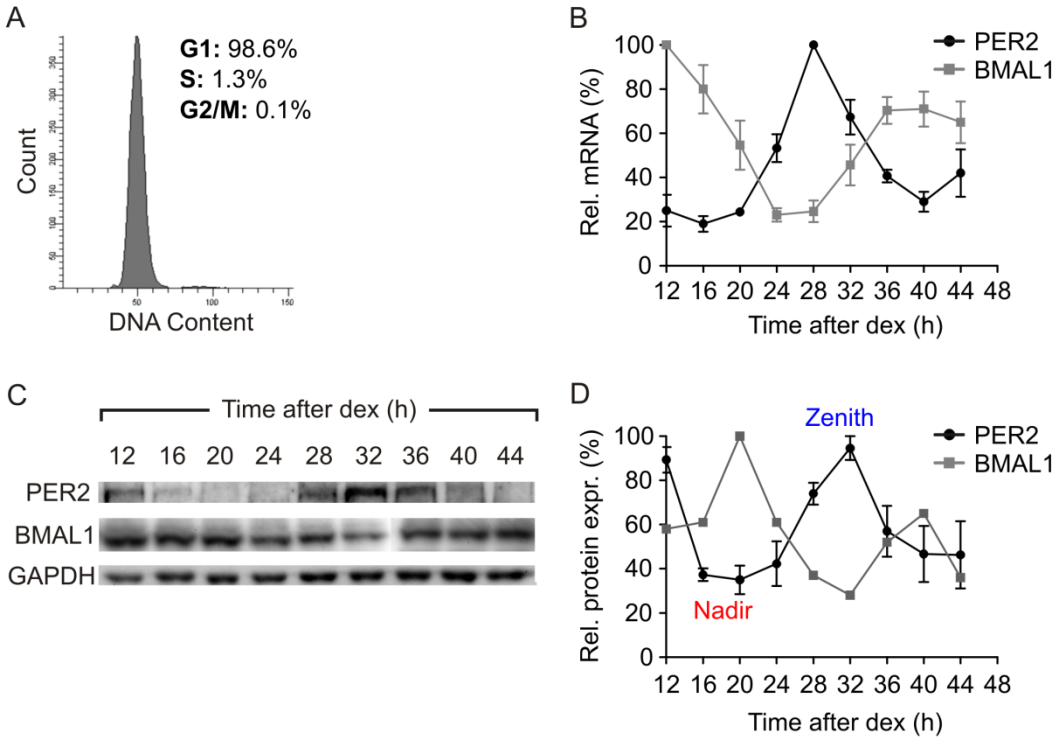

Figure 1 | The synchronization of quiescent skin fibroblasts. (A) The cell cycle distribution of C63 fibroblasts after 7 days in DMEM + 0.1% FBS. The X axis shows DNA content; the Y axis shows the number of cells. **(B)** The relative mRNA levels of PER2 and BMAL1 were analyzed every 4 h after synchronization over a 32 h interval **(C)** A representative Western Blot. **(D)** BMAL1 and PER2 relative protein levels measured every 4 h over a 32 h interval.

DNA Repair is Affected by Circadian Time

While it is well known that the phosphorylation of histone H2AX on S139 (γ-H2AX) after ATM activation is an important step in double-strand break (DSB) repair to assemble signaling and repair protein complexes, the functional role of this event after UV irradiation is less apparent. Experiments carried out in cells mutant on S139 showed that this site has no influence on UV damage response, indicating that γ-H2AX is a biomarker rather than a participant in the response (Cleaver 2011). The presence of γ-H2AX is correlated during the NER process to persistent DNA gaps created by the excision of photoproducts, and its disappearance signals that the gaps have been filled by dNTP polymerization (Cleaver 2011; Pontarin et al., 2012). Our next step, then, was to analyze γ-H2AX

content in skin fibroblasts irradiated at the zenith and nadir of PER2 protein by flow cytometry (Figure 2).

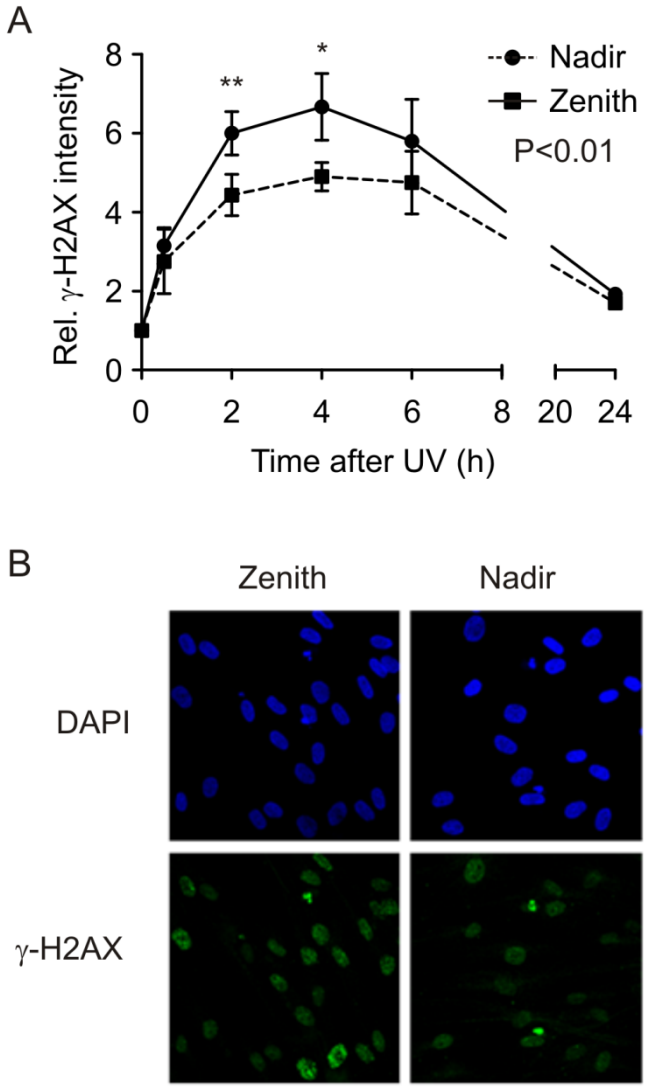

Figure 2: Histone H2AX phosphorylation after UV-induced DNA damage. (A) Flow cytometer analysis of γ-H2AX in C63 irradiated at the nadir and zenith values of PER2. **(B)** A representation of γ-H2AX (green) in quiescent C63 cells 4 h after irradiation. The nuclei were counterstained with DAPI (blue). The experiments were carried out in triplicate and plotted as mean ± SEM. The P-value refers to 2-way ANOVA. *P<0.05, **P<0.01, Bonferroni post-test.

The γ-H2AX signal started to increase 0.5 h after irradiation in the nadir-irradiated cells, reached a peak at 4 h, and decreased until 24 h at which time the

fluorescence intensity was similar to that of the non-irradiated cells. The kinetics of the γ-H2AX fluorescence signal in the zenith-irradiated fibroblasts followed the same parabolic trend as did the nadir-irradiated ones, but with significantly higher values, especially at 2 h (4.4 vs. 6, nadir vs. zenith, respectively) and 4 h (4.9 vs. 6.6, nadir vs. zenith, respectively) after irradiation.

The main classes of UV-induced photoproducts are cyclobutane pyrimidine dimers (CPDs), which represent 75% of all the dimers formed, and 6-4 pyrimidone photoproducts ([6-4]PPs), which represent the remaining 25%. During the early steps in the NER process, the pyrimidine dimers are recognized by protein complexes (XPC, XPA) which bind DNA and recruit specific endonucleases (XPG and XPF) that remove the dimers by cutting the DNA strands at the damaged site. Strand integrity is thus restored by repair synthesis activity after which the new polynucleotide segment is ligated to the DNA molecule.

Using specific antibodies, it was possible to monitor the kinetics of [6-4]PP removal and CPDs by Dot-blot assay (Figure 3|A and |B, respectively). Quiescent skin fibroblasts were synchronized with dexamethasone incubation and divided into two groups: one was irradiated at the CT corresponding to the nadir (CT 16) and the other at the one corresponding to the zenith (CT 28) of PER2 protein expression. The cells were harvested at different times (0, 0.5, 1, 3, 6 and 24 h) after UV irradiation, and total DNA was extracted. The results of Dot-blot showed that both groups efficiently removed the [6-4]PPs within the first 3 h after irradiation, although the kinetics of fibroblasts irradiated at the zenith (CT 28) were significantly slower with respect to the nadir (CT 16) time. The difference was marked at 0.5 h after irradiation (20% vs. 44% of 6-4PPs removed, zenith vs. nadir) and persisted up to 1 h after irradiation (32% vs. 69% of 6-4PPs removed, zenith vs. nadir).

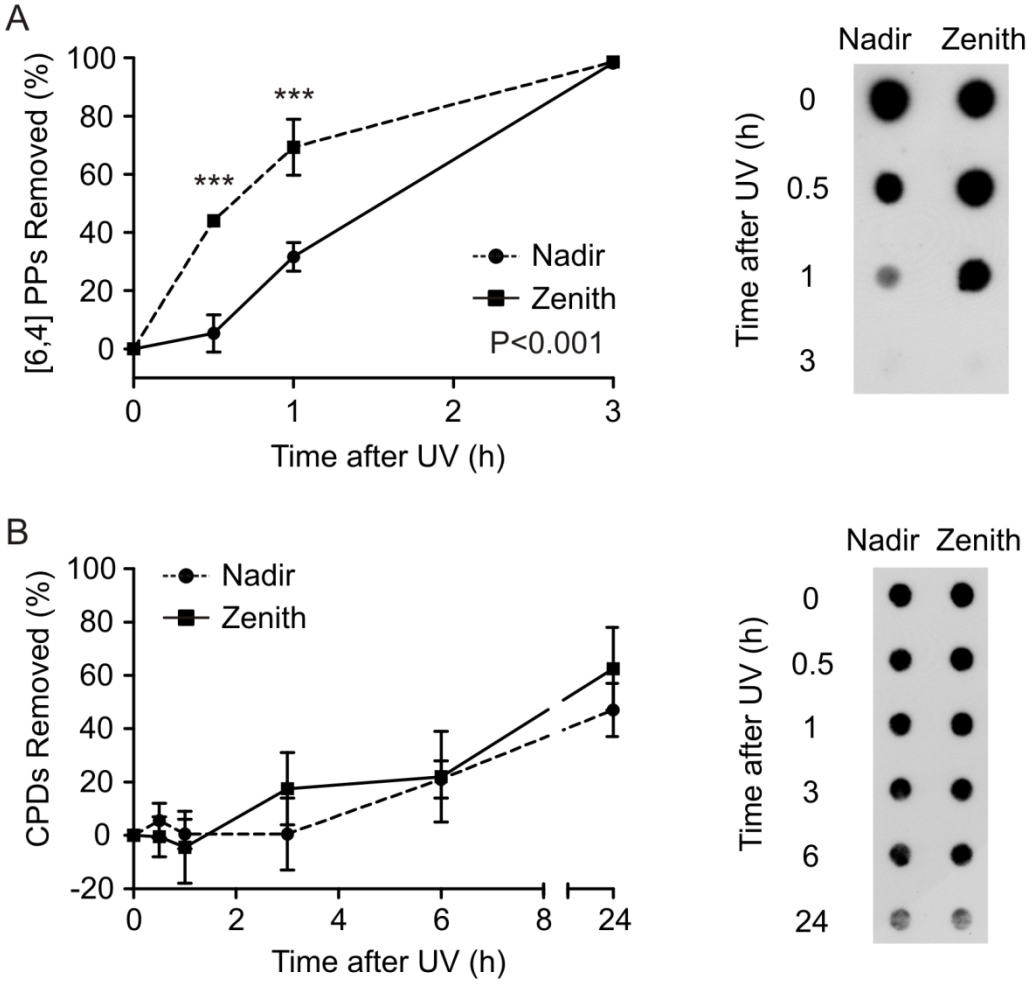

Figure 3: Analysis of [6-4]PP and CPD removal by Dot-blot. (A) The kinetics of [6-4]PP removal in C63 irradiated with 12 J/m^2 of UV light at the zenith (dashed line) and the nadir (solid line) of PER2 protein and a representative Dot-blot (right). **(B)** The kinetics of CPD removal in C63 irradiated with 12 J/m^2 of UV light at the zenith (dashed line) and nadir (solid line) of PER2 protein expression and a representative Dot-blot (right). The experiments were carried out in triplicate and plotted as mean ± SEM. The P-value refers to a 2-way ANOVA. ***P<0.001, Bonferroni post-test.

CPD removal took a considerably longer time with respect to [6-4]PP and nearly no repair took place within the first 6 h after irradiation (Figure 3|B). About 50% of the CPDs was removed within 24 h after irradiation, but there were no differences between the two groups, suggesting that the circadian clock affects the recognition and removal of damaged sites only during the early stages of the

repair process and, over time, dimer removal occurs efficiently at the zenith as well as at the nadir.

The second step in the NER process consists in restoring the integrity of the DNA molecule by filling in the 27–30 nucleotide gap created by the dimer removal. This process requires DNA polymerases δ or ε as well as the accessory replication proteins and a correctly balanced pool of dNTPs. Prior to the ligation step, alkali treatment of the nicked DNA produces single-stranded regions at the sites of the initial damage. The amounts of double-stranded DNA (dsDNA) provides, thus, a measure of the ongoing, although incomplete, repair process (Baumstark-Khan et al., 2000; Erixon et al., 1979). This parameter can be quantified by fluorometric analysis of DNA unwinding (FADU) (Pontarin at al., 2012) from the fluorescence of DNA-bound EtBr. Immediately after damage, the fluorescence of the DNA-bound EtBr shows a rapid drop that is proportional to the number of remaining gaps. When the nicks are sealed by resynthesis, the ensuing recovery of fluorescence indicates that the gap-filling process has been completed.

The FADU assay was used to investigate the time course of DNA repair in the clock-synchronized C63 cells irradiated with 12 J/m^2 of UV light at the nadir and the zenith of PER2 expression (Figure 4). In both groups the fluorescence intensity dropped immediately after irradiation following a rapid loss of dsDNA associated to the excision repair step. Proceeding slowly, the dsDNA recovery was nearly complete within 24 h, and interesting differences were noted between the zenith- and nadir-irradiated cells. First, the former contained less dsDNA at all the time-points with respect to the latter, suggesting that slower DNA repair kinetics reflected a higher residual damage. Second, after the initial drop in the dsDNA percentage, the nadir group began a rapid recovery, as opposed to the zenith one in which the quantity of dsDNA was unaltered for up to1 h after irradiation due to the slower kinetics of [6-4]PP removal and/or defective DNA synthesis. Finally, 6 h after irradiation, the zenith group contained only 68% of dsDNA, as opposed to 88% in the nadir group.

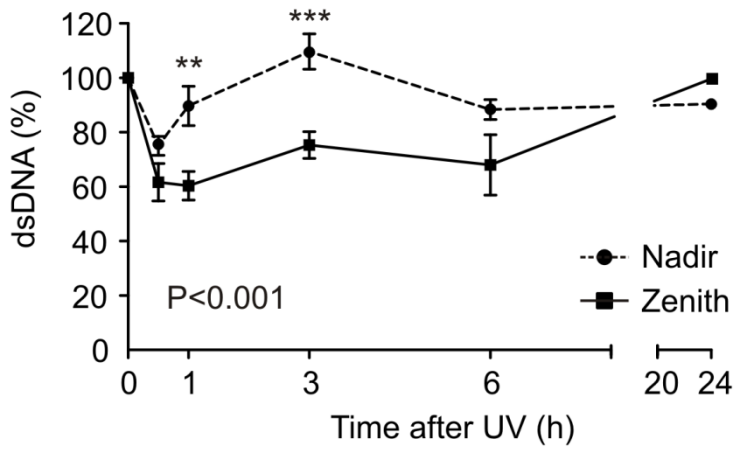

Figure 4 | Fluorometric analysis of DNA unwinding (FADU). The experiments were carried out in triplicate and plotted as mean ± SEM. The P-value refers to a 2-way ANOVA. **P<0.01, ***P<0.001, Bonferroni post-test.

XPA Is Not a Clock-Controlled Gene

We next assessed if differences in the removal of the photoproducts during early NER steps could be attributed to a different expression of the XPA protein during the initial phase of dimer recognition and signal transduction. Some investigators have recently reported that repair of UVB-induced DNA damage in mice is defective at night due to decreased levels of XPA-mediated excision repair (Gaddameedhi et al., 2011). Those same authors, however, later reported that mice mutant for different circadian clock genes are indistinguishable from the wild-type in their response to UV irradiation (Gaddameedhi et al., 2012).

We set out to verify if the amount of XPA protein, which is supposedly regulated by the circadian clock, shows oscillations during 12-44 hours of CT in quiescent C63 skin fibroblasts. Our results showed that there were no appreciable variations in XPA protein abundance during the 12-44 h time-interval in which protein expression controlled by the circadian clock could oscillate (Figure 5|A). We then analyzed XPA expression also in NIH-3T3 cells transfected with a plasmid coding for the firefly luciferase driven by a mouse XPA promoter (Figure 5|B). Once again, the cells were shocked with dexamethasone, and the

bioluminescence was monitored in real-time for 4 days using the Lumicycle apparatus (Actimetrics). Just as the C63 cells, XPA::luciferase did not show circadian rhythmicity, in particular when compared to BMAL1::luciferase and PER2::luciferase, which were considered the circadian positive controls, suggesting that XPA expression does not follow circadian rhythms.

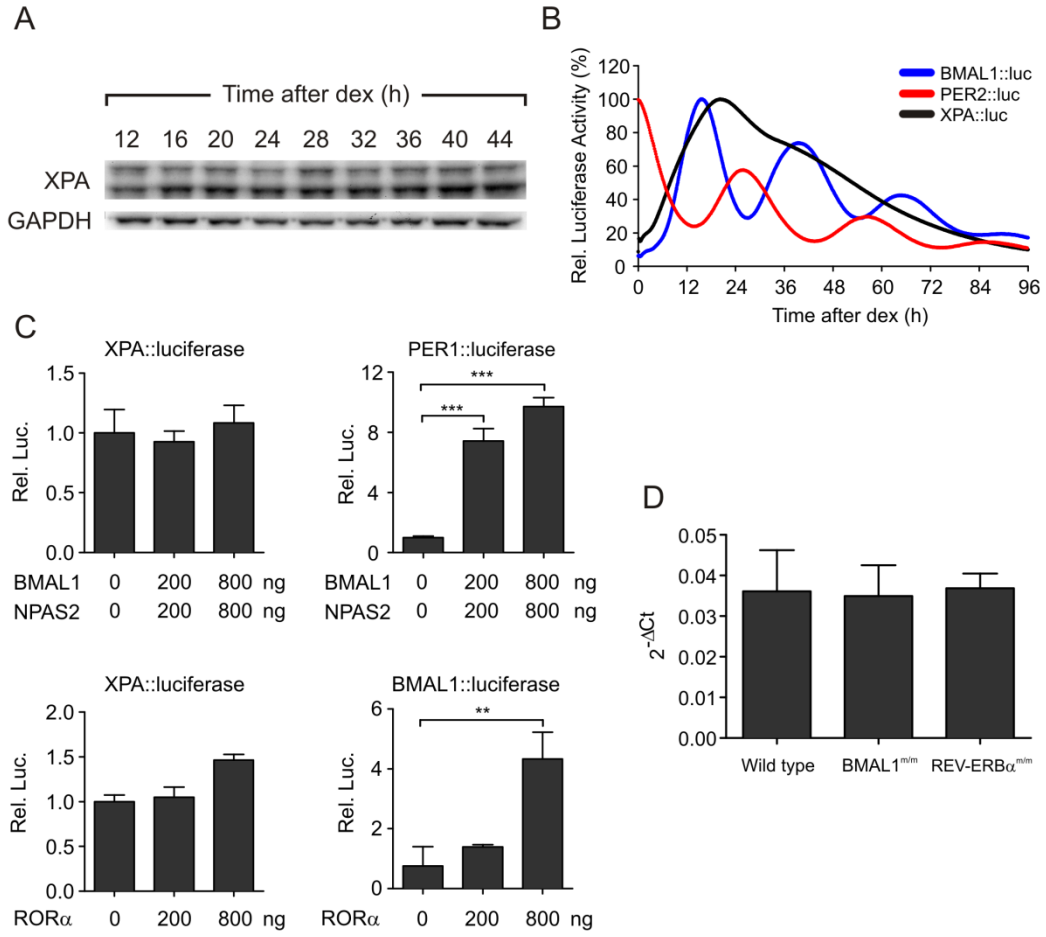

Figure 5 | The effect of the circadian clock on XPA expression. (A) The protein in XPA was analyzed in human quiescent C63 fibroblasts every 4 h after synchronization during a 32 h time-interval **(B)** Real-time bioluminescence of mouse XPA::luciferase, BMAL1::luciferase, and PER2::luciferase in NIH-3T3 cells after synchronization with dexamethasone. **(C)** Luciferase trans-activation assay. Mouse BMAL1-NPAS2 and RORα transcriptional activities were tested on mouse XPA::luciferase in NIH-3T3 cells. Data from 3-4 independent experiments are expressed as mean ± SEM. Transfection efficiency was normalized by βGal. **(D)** The relative level of XPA mRNA in primary dermal fibroblasts deriving from wild type, BMAL1 mutant and REV-ERBα mutant mice. ** $p<0.01$, *** $p<0.001$, ANOVA was followed by Bonferroni post-test.

We then attempted to verify if the main clock transcription factors interact with the XPA promoter and if they could be involved in its transcription. Utilizing a luciferase transactivation assay, we analyzed the dose response of XPA::luciferase to transfection by testing different amounts of BMAL1, NPAS2, and RORα coding plasmids (Figure 5|C). In contrast to the strong activation observed for PER1::luciferase, which was highly significant for both plasmid quantities assessed (7.6 folds and 10.4 folds, 200 ng and 800 ng, respectively. $p<0.001$), no relevant changes were detected in the expression of XPA::luciferase after co-transfection with BMAL1/NPAS2. As opposed to a strong activation of BMAL1::luciferase, transfection with RORα did not produce significant modifications in XPA::luciferase expression.

We investigated, finally, the effect of mutations in components of the circadian clock on XPA transcripts. Mouse dermal fibroblast (MDF) cultures were obtained from the dorsal flanks of wild type newborn mice and mice carrying mutations in BMAL1 or in REV-ERBα genes, and the relative amount of XPA transcript was analyzed by real-time PCR. mRNA expression was unmodified in both the $BMAL1^{m/m}$ and $REV\text{-}ERB\alpha^{m/m}$ mutants in the MDFs as compared to the transcripts collected from the wild type cells, demonstrating that the circadian clock does not control XPA transcription (Figure 5|D).

Clock Control of DNA Damage Sensitivity and Early Response to UV-irradiation

We next investigated if differences in the kinetics of dimers removal are correlated to different sensitivities to UV light when human fibroblasts are irradiated at various circadian times. To investigate the photoproduct amount formed immediately after UV irradiation more precisely, we analyzed CPD and [6-4]PP induction using an ELISA assay to evaluate the amount of photoproducts formed immediately after exposure to UV irradiation. Surprisingly, our results showed that in addition to the faster kinetics of [6-4]PPs removal, fibroblasts

irradiated at the nadir of PER2 induce a significantly higher formation of both [6-4]PPs and CPDs with respect to zenith-irradiated cells (Figure 6|A). This finding was confirmed by the outcome of DNA resynthesis by the Unscheduled DNA Synthesis assay (UDS). We found, in fact, a higher incorporation of [3H]-TdR within the first 30 min in nadir- with respect to zenith-irradiated fibroblasts (Figure 6|B). Over time, however, the incorporation of [3H]-TdR increased in both the cell groups as the repair resynthesis step of NER progressed, with little or no differences between them.

To evaluate if different sensitivities to UV-induced damage can be caused by the circadian time at which the cells are irradiated, we transfected the cells with siRNAs targeting BMAL1 gene expression. In those experimental conditions, fibroblasts were found to become arrhythmic even after dexamethasone shock (Figure S1); as a consequence, nadir and zenith cells had the same level of clock gene expression at the time of irradiation. Fibroblasts transfected with siBMAL1 or siCTRL were thus irradiated at CT 16 and CT 28, and dimer formation was analyzed immediately after UV exposure by ELISA assay. As expected, the difference in the amount of [6-4]PPs formed at the CT of radiation persisted in the fibroblasts transfected with siCTRL, which retained an intact circadian rhythmicity, but it was totally abrogated in cells transfected with siBMAL1 (Figure 6|C). The amount of dimers formed in siBMAL1-transfected fibroblasts was almost the same as that observed in siCTRL-transfected cells at the zenith of PER2 (when BMAL1 reached the minimum expression level), suggesting that BMAL1 could play an important role in DNA sensitivity to UV light. Interestingly, when the removal of photoproducts early after irradiation (0.5 and 1 h) was analyzed, we found that despite the low level of photoproducts formed at the time of irradiation, zenith-irradiated cells exhibited a delay in damage removal (Figure 6|D). One half hour after irradiation, in fact, no removal activity was observed in those cells as opposed to 44% of [6-4]PPs removed in nadir-irradiated cells. By silencing BMAL1 expression, the efficiency of DNA damage removal was markedly reduced in nadir-irradiated fibroblasts in which 23% of dimer had been removed 0.5 h after irradiation with respect to 55% in cells transfected with

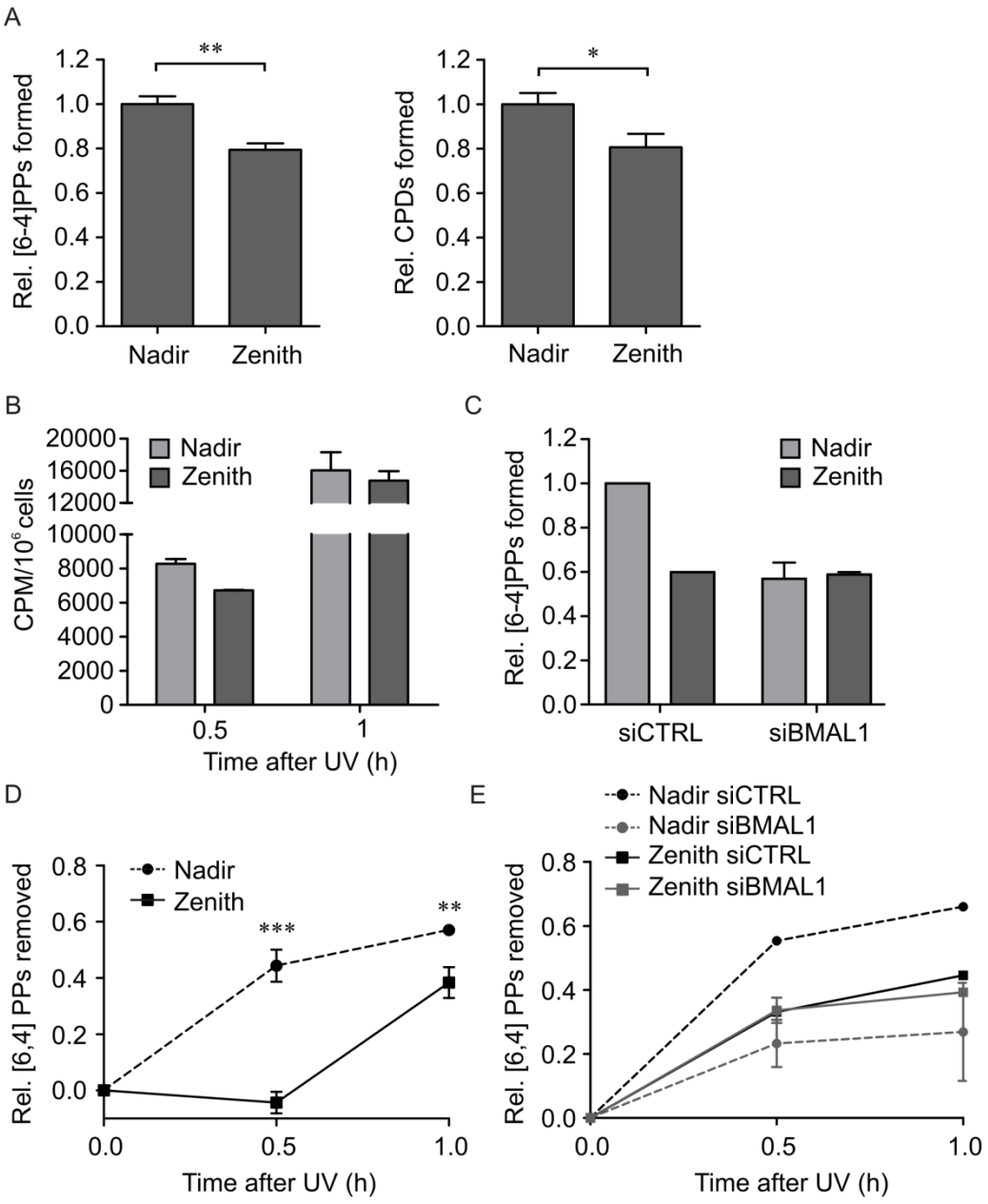

Figure 6 | Analysis of DNA sensitivity to UV and early DNA repair activity. (A) The quantity of [6-4]PPs and CPDs immediately after UV irradiation was determined using an ELISA assay. **(B)** Unscheduled DNA Synthesis (UDS) in nadir- and zenith-irradiated fibroblasts **(C)** [6-4]PPs in nadir and zenith-irradiated cells after they were transfected with siBMAL1 and siCTRL **(D)** The kinetics of [6-4]PP removal by ELISA assay in the nadir- and zenith-irradiated fibroblasts. **(E)** Transfection with siBMAL1 reduced the efficiency of [6-4]PP removal in nadir-irradiated cells. **P<0.01, ***P<0.001, Bonferroni post-test.

siCTRL and irradiated at the same circadian time (Figure 6|E). In that case as well, the efficiency of DNA repair in siBMAL1-transfected fibroblasts was almost the same as that observed in siCTRL-transfected cells at the zenith of PER2 when BMAL1 reached the minimum expression level, confirming BMAL1's role in the UV-induced DNA repair process.

Discussion

The role of the circadian clock in DNA damage response (DDR) has attracted increasing attention recently because of its possible implications to cancer development (Gery et al, 2010; Gaddameedhi et al., 2011). While the relationships between the circadian clock, cell cycle control, and apoptosis have been clarified to some extent (Gery et al., 2006; Kowalska et al., 2012), the effect of the circadian clock on DNA damage response pathways is still unclear (Gaddameedhi et al., 2012; Kondratov, 2012). This work aimed to analyze cell response to UV irradiation in clock-synchronized human skin fibroblasts in the attempt to evaluate if and how the efficiency of DNA repair varies over a 24 h time-interval. Quiescent fibroblasts were incubated with dexamethasone to induce a robust rhythmic expression of circadian clock genes. After clock synchronization, we identified two time-points separated by a 12 h interval at which cells could be irradiated when clock gene expression was at two opposite levels. Following PER2 protein expression, skin fibroblasts were irradiated at CT 16, which corresponds to the PER2 nadir, and at CT 28 h, which corresponds to its zenith.

Although preliminary, our results showed significant differences in DNA repair when UV irradiation was performed at the zenith and nadir of PER2 protein expression. Analysis of the γ-H2AX quantity and the state of winding of the DNA double helix revealed that greater residual damage persists in the zenith-irradiated cells due to slower DNA repair activity. This finding was supported by the Dot-blot kinetics of [6-4]PP removal, showing a significant delay within the first 3 hours after irradiation at the PER2 zenith with respect to its nadir. No difference was, instead, noted in CPD removal during the first hours after irradiation at the PER2 nadir and zenith circadian times. The kinetics of removal of this type of photoproduct was relatively slow and 24 h after irradiation 40-50% of the initial CPDs was still present; no significant differences were noted between the two irradiation groups. As opposed to authors reporting on the circadian oscillation of XPA protein expression (Kang et al., 2009; Gaddameedhi et al., 2011), we did not

observe any rhythmicity in its expression during a 32 h time-interval after circadian clock synchronization. Moreover, when fibroblasts were assessed for transactivation assay or derived from mice mutant in BMAL1 or REV-ERBα genes, there was no correlation between XPA and the circadian clock. Our results, in addition to reports that other proteins involved in the NER system (Kang et al., 2009) are not linked to circadian oscillations, led us to conclude that NER is not directly controlled by the circadian clock.

Interestingly, when we analyzed the induction of CPDs and [6-4]PPs immediately after irradiation, we found that fibroblasts irradiated at the nadir of PER2 formed a significantly higher amount of both photoproducts with respect to zenith-irradiated ones. Unscheduled DNA Synthesis assay (UDS) confirmed this result showing that, within the first 30 min of irradiation, the incorporation of [3H]-TdR during the resynthesis step of NER was higher in cells irradiated at the nadir of PER2 expression with respect to zenith-irradiated cells. By transfecting the fibroblasts with siRNAs targeting BMAL1 gene expression, which was reduced to 9%, the differences in the amounts of [6-4]PPs disappeared, but they persisted when the fibroblasts were transfected with siCTRL. Moreover, by silencing BMAL1 expression, the efficiency with which [6-4]PPs were removed was reduced with respect to control cells, and differences between the nadir and and the zenith-irradiated cells were abolished.

Taken together, these results led to two major conclusions. First of all, because cells transfected with siBMAL1 were arrhythmic with respect to siCTRL transfected cells, which retained an intact circadian clock, we demonstrated that DNA damage formation and repair efficiency are strictly dependent on the circadian time of UV exposure. Second, although BMAL1 is not essential to carry out DNA repair and the molecular mechanisms underlying it are not yet fully understood, we found that it enhances the efficiency of dimer removal.

Geyfman et al. (2012) recently reported that mouse epidermis had different susceptibilities to UVB-induced DNA damage at different times during a 24 hour period of the circadian clock. The authors correlated the higher amount of

photoproducts formed at Zeitgeber Time (ZT) 20, with respect to ZT 8, to the DNA replication phase that culminates at ZT 20, making DNA more sensitive to UV damage. Unlike the experiments carried out by those authors, ours were conducted in quiescent cells blocked in the G1/G0 phase; we cannot, as a consequence, explain the different susceptibilities to UV light by events dependent on cell cycle phases. As demonstrated by the higher amount of photoproducts formed in cells with relaxed as opposed to more condensed chromatin, chromatin conformation could also play an important role in susceptibility to UV-damage (Ogara et al., 2013). It is well known that the chromatin remodeling process is strictly regulated by the circadian clock, as demonstrated by the circadian modulation of RNAPII recruitment and the rhythmicity of chromatin remodeling on a genome-wide scale (Koike et al., 2012). Access to genomic DNA for activities such as DNA repair should be facilitated by processes that directly alter the chromatin structure leading to increased DNA accessibility. Since different conformational states of chromatin could affect both the susceptibility to DNA damage and the repair processes, we speculate that the circadian clock regulates DNA damage response by transcription-coupled chromatin remodeling.

Supporting information

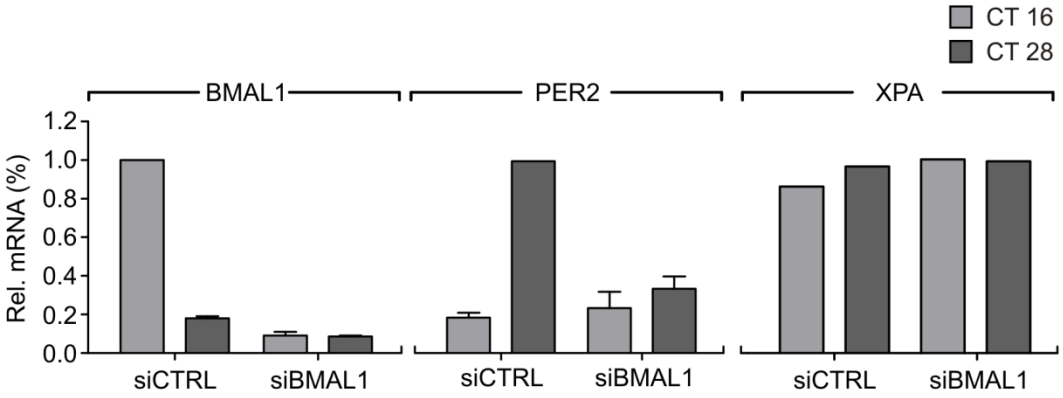

Figure S1 | Circadian clock disruption by transfection of C63 fibroblasts with siBMAL1. Fibroblasts transfected with siBMAL1 were arrhythmic even after dexamethasone shock; as a consequence, nadir and zenith cells had the same level of BMAL1 and PER2 expression at the time of irradiation. As expected, clock disruption had not influence on XPA gene expression.

CONCLUSIONS AND FUTURE PERSPECTIVES

In the first part of this project our attention was focused on evaluating if different levels of efficiency characterize DNA DSB repair during cell cycle progression. Since NHEJ and HR can virtually operate at the same time in the G2- with respect to the G1-phase (in the latter only NHEJ is active) we hypothesized that the efficiency of DSB repair could vary. We thus set out to examine the kinetics of γ-H2AX formation and disappearance after irradiation using increasing doses of γ-rays and comparing the efficiency of DSB rejoining during cell cycle progression. Using advanced fluorescence quantification techniques, we found that in the G2-phase cells, in which the frequency of gaps was significantly higher after irradiation, DNA repair proceeded faster with respect to that in G1 cells both immediately and long after irradiation. In agreement with these results, G2-phase cells treated with the HR inhibitor exhibited a higher level of unrepaired DSBs 6 hours after irradiation. When we compared the repair rate in G1- and G2-phase cells after a similar amount of initial DNA damage, we were, moreover, able to confirm that the HR repair system contributed to rejoining DSBs; repair efficiency was, in fact, higher in the G2 phase during which the HR and NHEJ cooperate with respect to that in the G1 cells in which only the NHEJ is active.

We then assessed if impairment in NHEJ affects the efficiency of HR in rejoining DSBs in CCD-34Lu treated with the DNA-PKcs inhibitor, NU7026, and in DNA-PKcs deficient M059J cells. In both conditions, the kinetics of γ-H2AX demonstrated that DSB repair was strongly affected by DNA-PKcs absence in all phases of the cell cycle, even in the G2-phase when HR should be active. This finding confirmed previous observations demonstrating that DSB rejoining is strictly dependent on the integrity of NHEJ repair system.

When we set out to grow human fibroblasts until they reached confluence followed by serum deprivation (0.1% FBS), we were able to maintain cell cultures in a long-term quiescence of up to 14 days with a good level of cell viability. Methods aiming to accurately quantify the repair of UV-induced DNA damage were utilized to assess if it was affected by the absence of the ribonucleotide

reductase subunit p53R2, which is responsible for the maintenance of the dNTP pool in quiescent cells. Consistent with the fact that dNTPs are required in NER only toward the end of the process after the damaged sites had been excised, our results showed that the early steps involving recognition and removal of the cross-links in the damaged DNA function normally in the quiescent mutant cells as well as in the control ones. The effect of mutations in DNA repair was evident during the FADU experiments when the irradiated mutant cells contained more single-stranded DNA after alkaline treatment and required more time to reseal the nicked DNA demonstrating that damage was more extensive and persistent in these cells with respect to normal ones. The mutant cells also differed from the control ones with regard to the level of phosphorylated histone H2AX. Kinetic flow cytometer analyses of UV-irradiated quiescent cells demonstrated larger amounts and a greater persistence of γH2AX in the mutant fibroblasts with respect to those in the control ones. Overall the results showed that p53R2 protein in quiescent cells is necessary for optimal DNA repair after UV damage.

We assessed, finally, if the circadian clock could modulate the response to UV-induced DNA damages. After a short treatment with dexamethasone, we successfully synchronized primary cultures of quiescent human skin fibroblasts. The rhythmicity of PER2 and BMAL1 clock genes and protein expression was confirmed by qRT-PCR and Western blot analysis. By irradiating the cells at the nadir and zenith of PER2 protein expression, we noted that the sensitivity of DNA to UV light and the repair of the UV-induced damages were both higher at the PER2 nadir (when BMAL1 was at its zenith). In contrast to what was reported by Gaddameedhi et al., (2011), in these conditions we did not observe any rhythmicity in the expression of XPA protein, the main rate-limiting factor in NER. Experiments in which fibroblasts were transfected with the specific siRNA targeting BMAL1 gene confirmed that DNA damage formation and repair efficiency were strictly correlated to the circadian time of irradiation, although no direct involvement of clock components has been demonstrated.

On the whole, our results indicate that DNA damage response is an event that is strictly modulated by the rhythmicity of the cell cycle and the circadian

clock, with its efficiency varying over the 24 h cycle. This means that the time of exposure to genotoxic stress such as ionizing radiation and/or UV can be a factor that contributes to increasing the risk of genomic instability. We observed that both the sensitivity of DNA to UV and repair were higher when PER2 reached its nadir (and therefore BMAL1 its zenith), perhaps as a consequence of a particular chromatin structure which leads to increased DNA accessibility. We observed, nevertheless, that DSB rejoining was more efficient in S-G2 phases when both HR and NHEJ co-operate in DNA repair. In mice it was found that the PER2 nadir occurred during the day while the PER2 zenith and the S- G2-phases occurred during the night, distant from the UV component of sunlight. We speculate that the temporal separation of these events is a form of adaptation to environmental conditions (such as sunlight) and the disruption of this oscillatory equilibrium affects the DNA repair process.

Future research will aim to examine the molecular link between the circadian clock and DNA damage and repair induced by UV light. The question if different conformational states of chromatin can affect DNA damage incidence as well as the efficiency of the repair processes will be investigated. It is well known that the chromatin remodeling process is strictly regulated by the circadian clock, as demonstrated by the circadian modulation of RNAPII recruitment and the rhythmicity of chromatin remodeling on a genome-wide scale. It is possible then that the circadian clock regulates DNA damage sensitivity and repair by a transcription-coupled chromatin remodeling mechanism.

REFERENCES

- Antoch MP, Kondratov RV (2010) Circadian proteins and genotoxic stress response. Circ Res. 2010 Jan 8;106(1):68-78.
- Balsalobre A, Brown SA, Marcacci L, Tronche F, Kellendonk C, Reichardt HM, Schütz G, Schibler U (2000) Resetting of circadian time in peripheral tissues by glucocorticoid signaling. Science 289(5488):2344-7.
- Bartek J, Lukas C, Lukas J (2004) Checking on DNA damage in S phase. Nat Rev Mol Cell Biol 5:792-804.
- Baumstark-Khan C, Hentschel U, Nikandrova Y, Krug J, Horneck G (2000) Fluorometric analysis of DNA unwinding (FADU) as a method for detecting repair-induced DNA strand breaks in UV-irradiated mammalian cells. Photochem Photobiol 72(4):477-84.
- Bee L, Fabris S, Cherubini R, Mognato M, Celotti L (2013) The efficiency of homologous recombination and non-homologous end joining systems in repairing double-strand breaks during cell cycle progression. PLoS One. 2013 Jul 11;8(7):e69061.
- Beucher A, Birraux J, Tchouandong L, Barton O, Shibata A, Conrad S, Goodarzi AA, Krempler A, Jeggo PA, Löbrich M (2009) ATM and Artemis promote homologous recombination of radiation-induced DNA double-strand breaks in G2. EMBO J. 28(21):3413-27.
- Borgs L, Beukelaers P, Vandenbosch R, Belachew S, Nguyen L, and Malgrange B (2009) Cell ‘‘circadian’’ cycle: new role for mammalian core clock genes. Cell Cycle 8, 832–837.
- Boucas J, Riabinska A, Jokic M, Herter-Sprie GS, Chen S, Höpker K, Reinhardt HC (2012) Posttranscriptional regulation of gene expression-adding another layer of complexity to the DNA damage response. Front Genet. 3:159.
- Chen Y, Sanchez Y (2004) Chk1 in the DNA damage response: conserved roles from yeasts to mammals. DNA Repair (Amst) 3(8-9):1025-32.
- Ciccia A, Elledge SJ (2010) The DNA damage response: making it safe to play with knives. Mol Cell. 40(2):179-204.

- Collis SJ, Boulton SJ (2007) Emerging links between the biological clock and the DNA damage response. Chromosoma 116(4):331-9.
- Cuadrado M, Martinez-Pastor B, Murga M, Toledo LI, Gutierrez-Martinez P, Lopez E, Fernandez-Capetillo O (2006) ATM regulates ATR chromatin loading in response to DNA doublestrand breaks. J Exp Med 203:297–303.
- Doi M, Hirayama J, Sassone-Corsi P (2006) Circadian regulator CLOCK is a histone acetyltransferase. Cell. 2006 May 5;125(3):497-508.
- Eccles LJ, O'Neill P, Lomax ME (2011) Delayed repair of radiation induced clustered DNA damage: friend or foe? Mutat Res 711:134–141.
- Erixon K, Ahnström G (1979) Single-strand breaks in DNA during repair of UV-induced damage in normal human and xeroderma pigmentosum cells as determined by alkaline DNA unwinding and hydroxylapatite chromatography: effects of hydroxyurea, 5-fluorodeoxyuridine and 1-beta-D-arabinofuranosylcytosine on the kinetics of repair. Mutat Res. 59(2):257-71.
- Esashi F, Christ N, Gannon J, Liu Y, Hunt T, Jasin M, West SC (2005) CDK-dependent phosphorylation of BRCA2 as a regulatory mechanism for recombinational repair. Nature, 434:598-604.
- Fabre F, Boulet A, Roman H (1984) Gene conversion at different points in the mitotic cycle of Saccharomyches cerevisiae. Mol Genet, 195:139-43.
- Franzolin E, Pontarin G, Rampazzo C, Miazzi C, Ferraro P, Palumbo E, Reichard P, Bianchi V (2013) The deoxynucleotide triphosphohydrolase SAMHD1 is a major regulator of DNA precursor pools in mammalian cells. Proc Natl Acad Sci U S A 110(35):14272-7.
- Friedberg EC (2001) How nucleotide excision repair protects against cancer. Nature Reviews Cancer 1:22-33.
- Gaddameedhi S, Selby CP, Kaufmann WK, Smart RC, Sancar A (2011) Control of skin cancer by the circadian rhythm. Proc Natl Acad Sci U S A. 108(46):18790-5.

- Gaddameedhi S, Reardon JT, Ye R, Ozturk N, Sancar A (2012) Effect of circadian clock mutations on DNA damage response in mammalian cells. Cell Cycle. 11(18):3481-91.
- Gandhi M, Evdokimova VN, Cuenco KT, Bakkenist CJ, Nikiforov YE (2013) Homologous chromosomes move and rapidly initiate contact at the sites of double-strand breaks in genes in G0-phase human cells. Cell Cycle 12(4): 547–52.
- Gery S, Koeffler HP (2010) Circadian rhythms and cancer. Cell Cycle 9(6):1097-103.
- Geyfman M, Kumar V, Liu Q, Ruiz R, Gordon W, Espitia F, Cam E, Millar SE, Smyth P, Ihler A, Takahashi JS, Andersen B (2012) Brain and muscle Arnt-like protein-1 (BMAL1) controls circadian cell proliferation and susceptibility to UVB-induced DNA damage in the epidermis. Proc Natl Acad Sci U S A 109(29):11758-63.
- Harrison JC, Haber JE (2006) Surviving the breakup: the DNA damage checkpoint. Annu Rev Genet 40:209-235.
- Hoeijmakers JH (2001) Genome maintenance mechanisms for preventing cancer. Nature 411(6835):366-74.
- Hughes M, Deharo L, Pulivarthy SR, Gu J, Hayes K, Panda S, Hogenesch JB (2007) High-resolution time course analysis of gene expression from pituitary. Cold Spring Harb Symp Quant Biol. 72:381-6.
- Johnson CH (2010) Circadian clocks and cell division: what's the pacemaker? Cell Cycle, 9(19):3864-73.
- Jenuwein T, Allis CD (2001) Translating the histone code. Science 293:1074–1080.
- Kang TH, Reardon JT, Kemp M, Sancar A (2009) Circadian oscillation of nucleotide excision repair in mammalian brain. Proc Natl Acad Sci USA. 106(8):2864-7.
- Kobayashi J, Iwabuchi K, Miyagawa K, Sonoda E, Suzuki K, Takata M, Tauchi H (2008) Current topics in DNA double-strand break repair. J Radiat Res. 49(2):93-103.

- Koike N, Yoo SH, Huang HC, Kumar V, Lee C, Kim TK, Takahashi JS (2012) Transcriptional architecture and chromatin landscape of the core circadian clock in mammals. Science 338(6105):349-54.
- Kondratov RV (2012) Cell-autonomous circadian DNA damage response: is the case closed? Cell Cycle. 11(20):3720-1.
- Kowalska E, Ripperger JA, Hoegger DC, Bruegger P, Buch T, Birchler T, Mueller A, Albrecht U, Contaldo C, Brown SA. NONO couples the circadian clock to the cell cycle. Proc Natl Acad Sci U S A. 110(5):1592-9.
- Kurz EU, Lees-Miller SP (2004) DNA damage-induced activation of ATM and ATM-dependent signaling pathways. DNA repair, 3:889-900.
- Lavin MF (2008) Ataxia-telangiectasia: from a rare disorder to a paradigm for cell signalling and cancer. Nat. Rev. Mol. Cell Biol. 9:759-769.
- Li Z, Musich PR, Serrano MA, Dong Z, Zou Y (2011) XPA-mediated regulation of global nucleotide excision repair by ATR Is p53-dependent and occurs primarily in S-phase. PLoS One 6(12):e28326.
- Li Z, Musich PR, Cartwright BM, Wang H, Zou Y (2013) UV-induced nuclear import of XPA is mediated by importin-α4 in an ATR-dependent manner. PLoS One 8(7):e68297.
- Lisby M, Rothstein R (2009) Choreography of recombination proteins during the DNA damage response. DNA Repair 8:1068–076.
- Matsuoka S, Ballif BA, Smogorzewska A, McDonald ER 3rd, Hurov KE, Luo J, Bakalarski CE, Zhao Z, Solimini N, Lerenthal Y, Shiloh Y, Gygi SP, Elledge SJ (2007) ATM and ATR substrate analysis reveals extensive protein networks responsive to DNA damage. Science 25;316(5828):1160-6.
- Meeran SM, Punathil T, Katiyar SK (2008) Interleukin-12- deficiency exacerbates inflammatory responses in UV irradiated skin and skin tumors. J Invest Dermatol 128: 2716–2727.
- Mellon I (2005) Transcription-coupled repair: a complex affair. Mutat Res. 577(1-2):155-61.

- Nakahata Y, Kaluzova M, Grimaldi B, Sahar S, Hirayama J, Chen D, Guarente LP, Sassone-Corsi P (2008) The NAD+-dependent deacetylase SIRT1 modulates CLOCK-mediated chromatin remodeling and circadian control. Cell 134(2):329-40.
- Nagoshi E, Saini C, Bauer C, Laroche T, Naef F, Schibler U (2004) Circadian gene expression in individual fibroblasts: cell-autonomous and self-sustained oscillators pass time to daughter cells. Cell 24;119(5):693-705.
- Nigg EA (1995) Cyclin-dependent protein kinases: key regulators of the eukaryotic cell cycle. Bioessays. 17(6):471-80.
- Ohnishi T, Mori E, Takahashi A (2009) DNA double-strand breaks: Their production, recognition, and repair in eukaryotes. Mutat Res 66:8-12.
- Palomera-Sanchez Z, Zurita M (2011) Open, repair and close again: Chromatin dynamics and the response to UV-induced DNA damage. DNA Repair, 10(2):119-25.
- Pontarin G, Ferraro P, Bee L, Reichard P, Bianchi V. (2012) Mammalian ribonucleotide reductase subunit p53R2 is required for mitochondrial DNA replication and DNA repair in quiescent cells. Proc Natl Acad Sci USA 14;109(33):13302-7.
- Rastogi RP, Richa, Kumar A, Tyagi MB, Sinha RP (2010) Molecular mechanisms of ultraviolet radiation-induced DNA damage and repair. J Nucleic Acids. 16;2010:592980.
- Rogakou EP, Boon C, Redon C, Bonner WM (1999) Megabase chromatin domains involved in DNA double-strand breaks in vivo. J Cell Biol. 146(5):905-16.
- Rothkamm K, Krüger I, Thompson LH, Lo¨brich M (2003) Pathways of DNA double-strand break repair during the mammalian cell cycle. Mol Cell Biol 23:5706-5715.
- Sahar S, Sassone-Corsi P (2009) Metabolism and cancer: the circadian clock connection. Nat Rev Cancer. 2009 Dec;9(12):886-96.
- Sahar S, Sassone-Corsi P (2013) The epigenetic language of circadian clocks. Handb Exp Pharmacol. 2013;(217):29-44.

- Sancar A, Lindsey-Boltz LA, Kang TH, Reardon JT, Lee JH, Ozturk N. (2010) Circadian clock control of the cellular response to DNA damage. FEBS Lett., 18;584(12):2618-25.
- Shrivastav M, De Haro LP, Nickoloff JA (2005) Regulation of DNA doublestrand break repair pathway choice. Cell Res 18: 134–147.
- Shrivastav M, Miller CA, De Haro LP, Durant ST, Chen BPC, et al. (2009) DNA-PKcs and ATM co-regulate DNA double-strand break repair. DNA Repair 8: 920–929.
- Torra IP, Tsibulsky V, Delaunay F, Saladin R, Laudet V, Fruchart JC, Kosykh V, Staels B (2000) Circadian and glucocorticoid regulation of Rev-erbalpha expression in liver. Endocrinology. 141(10):3799-806.
- Tracker J (2005) The RAD51 gene family, genetic instability and cancer. Cancer Lett 219: 125–135.
- Van Gent DC, Hoeijmakers JH, Kanaar R (2001) Chromosomal stability and the DNA double-stranded break connection. Nat Rev Genet. 2(3):196-206.
- Vilenchik MM, Knudson AG (2003) Endogenous DNA double-strand breaks: production, fidelity of repair, and induction of cancer. Proc Natl Acad Sci USA 100:12871–876.
- Ward JF (2000) Complexity of damage produced by ionizing radiation. Cold Spring Harb Symp Quant Biol 65:377-382.
- Weterings E, Chen DJ (2008) The endless tale of non-homologous end-joining. Cell Res. 18(1):114-24.
- Xue L, Yu D, Furusawa Y, Okayasu R, Tong J, Cao J, Fan S (2009) Regulation of ATM in DNA double strand break repair accounts for the radiosensitivity in human cells exposed to high linear energy transfer ionizing radiation. Mutat Res. 2;670(1-2):15-23.
- Yamamoto T, Nakahata Y, Tanaka M, Yoshida M, Soma H, Shinohara K, Yasuda A, Mamine T, Takumi T (2005) Acute physical stress elevates mouse period1 mRNA expression in mouse peripheral tissues via a glucocorticoid-responsive element. J Biol Chem. 280(51):42036-43.

- Zhou BB, Elledge SJ (2000) The DNA damage response: putting checkpoints in perspective. Nature 408:433–439.
- Zhou BB, Bartek J (2004) Targeting the checkpoint kinases: chemosensitization versus chemoprotection. Nat Rev Cancer. 4(3):216-25.

First of all I want to acknowledge my tutor Prof. Lucia Celotti for giving me the opportunity to work with her in these years. She always believed in my capabilities and under her guide I was able to grow as a researcher as well as a person.

Thanks to my co-tutor Prof. Urs Albrecht for hosting me for one year in his laboratory and for giving me good knowledge about the mechanism of the mammalian circadian clock.

A special thanks to Prof. Rodolfo Costa who always helped and supported my research, creating important opportunities that allowed me to pursue my career.

Thanks to Prof. Vera Bianchi and Prof. Peter Reichard for their precious help during these years, for including me in their fascinating project and for thesis revision.

Thanks to Sonia Fabris, Giovanna Pontarin, Paola Ferraro, Chiara Rampazzo and Elisa Franzolin. Everything I can do nowadays and allowed me to realize this work, I know I owe to you solely. Thanks to Jürgen A. Ripperger for your wise advices. Thanks to Selena Marini for your precious help in performing the laborious experiments about circadian clock & DNA repair topic. Thanks to Maddalena Mognato and Cristiano de Pittà for your willingness.

Thanks to Lia for making my life joyful.